KU BAND RF FRONT END RECEIVER OF A MOBILE TERMINAL FOR SATELLITE COMMUNICATION AND IOT SOLUTIONS

GUILHERME FELIX DE ANDRADE

DISSERTAÇÃO DE MESTRADO EM ENGENHARIA ELÉTRICA

DEPARTAMENTO DE ENGENHARIA ELÉTRICA

PROGRAMA DE PÓS-GRADUAÇÃO

UNIVERSIDADE DE BRASÍLIA

UNIVERSIDADE DE BRASÍLIA
PROGRAMA DE PÓS-GRADUAÇÃO
DEPARTAMENTO DE ENGENHARIA ELÉTRICA

KU BAND RF FRONT END RECEIVER OF A MOBILE TERMINAL FOR SATELLITE COMMUNICATION AND IOT SOLUTIONS

FRONT END RF DO RECEPTOR DE UM TERMINAL MÓVEL DE COMUNICAÇÃO VIA SATÉLITE EM BANDA KU E SOLUÇÕES IOT

GUILHERME FELIX DE ANDRADE

ORIENTADOR: PROF. DR. SÉBASTIEN R.M.J. RONDINEAU

DISSERTAÇÃO DE MESTRADO EM
ENGENHARIA ELÉTRICA

PUBLICAÇÃO: PPGEE.DM-802/22

BRASÍLIA/DF: DEZEMBRO - 2022

UNIVERSIDADE DE BRASÍLIA
PROGRAMA DE PÓS-GRADUAÇÃO
DEPARTAMENTO DE ENGENHARIA ELÉTRICA

KU BAND RF FRONT END RECEIVER OF A MOBILE TERMINAL FOR SATELLITE COMMUNICATION AND IOT SOLUTIONS

GUILHERME FELIX DE ANDRADE

DISSERTAÇÃO DE MESTRADO SUBMETIDA AO DEPARTAMENTO DE ENGENHARIA ELÉTRICA DA PROGRAMA DE PÓS-GRADUAÇÃO DA UNIVERSIDADE DE BRASÍLIA COMO PARTE DOS REQUISITOS NECESSÁRIOS PARA A OBTENÇÃO DO GRAU DE MESTRE.

APROVADA POR:

_____

Prof. Dr. Sébastien Roland Marie Joseph Rondineau – ENE/Universidade de Brasília - UNB
Orientador

_____

Prof. Dr. Leonardo Rodrigues Araujo Xavier de Menezes – ENE/Universidade de Brasília
Membro Interno

_____

Prof. Dr. Daniel Orquiza De Carvalho – ENE/Universidade de Brasília
Suplente

_____

Prof. Dr. Gefeson Mendes Pacheco – Instituto Tecnologico de Aeronautica - ITA
Membro Externo

BRASÍLIA, 30 DE DEZEMBRO DE 2022.

FICHA CATALOGRÁFICA

ANDRADE, GUILHERME FELIX DE
Ku Band RF Front End receiver of a mobile terminal for satellite communication and IoT solutions [Distrito Federal] 2022.
xvi, 80p., 210 x 297 mm (ENE/FT/UnB, Mestre, Engenharia Elétrica, 2022).
Dissertação de Mestrado – Universidade de Brasília, PROGRAMA DE PÓS-GRADUAÇÃO.
Departamento de Engenharia Elétrica

1. Front End RF	2. Receptor
3. Comunicação Satélite	4. IoT
I. ENE/FT/UnB	II. Título (série)

REFERÊNCIA BIBLIOGRÁFICA

ANDRADE, GUILHERME FELIX DE (2022). Ku Band RF Front End receiver of a mobile terminal for satellite communication and IoT solutions . Dissertação de Mestrado em Engenharia Elétrica, Publicação PPGEE.DM-802/22, Departamento de Engenharia Elétrica, Universidade de Brasília, Brasília, DF, 80p.

CESSÃO DE DIREITOS

AUTOR: Guilherme Felix De Andrade
TÍTULO: Ku Band RF Front End receiver of a mobile terminal for satellite communication and IoT solutions .
GRAU: Mestre ANO: 2022

Guilherme Felix De Andrade

Departamento de Engenharia Elétrica (ENE) - FT
Universidade de Brasília (UnB)
Campus Darcy Ribeiro
CEP 70919-970 - Brasília - DF - Brasil

I dedicate this work to my family who always supported me.

ACKNOWLEDGMENTS

First of all, I thank God to guide all my steps until here.
My sincere acknowledgment to my family who has always been supported and always stand by my side among the difficulties along the way, especially my mother Francelite, my father Marcelo, and my sister Camila.
Thank you to my dissertation advisor, Sébastien Rondineau, for taught me and guided me to follow the radio frequency specialty and provided me with knowledge and opportunities for several jobs to evolve professionally and be inserted into the job market.
Thank you to my co-workers Vitor Almeida, Daniel Carvalho, Elpidio Araújo, Vinicius Lisboa, Jeann Feitosa, Matheus Pereira, and Eric Barbosa, who helped me during my academic life, disciplines, and projects.

RESUMO

Título: Front end RF do receptor de um terminal móvel de comunicação via satélite em banda Ku e soluções IoT
Autor: Guilherme Felix De Andrade
Orientador: Prof. Dr. Sébastien R.M.J. Rondineau
Programa de Pós-Graduação em Engenharia Elétrica
Brasília, 30 de dezembro de 2022

Os sistemas de comunicação via satélite precisam recuperar o sinal transmitido, processá-lo adequadamente e adicionar o mínimo possível de ruído ao sistema, pois o sinal é bastante atenuado pelo espaço livre e pela chuva. Este trabalho apresenta o desenvolvimento, simulações sistêmicas e medições do receptor heteródino de rádio frequência para um terminal móvel de comunicação via satélite operando na banda Ku, juntamente com um sistema baseado na comunicação LoRa para dispositivos e adição de funcionalidades IoT ao produto. Além disso, é apresentado o projeto e procedimentos de design de filtros passivos, mixer e LNA utilizando o software Advanced Design System. Este trabalho apresenta uma compilação de subitens de três projetos cujo o foco é comunicação satélite e LoRa, desenvolvido ao longo do mestrado.

Palavras-chave: Front End RF, Receptor, Comunicação Satélite, IoT.

ABSTRACT

Title: Ku Band RF Front End receiver of a mobile terminal for satellite communication and IoT solutions
Author: Guilherme Felix De Andrade
Supervisor: Prof. Dr. Sébastien R.M.J. Rondineau
Graduate Program in Telecommunications and Communications Network Engineering
Brasília, December 30th, 2022

Satellite communication systems must recover the transmitted signal, process it correctly, and add as little noise as possible, as free space and rain significantly attenuate the signal. This work presents the heterodyne radio frequency receiver development, systemic simulations, and measurements for a mobile satellite communication terminal operating in the Ku band, along with a system based on the LoRa communication for devices and adding IoT functionality to the product. In addition, the passive filters, mixer, and LNA was projected and designed using Advanced Design System software. The work is part of a larger project, which deals with the design of the complete mobile terminal. This work presents a compilation of sub-items from three projects focused on satellite communication and LoRa, developed throughout the master's degree.

Keywords: Front End RF, Receiver, Satellite Communication, IoT.

SUMMARY

LIST OF FIGURES

LIST OF TABLES

LIST OF SYMBOLS

Greek symbols

Γ	Reflection coefficient	
Ω	Steradian	[sr]
ϵ_r	Relative permittivity, dielectric constant	
ϵ	Electric permittivity	[F/m]
λ	Wavelength	$[\mathrm{m}]$
∇	Nabla operator	
ω	Angular frequency	[rad/s]
ϕ	Azimuth angle	[°]
θ	Elevation angle	[°]

Latin symbols

D	Directivity	
P	Power intensity	$[\mathrm{W}]$
S	S-parameter	
f	Frequency	[Hz]
r	Distance	$[\mathrm{m}]$

LIST OF ACRONYMS AND ABBREVIATIONS

ADS Advanced Design System. , 1

BER Bit error rate. , 1, 7, 9

dB decibel. , 1
dBm decibel miliwatt. , 1

GPS Global positioning system. , 1

IF Intemediate frequency. , 1, 2, 9
IoT Internet of Things. , 1, 2
ITU International Telecommunication Union. , 1, 6

LNA Low Noise Amplifier. , 1, 10
LO Local Oscilator. , 1, 10, 18, 19
LoRa Long Range. , 1–3

RFFE Radio frequency front end. , 1, 3

1 INTRODUCTION

1.1 PREFACE

Satellite communications take radio waves (usually microwave frequencies between 1 GHz and 300 GHz) sent by satellites in Earth's orbit to transmit the data. Satellites are used in mobile communication, television, radio, and GPS, among others (RODDY, 2006).

Vehicle tracking services are in constant development. To present high quality and reach regions with no GPS signal, companies use the satellite communication technology for vehicle tracking, keeping ahead of the market competition.

The RF front end (RFFE) consists of all circuity needed to interface between antennas and the digital section in a mobile terminal system. The digital block contains the processor that sends and receives data, which then needs to interface with the RF source and support circuity in the signal chain. The RFFE transceiver contains several components that work together to ensure signal integrity throughout the bandwidth, including preparing a signal for transmission and demodulating a signal received on the Rx side (LEENAERTS D.; TANG, 2001).

Figure 1.1 describes a transceiver general block diagram. This project is part of a complex communication system in vehicle tracking systems based on satellite communication operating in the Ku band with electronic pointing from antenna arrays, Rotman lenses, and mobile terminals.

This project focuses on the RFFE receiver chain in the Ku band composed of selected commercial components and individual LNA and mixer designs for future low-cost products.

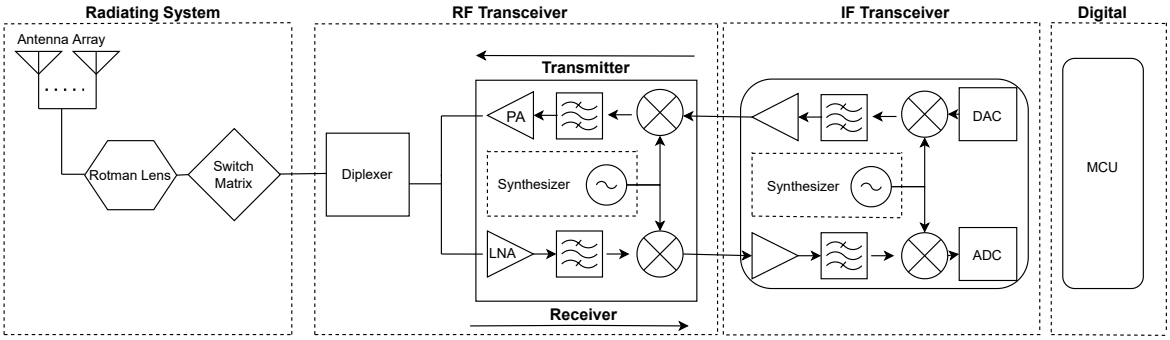

Figure 1.1 – Diagram of the overall full duplex system of the project showing the IF transceiver, RF transceiver, and the radiating system with its subsystems. Source: Own elaboration.

This work focuses on applied engineering, showing the stages of the product development cycle for the two projects mentioned below. The project's main focus was measurement results obtained to gather the maximum information and develop an optimized entire solution.

Due to the pandemic scenario during the project, the funding company decided to stop the project for economic reasons. As a result, developing the transceiver reception chain in the intermediate frequency for the satellite communication project was not possible.

Another communication project emerged with the Clamper company, which focuses on monitoring surge protection devices that incorporate LoRa communication, sensing, and monitoring systems, with an idea for IoT (Internet-of-Things) applications in low-voltage lightning arrester protection devices.

LoRa's project focused on the receiver and transmission chain, guided by the STM application note (STMICROELECTRONICS, 2020). In the receiver, it is necessary to perform impedance matching and filtering for the connection to the antenna. Beyond the impedance matching, the transmitter must filter the signal due to harmonics generated at the microcontroller transceiver output.

Basic peripheral circuits were developed in the LoRa communication project, such as DC power supplies, voltage, current, and temperature sensors, that will not be shown in this project to avoid deflect from the focus on radio frequency.

Companies with vehicle tracking products are constantly searching and developing to meet market demand so that the satellite communication project can be incorporated into the LoRa for communication between devices. Therefore, changing the IF frequency from 3 GHz to 915 MHz and adding a switch to select satellite communication or the LoRa antenna directly.

1.2 JUSTIFICATION

The company funding the satellite communication project decided to develop its own technology system antenna with accurate pointing and reduce product costs. Changing the antenna pointing and parameters, a new mobile terminal was designed to meet signal demodulation's power, noise, and phase specifications.

The company Clamper aims to keep up with innovating technology in actual devices by adding functionality to its product to deliver to customers a product containing LoRa communication. Monitoring surge protection devices and sensing current, voltage, and temperature with an idea for IoT applications in low-voltage lightning arrester protection devices 280 V.

1.3 OBJECTIVE

1.3.1 General Objective

To present the RFFE receiver studies, strategies, architectures, simulations, and measurements to be integrated into the mobile transceiver via satellite operating in the Ku band.

To present the LoRa communication system studies, strategies, architectures, simulations, and measurements to be integrated into the Clamper products.

1.3.2 Specific Objectives

- To design and characterize RFFE receiver;
- To design and characterize LNA;
- To design and characterize Mixer;
- To design and characterize Filters;
- To design and characterize RF LoRa circuit.

1.4 DISSERTATION STRUCTURE

This work is organized in 5 chapters, as follows

- Chapter 1 - Introduction - Presents the research theme, the justifications, the general and specific objectives, and dissertation structure.
- Chapter 2 - Fundamental concepts - Exposes the knowledge needed to understand the project, such as explanations of the general project, transceivers, LNA, mixers, filters, and LoRa.
- Chapter 3 - Methodology - It describes the methods used to obtain the results, such as calculations, simulations, and optimizations.
- Chapter 4 - Results and Discussion - Presents the measurement results of RFFE receiver, LNA, mixer, passive components, and LoRa project.
- Chapter 5 - Conclusion - Concludes the work with a general outline and presents the suggestion of future works.

2 FUNDAMENTAL CONCEPTS

It is necessary to understand the proposed system of which the RFFE receiver is part beyond the knowledge of the RFEE receiver itself.

2.1 SATELLITE COMMUNICATION SYSTEM

An artificial Earth satellite in orbit, known as a communications satellite, receives a communications signal from a transmitting ground station, amplifies it, and may even process it before sending it back to the Earth for reception by one or more receiving ground stations. The satellite is neither the point of origin nor the destination for communications data. Instead, the satellite is an active transmission relay, a role relay tower in terrestrial microwave communications (IPPOLITO; JR, 2017).

For different types of satellite communication services, such as fixed satellite service (FSS), broadcasting satellite service (BSS), mobile satellite services, navigational satellite services, and meteorological satellite services, there are allocation frequencies bandwidth options that follow International Telecommunication Union (ITU) rules. At allocation frequency band designations are presented in figure 2.1, where the Ku band is found in the frequencies from 12 GHz to 18 GHz (IPPOLITO, 2012).

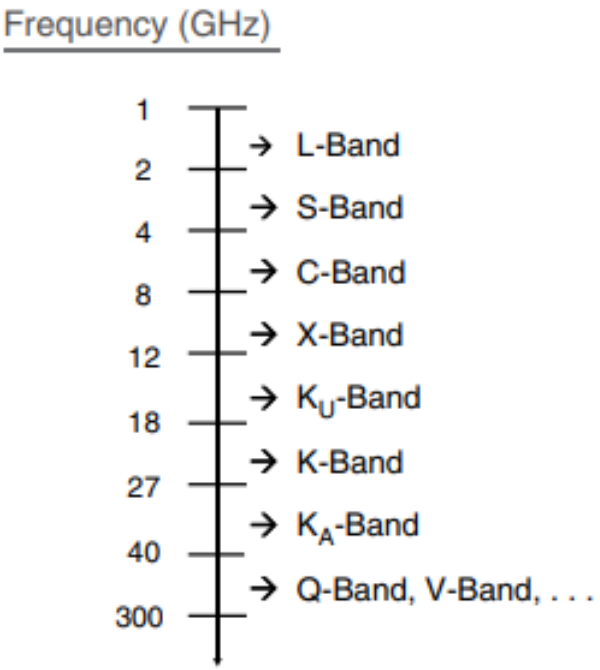

Figure 2.1 – Frequency Band Designations. Source: (IPPOLITO, 2012)

.

Satellites can be categorized by their altitude above the Earth's surface. There are LEO (low Earth orbit), MEO (medium Earth orbit), and GEO (geostationary Earth orbit). The Star One C1 satellite chosen for this project operates in the Ku band range, with the uplink in the frequency range from 14.0 GHz to 14.5 GHz and the downlink from 11.7 GHz to 12.2 GHz, using 36 MHz and 72 MHz bandwidth transponders, in both horizontal (H-pol) and vertical polarization (V-pol) (EMBRATEL, 2017).

Satellite links are used to provide communications over vast distances. A ground station relays a signal up to the satellite at a frequency known as the uplink frequency. The satellite receives this signal and re-broadcasts it on a downlink frequency to another ground station. If digital communications signaling is used, the signal may be regenerated before it is re-transmitted to Earth (MINOLI, 2015).

Three network elements compose the satellite communication system for vehicle tracking, shown in figure 2.2. First, the ground station controls vehicle tracking and monitoring a mobile terminal connected to the vehicle, which has access to relevant information for tracking, such as vehicle location and mobility, and the geostationary satellite, which allows communication between the ground station and terminal mobile.

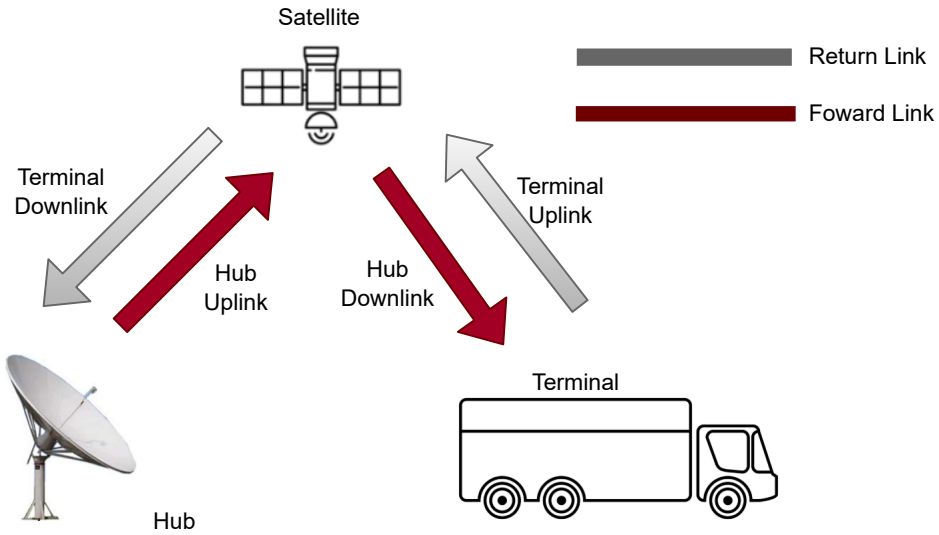

Figure 2.2 – Satellite communication system for vehicle tracking. Source: Own elaboration.

In satellite telecommunications terminology, uplink means the signal sent from Earth to the satellite, and downlink means the signal from the satellite to Earth. The uplink and downlink signals to and from a specific satellite must differ. The satellite constantly sends a specific downlink frequency that identifies it from other satellites. The transmit signal must be strong enough to reach the Earth stations. A Ground station constantly sends a specific uplink frequency that identifies it from other stations (RODDY, 2006).

The Ku-band is widely used in today's satellite communication. For example, users on this band receive satellite TV, such as Sky and Claro. The Ku band is defined by the ITU (International Telecommunication Union) by radio signals between 12 GHz and 18 GHz.In the telecommunications system, there are subdivisions for the uplink (11,7-12,2 GHz), and downlink (14,0-14,5 GHz) (IPPOLITO; JR, 2017).

Figure 2.3 shows the losses that must be determined and accounted for in any microwave link design. The figure compares typical downlink values for L, C, Ku, and Ka-bands. Certain losses are critical in all satellite systems, while others are of concern only in specific cases.

Propagation Mode	*Relative Importance on Satellite Links*	*L-Band (1.6/1.5 GHz)*	*C-Band (6/4 GHz)*	*Ku-Band (14/12 GHz)*	*Ka-Band (30/20 GHz)*
Free space downlink	Dominating factor	187	196	205	210
Atmospheric	Relatively small and nearly constant at high elevation angles	0.1	0.2	0.3	0.5
Rain attenuation	Severe as frequency and elevation angle increases	0.1	0.5	2	6
Refraction	Significant at times at low elevation angles	6	3	2	1
Scattering	Produces local RFI				
Diffraction	Considered for mobile links without line of sight	6 to 12			
Ionospheric scintillation (multipath)	Occasional wide signal variation	3 to 6	1 to 3	<1	
Doppler	Frequency shift for moving vehicles or satellites				

Figure 2.3 – Comparison of Significant Propagation and Fading Modes and Resulting Losses That Affect Microwave Links over GEO Paths (Values Are Rough Order of Magnitude, in Decibels). Source: (ELBERT, 2008).

2.1.1 Free Loss space

The free-space path between the transmitter and receiver may pass through a combination of ground obstructions and atmospheric phenomena. In free space, the satellite is considered a point source of power uniformly radiated in all directions (FREEMAN, 2007). The losses reduce the strength of the received signal and can cause its level to vary over time, even to the point where the signal fades away.

Free space losses in their linear form are explained in the Friis transmission equation 2.1, where the ratio of received power to transmitted power depends on the wavelength λ and the distance between the antennas r. This equation is valid for the Fraunhöfer region, r>$2D^2/\lambda$,

where D is the largest dimension of antennas (IPPOLITO, 2012).

$$\frac{P_r}{P_t} = \left(\frac{\lambda}{4\pi r}\right)^2 G_r G_t \tag{2.1}$$

Converting the Friss equation to the logarithmic scale, we get:

$$P_{RXdBm} = P_{TXdBm} + G_{TXdB} + G_{RXdB} - 20 \cdot \log_{10}\left(\frac{4\pi r}{\lambda}\right) \tag{2.2}$$

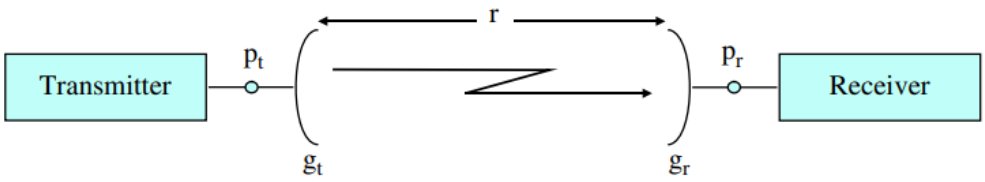

Figure 2.4 – Basic communications link. Source: (IPPOLITO; JR, 2017).

2.1.2 Rain atenuattion

In figure 2.5, it is evident that the difference in the attenuation level in the Ku band for lower frequency ranges is very high. Thus, satellite communication systems apply adaptive coding and modulation to mitigate errors and link loss, performed in the transmission burst coding, using source coding with low bit error rate (BER) and error correcting codes, which reduce BER inserting redundancies in the receiver code (IPPOLITO; JR, 2017).

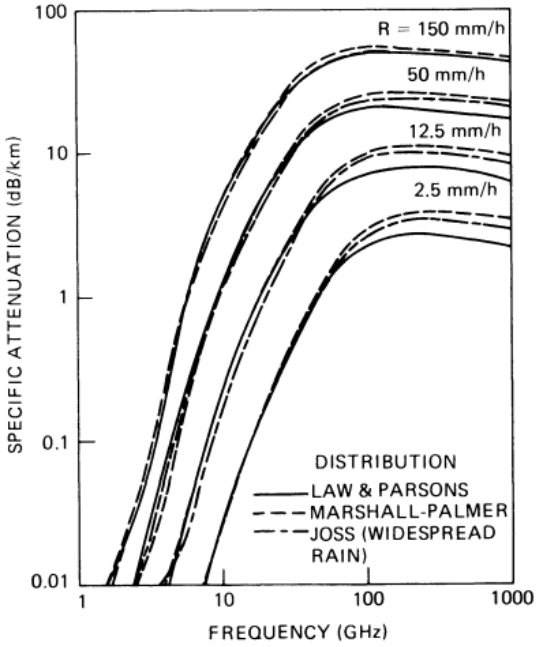

Figure 2.5 – Specific Attenuation of rain for three drop size distributions. R is the rain rate in mm/h, high signal attenuation in Ku-band when compared to the attenuation levels in lower frequencies. Source: (IPPOLITO, 2012).

2.1.3 EIRP

Equivalent isotropic radiated power (EIRP) is the power that must be radiated by a hypothetical isotropic antenna to achieve the same signal level in the antenna's maximum radiation direction. It is defined as the transmitted power (P) times the antenna gain (G), shown in the equation 2.3 (IPPOLITO; JR, 2017; MINOLI, 2015; RODDY, 2006).

$$EIRP = P \cdot G \tag{2.3}$$

2.2 LORA COMMUNICATION

The Internet of Things (IoT) has evolved into a typical application scenario with the speedy growth of the smart city, smart home, environmental monitoring, and other applications (ZHANG et al., 2022).

The LoRa benefit on the Internet of Things applications it is the lowest power needed and long-distance connectivity. Moreover, the LoRa node device transmits radiofrequency waves that carry data gathered from sensors. To achieve monitoring over a large geographical area, it requires a low power wide-area network (LPWAN) for an application called LoRaWAN in the IoT based LoRa connection (KARUNAMURTHY et al., 2021).

The LoRaWAN is a protocol communication method for terrestrial IoT networks, a novel frequencyshift chirp-spread-spectrum-modulation technique known as LoRa. The Semtech company develop the LoRa technology. It has a proprietary Chirp Spread Spectrum (CSS) modulation, which is more resilient than others to interference, jamming, and transmits in unlicensed ISM bands (FERKO et al., 2022).

2.3 TRANSCEIVER

The transceiver is a device capable of receiving and transforming signals from antennas into signals that can be converted digitally. The transmitter converts the baseband signal to an intermediate frequency, later to the same used by the satellite to be delivered to the antennas. It consists of a receiver circuit (RX) and a transmitter (TX). It is classified as a full duplex if it can transmit and receive simultaneously and half-duplex otherwise (ROGERS, 2003).

In the Receiver, the RFFE converts the radio frequency signal from 11.95 GHz to around 3 GHz for the intermediate frequencY (IF) transceiver to do the frequency conversion to the baseband. In the transmitter, the first stage converts a baseband signal to an IF of 3 GHz. The second stage raises this frequency with local oscillators and a mixer, passing through a filter in the band intended for transmission in the Ku band. Then the signal is boosted by a power amplifier and the information is delivered to the satellite.

2.4 RECEIVER

Receivers are fundamental in modern communication systems to recover the transmitted RF signal, process it properly, select the desired frequency band, reject adjacent ones, and translate the signal to IF, providing a minimum noise figure enough and amplification for system operation.

A receiver should have a low noise figure, low intermodulation distortion, high dynamic range, satisfactory gain flatness across the band, low phase noise, sufficient selectivity, and suitable BER. This can be considered the most critical specification for any architecture. The preferred receiver design should be lower in cost for successful implementation (LATHI; DING, 2012). Two available architecture types for designing the receiver are Homodyne and Heterodyne receivers.

2.4.1 Homodyne Receiver

It is also called “direct conversion” or “zero IF” architecture since the received signal is directly down-converted to the baseband. In a homodyne receiver, the desired signal is first selected by a filter, amplified by an LNA, and then frequency translated by a mixer to DC. Direct conversion needs a more linear mixer to attain the same performance as heterodyne (ABIDI, 1995).

2.4.2 Heterodyne Receiver

The heterodyne receiver performs frequency conversion in two (or more) stages, converting the signal from an RF source with frequency F_1 to an intermediate frequency F_{IF}, with an oscillator centered at frequency F_2. Then the mixer translates the frequency F_{IF} to a baseband frequency F_4, with an oscillator centered at frequency F_3 according to figure 2.6 (LATHI; DING, 2012).

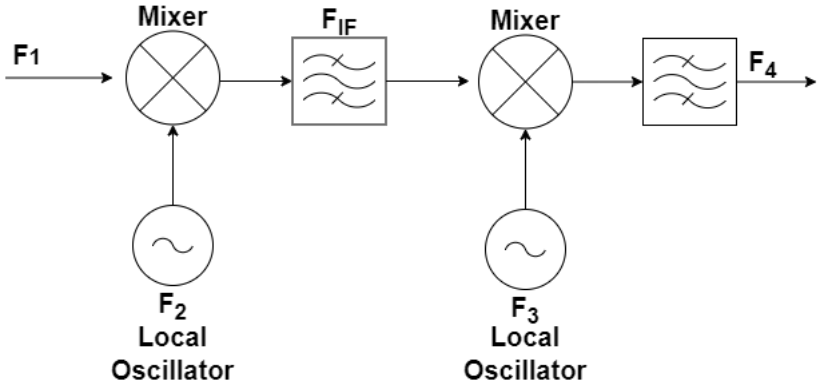

Figure 2.6 – Heterodyne receiver with 2 conversion stages diagram. Source: Own elaboration.

In a heterodyne architecture, the bands symmetrically located above and below the local oscilator (LO) frequency are down-converted to the same center frequency. If the receiver band of interest is $F_1 = F_2 - F_{IF}$, then the image is around $2F_2 - F_1 = F_2 + F_{IF}$. The most common approach to suppress the image is putting an image reject filter in the receiver. Both images reject the filter, and the IF filter requires a highly selective transfer function for conventional heterodyne architecture. Since the image reject filter is placed off-chip, the LNA needs to drive 50 Ω load for this architecture (RAZAVI, 2011).

2.5 NOISE

In the presence of noise, signal detection it is more challenging. The receiver is collecting background noise from the rest of the universe in addition to the desired signal. Thermal energy is present in all matter above 0 K. This thermal energy moves atoms and electrons around in a random way, leading to random currents in circuits, which are also noising. The noise can also come from man-made sources such as microwave ovens, cell phones, pagers, and radio antennas (ROGERS, 2003).

In communication systems, noise is the main factor that determines the functioning of receiver operation since the signal has a low amplitude, usually in picowatts, due to the loss of free space. In the presence of noise, signal detection is more challenging (IPPOLITO; JR, 2017).

There are several sources of noise, such as diffusion ones, shot noise caused by fluctuations in electron emissions or gaps at junctions in semiconductor materials with different dopings, flicker noise caused by defects in the crystalline structure of semiconductors, thermal noise resulting from the random fluctuation of voltage or current in a material, due to energy exchange with the surrounding environment (VASILESCU, 1999).

The main noise in radiofrequency systems is the thermal one caused by the movement of electrons in the devices that make up the receiver, being they active, such as amplifiers, mixers, switches, synthesizers, as well as the passive ones, antenna, beamformer, diplexer, filters, and splitters (ROGERS, 2003).

2.5.1 Thermal Noise

Originated from the effect of energy absorption by a black body in the presence of heat, impacting the vibration of the material molecules due to temperature. When raising At the temperature of a material, electrons acquire kinetic energy and move randomly, generating random voltage fluctuations at the component's terminals (POZAR, 2012).

From a resistor with a specific temperature in Kelvin [K], the electrons present in this resistor have a random movement, having a part of their kinetic energy converted into heat. With this, random fluctuations in the voltage at the resistor terminals are obtained over time, calculated from the equation 2.4, where h is Plank's constant, k is Boltzmann's constant, B is the bandwidth, f the center frequency, and R the resistance (POZAR, 2012).

$$V_n = \sqrt{\frac{4\,\mathrm{h}\,f\,B\,R}{e^{\frac{hf}{\mathrm{k}T}} - 1}} \tag{2.4}$$

As h$f \ll$ kT for frequencies smaller than 100 GHz, use Taylor's series first term to $e^{\frac{hf}{\mathrm{k}T}} -$

$-1 \simeq \frac{hf}{\mathrm{k}T}$ simplifying equation 2.4 into:

$$V_n = \sqrt{4\,\mathrm{k}\,T\,B\,R} \tag{2.5}$$

For a maximum power transfer using a load R, the noise power transferred to the load is given by the equation 2.7, and the noise power spectral density is constant at all frequencies (RAZAVI, 2011).

$$P_n = \left(\frac{V_n}{2\,R}\right)^2 R \tag{2.6}$$

$$P_n = \mathrm{k}\,T\,B \tag{2.7}$$

2.5.2 Noise Figure

One way to quantify noise in telecommunications systems it is from the noise figure. Noise from the electronics is described by noise factor F, which is a measure of how much the signal-to-noise ratio is degraded through the system (ROGERS, 2003).

$$S_0 = G \cdot S_i \tag{2.8}$$

where S_0 is the output signal power, S_i is the input signal power, G is the power gain $\frac{S_0}{S_i}$, SNR_i is the signal-to-noise ratio at input, and SNR_0 is the signal-to-noise ratio at output. Deriving the following equation for noise factor:

$$F = \frac{SNR_i}{SNR_0} = \frac{\frac{S_i}{N_i}}{\frac{S_0}{N_0}} = \frac{N_0}{G \cdot N_i} \tag{2.9}$$

For noise figure calculation, the component is considered to be equivalent resistor, so the noise power at the input is N_{in} = k T_0 B, the output noise power is the sum of input amplification and internally generated noise, so N_0 = k G B(T_0+T_e) where T_e is the equivalent noise temperature and T_0 is the room temperature 290 K, then we get the equation 2.10 (POZAR, 2012).

$$F = \frac{S_{in}\,\mathrm{k}\,G\,B(T_0 + T_e)}{\mathrm{k}\,T_0\,B\,G\,S_{in}} = 1 + \frac{T_e}{T_0} \tag{2.10}$$

$$T_e = (F - 1)\,T_0 \tag{2.11}$$

2.5.3 The Noise Figure of Components in Series

In receivers, several stages of components appear in order to have the amplification, mix, and filter of the corresponding signal for it is proper modeling and detection. Each stage has corresponding noise figure, and the noise added by all stages is combined to calculate the performance of the entire receiver chain (RAZAVI, 2011).

According to figure 2.7, each subsystem has it gain (G_i), noise figure (NF_i), and noise (N_i). The receive chain input noise power (N_{in}) it is calculated according to equation 2.7, amplified at the output $N_{out} = \mathrm{k}TBG_i$ according to the elements present in the reception chain, and $S_{out} = S_{in}(G_1\,G_2 \cdots G_i)$ (ADAM, 1969). Therefore the overall system noise figure equation is obtained by equation 2.12 (LEUNG, 2011).

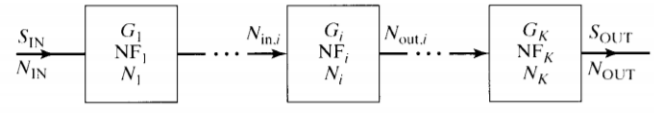

Figure 2.7 – K stages cascade in the receiver. Source: Leung (2011, p. 88).

$$NF = NF_1 + \frac{NF_2 - 1}{G_1} + \frac{NF_3 - 1}{G_1\,G_2} + \cdots + \frac{NF_k - 1}{G_1\,G_2 \cdots G_{k-1}} \tag{2.12}$$

Another way to characterize the system instead of the noise figure is with the receiver noise temperature (T_R), so we have the equation 2.13 according to Kraus (1988).

$$T_R = T_1 + \frac{T_2}{G_1} + \frac{T_3}{G_1\,G_2} + \cdots + \frac{T_k}{G_1\,G_2 \cdots G_{k-1}} \tag{2.13}$$

2.5.4 Antenna noise temperature

The noise temperature of an antenna is the physical temperature of a fictitious resistor that, when positioned in place of the antenna, generates the same noise power as the antenna, both matched to the transmission line or receiver to which they are connected. The noise appearing at the antenna terminals is formed by contributions from galactic, atmospheric, and terrain noise and by ohmic losses in the antenna itself (KRAUS, 1988; XU; RAHMAT-SAMII, 2011).

The antenna noise temperature (T_A) in Kelvin varies as a function of its pointing direction, brightness temperature $\big(T_s(\theta,\phi)\big)$ and the directivity of the antenna $\big(D_n(\theta,\phi)\big)$ according to the equation 2.14 (KRAUS, 1988).

$$T_A = \frac{1}{4\pi} \int_{4\pi\Omega} T_s(\theta,\phi)\, D(\theta,\phi)\, d\Omega(\theta,\phi) \tag{2.14}$$

Another useful figure of merit for receive antennas is the G/T ratio, this parameter defined above is a valuable figure of merit for a receive antenna because it characterizes the total noise power delivered by the antenna to the input of a receiver, concerns the quality or efficiency of the receiver, saying that for each Kelvin of noise temperature what is the minimum amount in dB that is needed on the antenna to ensure a satellite communication link works (IPPOLITO; JR, 2017; POZAR, 2012).

$$(G/T)_{[dB]} = 10 \log_{10} \frac{G}{T_A} [dB/K] \tag{2.15}$$

2.5.5 Sensibility

For a communication system, the receiver's sensibility it is essential for the operation. The sensibility S is defined as the required signal level that will allow the system to work most effectively for a given application (HERNANDEZ, 2014).

$$S = MDS + SNR \tag{2.16}$$

$$MDS = -174\,dBm + 10\,log_{10}(B) + NF \tag{2.17}$$

The minimum detectable signal (MDS) is the lowest signal level detected by a radio receiver. It can be processed by the analog and digital signal chain, demodulated by a receiver to provide useful information at the exit. B is the equivalent bandwidth, and NF is the system noise figure. Receivers require a proper signal with power above MDS to retrieve information with quality (HERNANDEZ, 2014).

2.6 SCATTERING MATRIX

The relationship between the incident and reflected voltage waves at the gates of the circuit employs for the characterization of linear microwave circuits. These relationships, called scattering parameters, are grouped in a matrix (POZAR, 2012).

The equation 2.18 defines the scattering matrix with an *N* ports network, where V_N^+ is the amplitude of the incident voltage wave on the *N* port and V_N^- is the amplitude of the voltage waveform reflected at the *N* gate.

$$\begin{bmatrix} V_1^- \\ V_2^- \\ \vdots \\ V_N^- \end{bmatrix} = \begin{bmatrix} S_{11} & S_{12} & \cdots & S_{1N} \\ S_{21} & & & \vdots \\ \vdots & & & \\ S_{N1} & \cdots & & S_{NN} \end{bmatrix} \begin{bmatrix} V_1^+ \\ V_2^+ \\ \vdots \\ V_N^+ \end{bmatrix} \tag{2.18}$$

$$S_{ij} = \left. \frac{V_i^-}{V_j^+} \right|_{V_k^+ = 0 \; for \; k \neq j} \tag{2.19}$$

The scattering parameter is determined by inserting an incident wave into port *j* and measuring the outgoing wave into port *i*. The incident wave on all ports must be null, except on port *j*. Thus, S_{ii} is the reflection listener on port *i* and S_{ij} is the transmission listener between port *i* and *j*. $|S_{ii}|^2$ is the power loss to reflection at the gate *i* and $|S_{ij}|^2$ is the power gain between the gates *i* and *j* (POZAR, 2012).

2.7 LOW NOISE AMPLIFIER

In receivers, the low noise amplifier is usually the first component an active part of the RFEE, the most critical subsystem in the reception chain for inserting noise into the system (JHA; GUPTA, 2012; SULAEMAN et al., 2016).

One of the main purposes of low noise amplifiers in the reception system it is to provide a high enough gain at the low power level in signal reception at the RFEE and introduce the minimum possible noise power to the signal. Therefore, the total noise figure in the system will guarantee a low signal-to-noise ratio (SNR), according to equation 2.12 (LIU et al., 2013).

With the improvements and innovations in solid-state technology, most RF and microwave amplifiers today utilize transistor devices such as Si BJTs, GaAs or SiGe HBTs, Si MOSFETs, GaAs MESFETs, or GaAs or GaN HEMTs (POZAR, 2012).

Figure 2.8 shows a generic single-stage amplifier configuration with a transistor between input and output matching networks. The matching networks are used on both sides of the transistor to transform the input and output impedance Z_0 to the source and load impedances Z_S and Z_L (SULAEMAN et al., 2016).

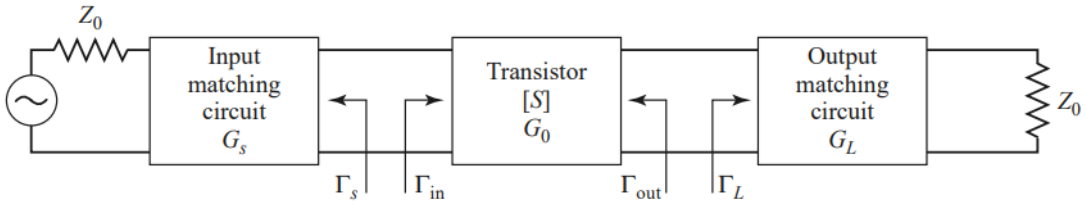

Figure 2.8 – The general transistor amplifier circuit. Source: (POZAR, 2012)).

From Equation 2.12, note that the LNA design considers not only the noise it inserts into the system but also gains, which must be big enough to suppress the noise of the subsequent ones.

The LNA has to be stable, considering that, as it is the first element of the reception chain, the existence of feedback amplifiers can be made to oscillate for a given combination of source and load impedances, as the source impedance value can change due to external conditions imposed on the antenna (RAZAVI, 2011).

An effective method for available LNA stability is through the condition of Rollet stability, or factor of Stern's stability, defined by:

$$K = \frac{1 - |S_{11}|^2 - |S_{22}|^2 + |\Delta|^2}{2|S_{12}||S_{21}|} \geq 1 \tag{2.20}$$

The combination K > 1 and Δ < 1 guarantees, if simultaneously satisfied, the unconditional stability of the LNA, Δ is the matrix determinant. It is worth mentioning that this factor does not indicate a metric since its value depends on two distinct quantities, which can alternatively be performed by the μ-test, as described by (Edwards; Sinsky, 1992).

$$\mu = \frac{1 - |S_{11}|^2}{|S_{22} - \Delta S_{11}^*| + |S_{12}S_{21}|} \geq 1 \tag{2.21}$$

2.8 THE QUADRATURE HYBRID

Quadrature hybrid couplers are microwave four ports circuit elements capable of splitting input wave power equally to two ports output (signal at each port 3 dB below that received by the input), with a 90 ° phase difference and the fourth completely isolated (POZAR, 2012). Figure 2.9 describes the quadrature hybrid coupler topology, Z_0 is the characteristic impedance, and λg is a guide wavelength.

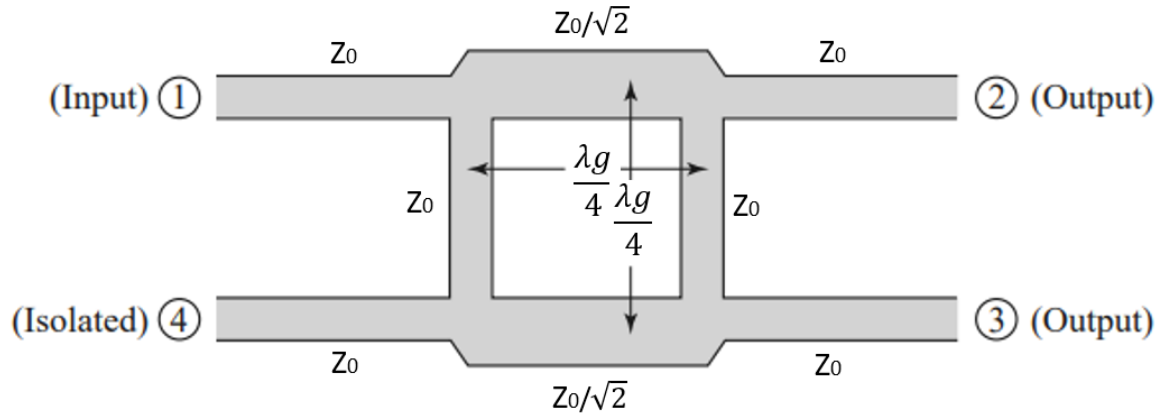

Figure 2.9 – Quadrature hybrid coupler, internal lines with λg/4 length and characteristic impedances of Z_0 or $Z_0/\sqrt{2}$ depending on the indicated path. Source: (POZAR, 2012)).

Given the matrix in Equation 2.22, note that ideally, there is no reflection at the input port (1), the path to the output port direct output (2) dephases the input signal by 90 ° because λ_g/4 path traveled. The signal to the coupled output (3) has a phase shift of 180 ° by traveling λ_g/2 path, and the signal at the port of the computer (4) is null due to the cancellation of the signal that travels along the path 1 - 2 (with 90 ° phase shift) with the signal traveling 1 - 2 - 3 - 4 (with phase shift from 270 °) (POZAR, 2012).

$$[S] = \frac{-1}{\sqrt{2}} \begin{bmatrix} 0 & j & 1 & 0 \\ j & 0 & 0 & 1 \\ 1 & 0 & 0 & j \\ 0 & 1 & j & 0 \end{bmatrix} \tag{2.22}$$

2.9 FREQUENCY CONVERSION

2.9.1 Diode conversion

The current in a diode is modeled by Equation 2.23, where I_s it is the saturation current, V is the voltage across the diode terminals, and $\alpha = nkT$, with α being the electron charge, k the Boltzmann constant, and T the temperature in Kelvin.

$$I(V) = I_s(e^{(\alpha V)} - 1) \tag{2.23}$$

Using the small-signal model and expanding equation 2.23 into a Taylor series (POZAR, 2012):

$$I(V) = I_0 + v\frac{dI}{dV}\bigg|_{V_0} + \frac{1}{2}v^2\frac{d^2I}{dV^2}\bigg|_{V_0} + \cdots = I_0 + \sum_{n=1}^{\infty}\frac{v^n}{n!}\frac{d^nI}{dV^n}\bigg|_{V_0} \tag{2.24}$$

$I(V_0) = I_0$ is bias current (DC), the dynamic conductance (G_d) defines the Taylor series first term or the junction resistance inverse $\frac{1}{R_j}$

$$\frac{dI}{dV}\bigg|_{V_0} = G_d = \frac{1}{R_j} \tag{2.25}$$

$$I(V) = I_0 + v\,G_d + \frac{v^2}{2}\,G'_d + \cdots \tag{2.26}$$

As it is a nonlinear system, the diode can be used for frequency conversion. According to equation 2.32, for nonlinear systems in general, when two frequency signals ω_1 and ω_2 are inserted, generate signals at (LIU et al., 2013):

$$\omega_0 = \mid m\omega_1 + n\omega_2 \mid, (m, n) \in \mathbb{Z} \tag{2.27}$$

2.9.2 FET conversion

Frequency multipliers with transistors are more efficient, offering greater bandwidth and lower losses, and there is a possibility of conversion gain. The FET transconductance high non-linearity is used for the conversion when polarized close to the pinch-off region. The local oscillator changes the transistor between low and high transconductance states, according to the equation 2.28 (POZAR, 2012).

$$g(t) = g_0 + 2\sum_{n=1}^{\infty} g_n \cos(n\omega_0 t), \tag{2.28}$$

g_0 is the transconductance in the polarization region, in this case, the pinch-of region.

2.9.3 Mixer

The mixer is a three-port device that multiplies twice domain input signals to perform frequency conversion. In an ideal mixer, the multiplication of the input signals results in an output signal representing the input frequencies sum and difference. The amplitude is proportional to the product of the RF and LO amplitudes and is verified mathematically through the trigonometric relationship of the equation 2.29 (STEER, 2010; LEE, 2004).

$$A\cos(w_1\,t).B\cos(w_2\,t) = \frac{AB}{2}[\cos(w_1 - w_2)t + \cos(w_1 + w_2)t] \tag{2.29}$$

The equations in section 2.9 show that infinite components are generated at other frequencies due to the nonlinearities in a real mixer implemented with a diode. This effect is also observed in other families of mixers implemented with transistors, for example.

Radiofrequency and microwave mixers are usually designed with non-linear devices, whether diodes or transistors. Such devices generate undesirable harmonics at various frequencies (POZAR, 2012).

The mixers can be classified as active when the signal at the output gives a gain concerning the input signal or passive when translation occurs frequency without any gain being added to the signal.

In upconverter mixers, the input is the IF signal, and the output is the RF signal, whereas, in the downconverter, the input is the RF signal, and the output is the IF signal.

Figure 2.10 – (A) Upconverter mixer, (B) Downconverter mixer. Source: (POZAR, 2012)).

The signal coming from the LO is periodic and generally has a fixed amplitude. The output of the mixer is sensitive to any modulation, whether desirable or not, of one of its inputs. Such undesirable modulations can be any non-linear interaction that happens with the input signal and any other signal (RAZAVI, 2011).

2.9.3.1 Balanced Mixer

Balanced mixers consists of two single-ended mixers combined with a hybrid junction are preferred in the RFEE transceiver operating in Ku Band downconverters to their superior suppression of spurious mixing products, zero dc power consumption, and good port-to-port isolation (ZHANG et al., 2018).

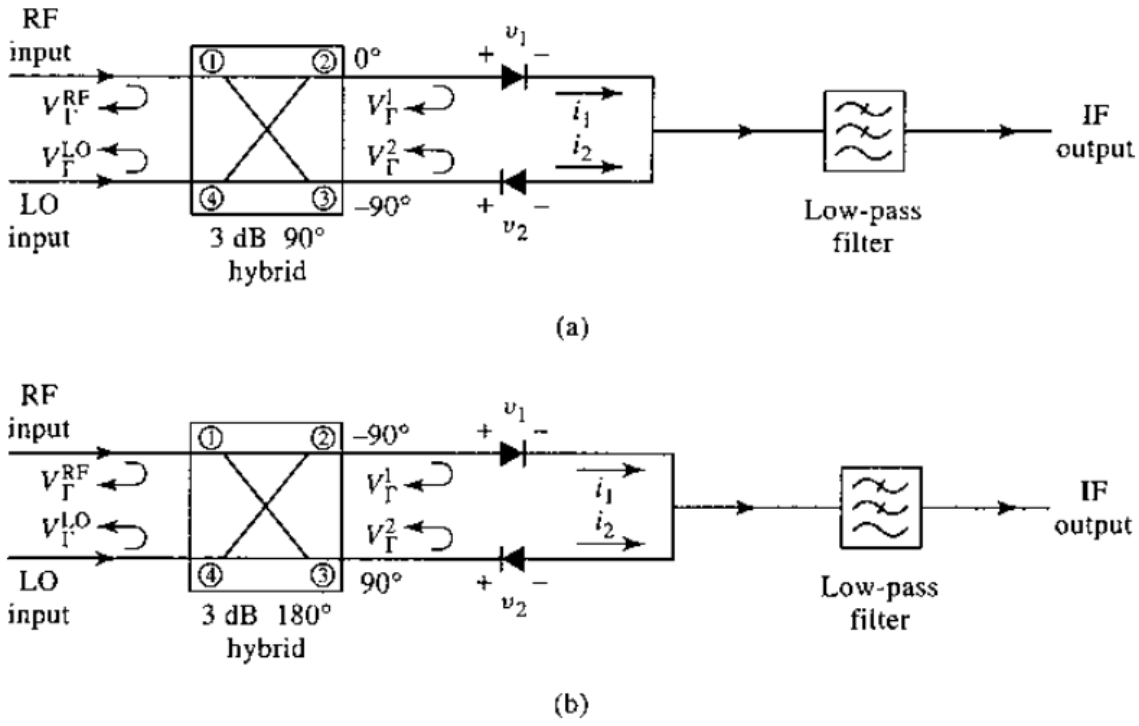

Figure 2.11 – (Balanced mixer circuits. (a) Using a 90 ° hybrid. (b) Using a 180 ° hybrid. Source: (POZAR, 2012)).

The LO and RF ports are isolated by the hybrid coupler. The IF output port should provide a low-impedance ground return for the RF and LO frequencies. To provide this return, the mixer module places a lowpass filter at the IF output (ZHAO; ZHANG; ZHAN, 2010).

2.10 INTERMODULATION

In a system with two input frequencies (ω_1 and ω_2), for example, the superimposed signals will be generated according to equation 2.30. The *n* signals in equation 2.30 are called "*n* order intermodulation products" or IP_n (POZAR, 2012; GUTTA; FATTORINI; PARKER, 2006).

$$v_0 = \sum_{n=0}^{\infty} a_n(\cos(w_1 t) + \cos(w_2 t))^n \tag{2.30}$$

The non-ideality of the mixer causes the intermodulation effect when two signals with different frequencies are applied to the non-linear system input, which presents a transfer function approximately to a Taylor series shown in equation 2.31. Its output displays components that are not harmonics but the intermodulation effect that generates superimposed

signals according to the equation 2.30 (RAZAVI, 2011; TERROVITIS; MEYER, 2000).

$$y(t) = a_0 + a_1 x(t) + a_2\, x^2(t) + a_3\, x^3(t) + \cdots + a_n\, x^n(t) + \cdots \tag{2.31}$$

It is possible to apply trigonometric identity properties to obtain the frequencies at which the resulting signals will be generated (POZAR, 2012; LIU et al., 2013):

$$\begin{aligned} v_o =& a_0 + a_1 V_0(\cos(\omega_1 t) + \cos(\omega_2 t)) + \\ &+ a_2 V_0^2 \left\{ \frac{1}{2}[1 + \cos(2\omega_1 t) + \frac{1}{2}[1 + \cos(2\omega_2 t) + \cos[(\omega_1 - \omega_2)t] + \cos[(\omega_1 + \omega_2)t] + ... \right\} \end{aligned} \tag{2.32}$$

2.11 SYNTHESIZER

The local oscillator is implemented by a voltage-controlled oscillator (VCO), whose output frequency varies according to the input voltage level. However, such circuits have accuracy that meets the needs of a modulator for communication systems, as their characteristics can vary with temperature and wear over time (RAZAVI, 2011).

The VCO has an output frequency controlled by the input voltage. It uses a low input frequency generated by a crystal oscillator as a reference and a feedback loop that maintains control voltage applied to the VCO so that its output precisely follows the reference frequency (RAZAVI, 2011; GOLDBERG, 2001). Figure 2.12 describes a typical phase-locked loop diagram.

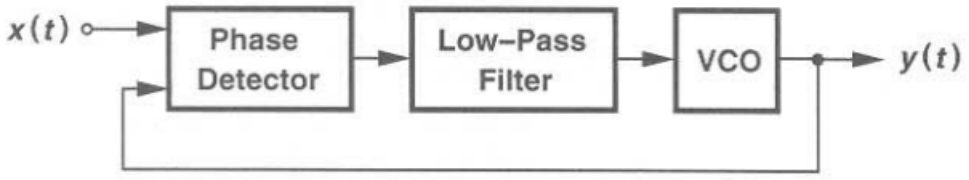

Figure 2.12 – Basic phase-locked loop, the VCO is controlled by the feedback system, which works by comparing the y(t) output frequency to a lower and more accurate reference frequency at x(t). Source: (RAZAVI, 2011)).

2.12 FILTERS

Filters are two-port components that contain the transfer function defined by the general equation 2.33. All telecommunications systems containing transmitters and receivers employ

filters, constituted by the association of reactive elements (inductors and capacitors), which can be discrete components, transmission line sections, or resonant elements. They aim to reject signals at undesirable frequencies for selecting specific frequency bands (HONG; LANCASTER, 2004).

Heterodyne receiver mixers generate one copy of the signal centered on $f_1 + f_2$ and the other on $f_1 - f_2$, which pollutes the receiver band unnecessarily and affects the low noise amplifier dynamic range. So, it is necessary to use a filter to select only the band of interest and suppress spurious signals coming from nonlinearities (WANG et al., 2017).

In the equation 2.33 ϵ and F_n are, respectively, the ripple and the characteristic function, with omega being the frequency variable (HONG; LANCASTER, 2004).

$$|S_{12}(j\Omega)|^2 = \frac{1}{1 + \epsilon^2 \, {F_n}^2(\Omega)} \tag{2.33}$$

The most common filters in communications systems are low-pass filters that pass low frequencies and reject high frequencies, high-pass filters that allow high frequencies to pass and reject low frequencies, band-pass filters that select a specific range of frequencies and reject all others, and band-stop filters that reject a specific frequency range and let the other frequencies pass (LATHI; DING, 2012).

2.12.1 Band-pass filter

Band-pass filter design consists of the low-pass filter generic sections normalized elements according to figure 2.13 and then transforms to band-pass with equations 2.34,2.35, 2.36, and 2.37.

For microwave frequencies, including Ku-band, coupled resonators have been vastly used as bandpass filters in microstrip technology. The most prevalent forms are the end-coupled half-wavelength resonator, hairpin line, interdigital, and square Open-Loop Resonator (SOLR) (KHAN et al., 2015).

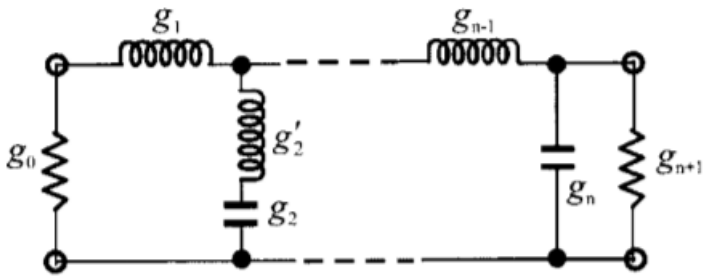

Figure 2.13 – Generic Multi-Session Low-Pass Filter with Normalized Elements. Source: (HONG; LANCASTER, 2004).

The equations 2.34 and 2.35 represent the inductances and capacitances transformations from low-pass to band-pass. *FBW* is the fractional width of the filter $\left(\frac{f_2-f_1}{f_0}\right)$, γ_0 the impedance scaling factor, w_c the cutoff frequency, g the characteristic impedance and Ω_c the central frequency variable (HONG; LANCASTER, 2004).

$$L_s = \left(\frac{\Omega_c}{FBW\, w_0}\right)\gamma_0\, g \tag{2.34}$$

$$C_s = \left(\frac{FBW}{w_0\, \Omega_c}\right)\frac{1}{\gamma_0\, g} \tag{2.35}$$

The equations 2.36 and 2.37 represent the inductances and capacitances transformations from low-pass to band-pass.

$$C_p = \left(\frac{\Omega_c}{FBW\, w_0}\right)\frac{g}{\gamma_0} \tag{2.36}$$

$$L_p = \left(\frac{FBW}{w_0\, \Omega_c}\right)\frac{\gamma_0}{g} \tag{2.37}$$

2.12.1.1 Coupled Open-Loop Resonators Filter

The Coupled Open-Loop Resonators (COLR) filters are high-selectivity bandpass filters. They are intermediaries between Chebyshev and elliptical function filters (HONG; LANCASTER, 2004).

In specific resonant frequencies, a resonator is a device that can store a significant amount of electromagnetic energy while wasting only a small portion of the stored energy. Generally, a circuit's resonance happens when the amount of stored electric and magnetic energy equals (CHIANG; HSIEH; CHUNG, 2006; SANTANA; BARBOSA; RONDINEAU, 2020).

The association of two or more resonators close enough to fringing fields makes them get coupled. The coupling coefficient value quantifies the coupling effect, which is the ratio between the coupled to stored energy in the resonator. The resonators number determines the filter order, and the total loop length must be $\lambda/2$ (HONG, 2000; SANTANA; BARBOSA; RONDINEAU, 2020).

Figure 2.14 describes the four-pole filter configuration that uses electric, magnetic, and mixed couplings in its structure.

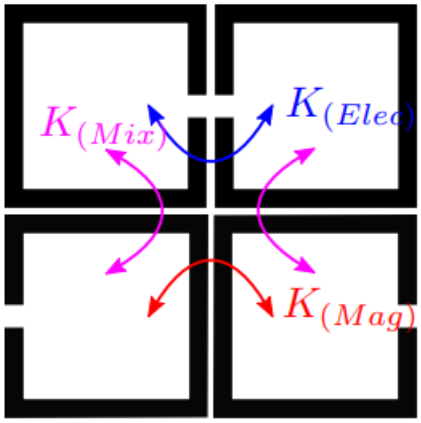

Figure 2.14 – Geometry of a basic four-pole order coupled open-loop resonator filter indicating the types of couplings in the structure. Source: (SANTANA; BARBOSA; RONDINEAU, 2020).

2.12.1.2 Parallel-Coupled Filter

Bandpass filters with high bandwidths can be developed from cascaded sections of lines parallel coupled to each other. The calculations for their implementation are those of equations 2.38, 2.39, and 2.40. For example, figure 2.15 shows the topology (POZAR, 2012).

In the equations 2.38, 2.39 and 2.40 g_n are the prototype low-pass filter elements, $J_{i,j}$ are the elements immittances, Δ is the fractional filter bandwidth $\left(\frac{f_2 - f_1}{f_0}\right)$ and Z_0 is the input characteristic impedance (HONG; LANCASTER, 2004).

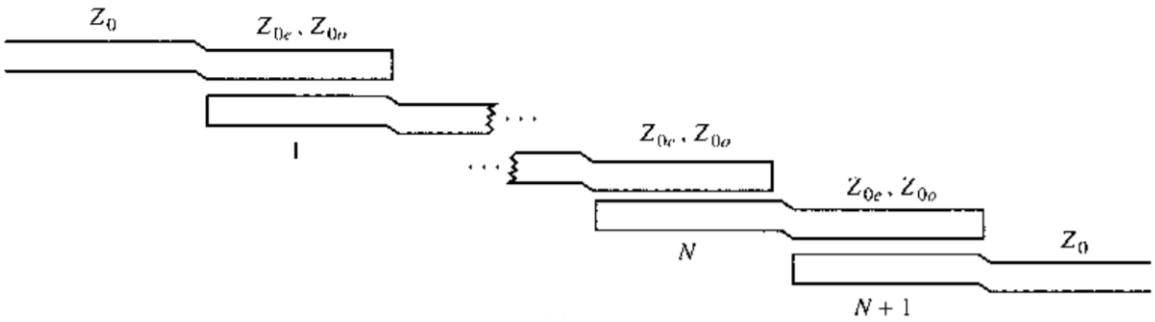

Figure 2.15 – Parallel coupled microstrip filter. Source : (POZAR, 2012)).

$$Z_0 J_1 = \sqrt{\frac{\pi \Delta}{2 g_1}} \tag{2.38}$$

$$Z_0 J_n = \frac{\pi \Delta}{2 \sqrt{g_{n-1} g_n}} \tag{2.39}$$

$$Z_0\, J_{N+1} = \sqrt{\frac{\pi\,\Delta}{2\,g_N\,g_{N+1}}} \tag{2.40}$$

From equations 2.38, 2.39, and 2.40, it is possible to determine the even and odd impedance modes according to equations 2.41 and 2.42 and obtain the track's width and the spacing between them.

$$(Z_{0\,par})_{j,j+1} = \frac{1}{Y_0}\left[1 + \frac{J_{j,j+1}}{Y_0} + \left(\frac{J_{j,j+1}}{Y_0}\right)^2\right] \tag{2.41}$$

$$(Z_{0\,impar})_{j,j+1} = \frac{1}{Y_0}\left[1 - \frac{J_{j,j+1}}{Y_0} + \left(\frac{J_{j,j+1}}{Y_0}\right)^2\right] \tag{2.42}$$

3 METHODS

To describe the methods used to obtain the results, such as calculations, simulations, and optimizations.

3.1 PROJECT

The project's methodology was map in the flowchart of figure 3.1, where the subsystems were simulated at the block level in an ideal architecture, and the general specifications required for the system's operation were established.

With the parameters already defined in the general system, each subsystem was designed, simulated, and optimized from this methodology. Finally, the printed circuit board project was sent for manufacturing and carried out the necessary tests for validation.

The simulations setup in ADS software is a frequency in the range of 9.7 GHz to 16.2 GHz, with 120 cells per wavelength mesh in the microstrip lines, where the wavelength is at the highest frequency and with edge mesh enabled.

The subsystems were all designed with a characteristic impedance of 50 Ω, so impedance matching between commercial components mixer, synthesizer, and LNA chosen for the project is not required.

The Ku-band receiver operating frequency was determined with a central frequency of 11.95 GHz with a bandwidth of 500 MHz, according to Star One C1 satellite operating range (EMBRATEL, 2017). The Ku band is contained in the SHF frequency band, classified by ANATEL (2018a).

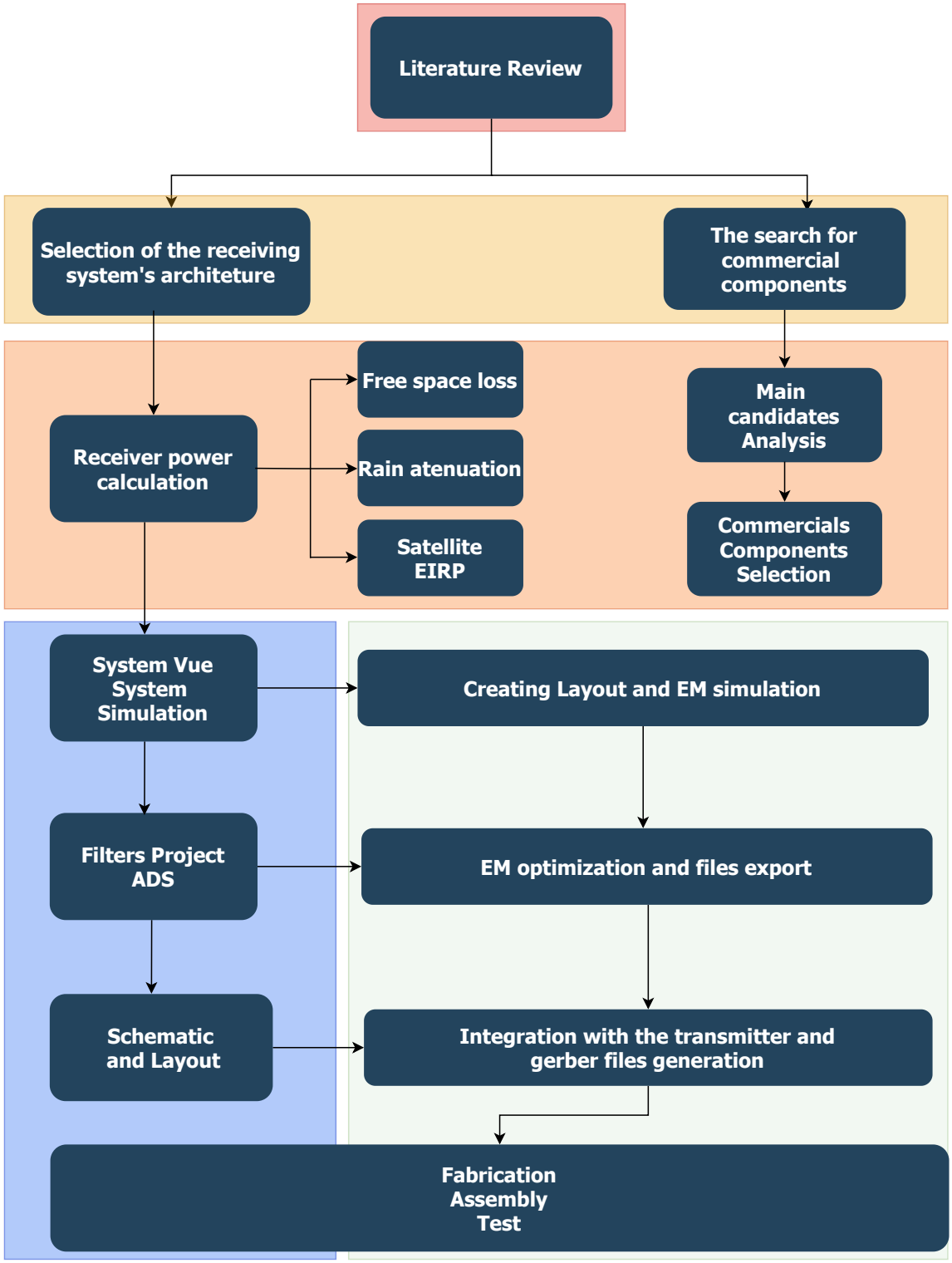

Figure 3.1 – Project flowchart. Source: Own elaboration.

3.2 RECEIVER ARCHITECTURE

A receiver that can operate in the receiver band from 11.7 GHz to 12.2 GHz with 24 MHz channels accessible of the transponder and be able to switch between the channels in the entire band of 500 MHz was projected to attend Ku-band reception requirements.

The indirect conversion architecture (heterodyne architecture) was chosen in two stages, converting the RF signal from 11.95 GHz to around 3 GHz for the IF transceiver to do the frequency conversion to the baseband. Then, in the IF synthesizer, channel selection will be made with a control planned to generate the oscillation frequencies needed to translate the signal to the desired channel.

3.3 RECEIVER POWER

The wavelength λ for the Ku-band descent frequency is 2.5105 cm calculated by the equation 3.1, where c is the speed of light in a vacuum $3 \cdot 10^8$,m/s and f is the center operating frequency of 11.95 GHz

$$\lambda = \frac{c}{f} \tag{3.1}$$

Free space losses 205.2 dB for the Ku band in the downlink of the system were calculated from equation 2.2 with *R* equal to 36,382 Km, center frequency of 11.95 GHz and λ of 2.5105 cm.

The rain attenuation for the worst scenario is 18 dB, taking into account consideration that in 1 year, there is a possibility of 0.01 % of rainfall with a maximum rate of 90 mm/h, according to the recommendation (ITU-R, 2017).

According to Embratel (2017), the typical satellite *Star One C1* EIRP is 46 dBW, 1 dB/K typical *G/T*, and 4 dB output backoff, all of these around the Mercosur region, the HUB output estimation is 5.9 dB. So with this, we have a 40.1 dBW downlink EIRP, discounting the HUB output backoff in the typical satellite EIRP.

In Ippolito e Jr (2017) and Roddy (2006), it is demonstrated how to calculate the receiver signal power according to the equation 3.2. With the downlink EIRP parameters extracted from the *Star One C1* satellite, the calculated free space losses, the estimated gain 27 dB of the antenna array, and 3 dB of polarization loss due to the fact since the mobile terminal antenna is circularly polarized, and the satellite is linearly polarized, reception power of -141.1 dBW was obtained, or -111.1 dBm according to 3.4.

$$P_r[dBW] = EIRP_d + G_r - L_{fs} \tag{3.2}$$

$$P_r = -141,1\,[dBW] \tag{3.3}$$

$$P_{[dBm]} = P_{[dBW]} + 30 \tag{3.4}$$

3.4 RFFE TRANSCEIVER

The transceiver board followed the steps of simulation and optimization of circuits and transitions, schematic design with its associated symbols, the footprint of the component's commercials following datasheet recommendations, and complete board layout.

The resistor and inductor components are all SMD 0402 packaging, the LNA's and Synthesizer are QFN encapsulation, and the TDFN encapsulation mixer.

The substrate chosen for the project is AD250C from Rogers Corporation, having the low dielectric constant (ϵ_r = 2.5). Obtaining microstrip tracks wider and having more design freedom in terms of characteristic impedances of the lines, moving away from the minimum width that the manufacturer can produce. In addition, the tracks become less sensitive to variations in width.

This substrate is a polymer, having high flexural strength since the transceiver will be a product subjected to mechanical vibrations in the movement of vehicles.

The loss tangent for this substrate is low ($\tan\,\delta = 0.0014$), causing the material to have a lower loss. The chosen substrate thickness was 0.508 mm and 0.5 oz thick copper.

To manufacture the RFFE transceiver PCB, Lauquen was selected because they work with the IPC-6018 standard, which is suitable for manufacturing high-frequency boards. Table 3.1 describes the capabilities, and table 3.2 defines the layer stack.

Table 3.1 – Lauquen printed circuit manufacturing capability.

Parameter	Value
Minimum spacing between tracks	4 mil (102 μm)
Minimum track width	4 mil (102 μm)
hole diameter	6 mil (0.15 mm)

The RF fornt end receiver development depends on the Lauquen technical capabilities.

The limitations that most affect the design are the width and isolation of tracks, table 3.1. Circuit design cannot be outside of these Lauquen manufacturing limits.

The Top Layer, which is the first copper layer, was used to make the tracks RF signal. The second copper layer is exclusively GND, making the tracks of the first layer microstrip.

Table 3.2 – RFFE Transceiver Layer Stack.

Layer	Name	Material	Thickness	Dielectric Constant
1	Top Overlay	Silk screen		
2	Top Solder	Solder Resist	0,01 mm	
3	Top Layer	Copper	0.5 oz/ft^2	
4	Dieletric 1	AD250C	0.508 mm	2.5
7	Bottom Layer	Cooper	0.5 oz/ft^2	
8	Bottom solder	Solder Resist	0,01 mm	
9	Bottom Overlay	Silk screen		

For the connection to GND, a series of shielded vias were placed inside the ground planes of the plate at a 1.5 mm spacing (space $< \frac{\lambda_g}{8}$ @ $f = 15$ GHz), is this group of roads inserted in the edges of the land plane, closer to the track. Already inside the rest of the ground plane, groups of vias stitching were evenly inserted spaced 2.5 mm inside the ground planes, this track group being used to fill in the spaces that may resonate if they are not terminated with GND.

In the top layer, the empty spaces were filled with a ground plane (GND) spaced 3 mm apart from the RF signal tracks to avoid coupling. The 250 μm through vias diameter connect the top layer ground plane to the board GND layer. Therefore, the pathways were evenly arranged at the ends and inside the ground plane of the top layer.

Figures 3.2,3.3, and 3.4 show the top and bottom layer layouts.

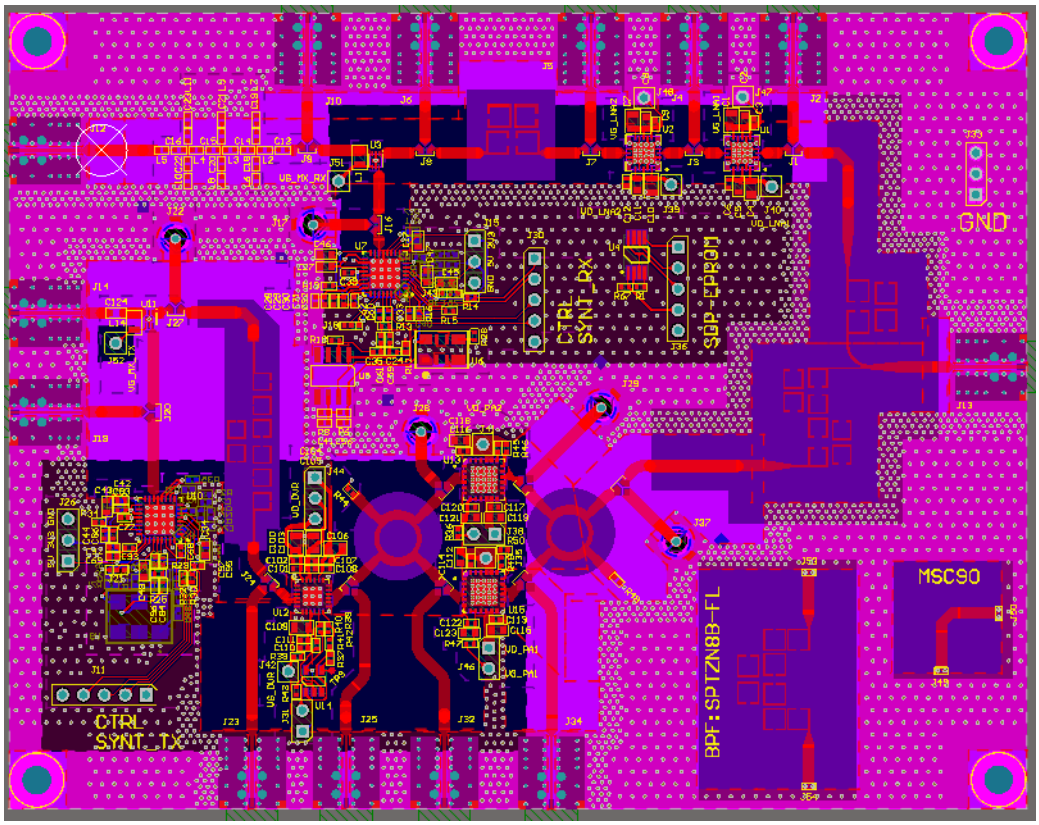

Figure 3.2 – RFFE transceiver Layout. Source: Own elaboration.

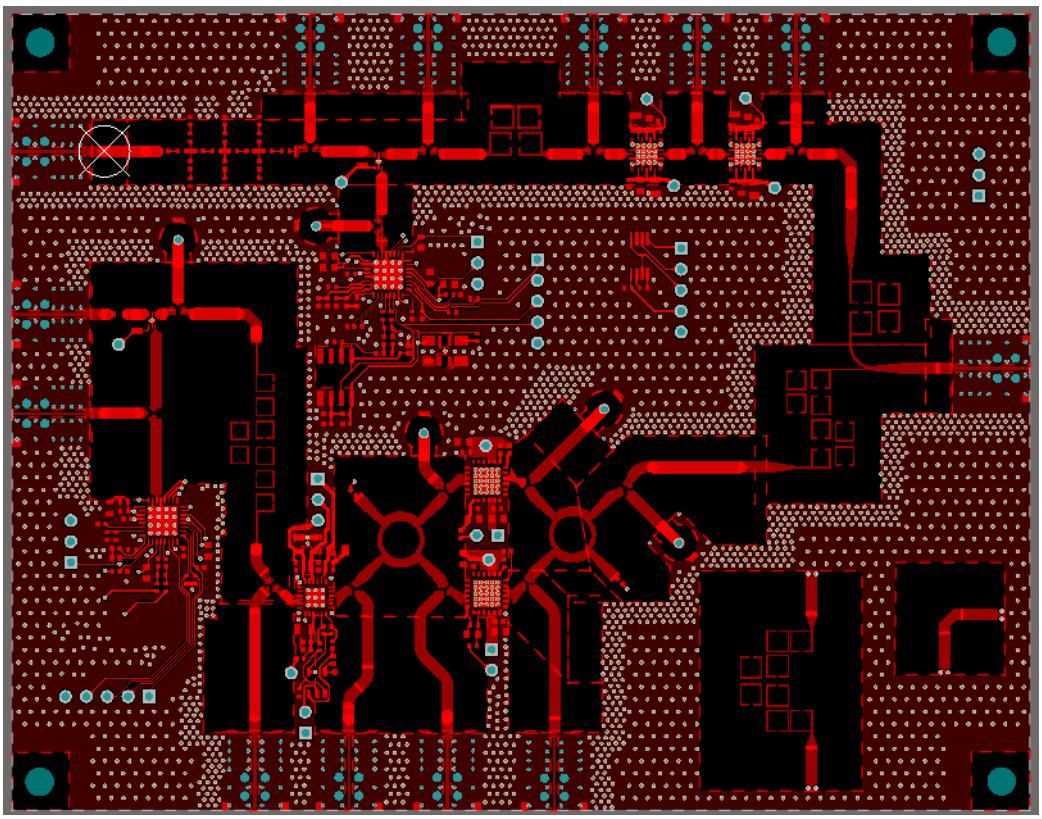

Figure 3.3 – RFFE transceiver Top Layer. Source: Own elaboration.

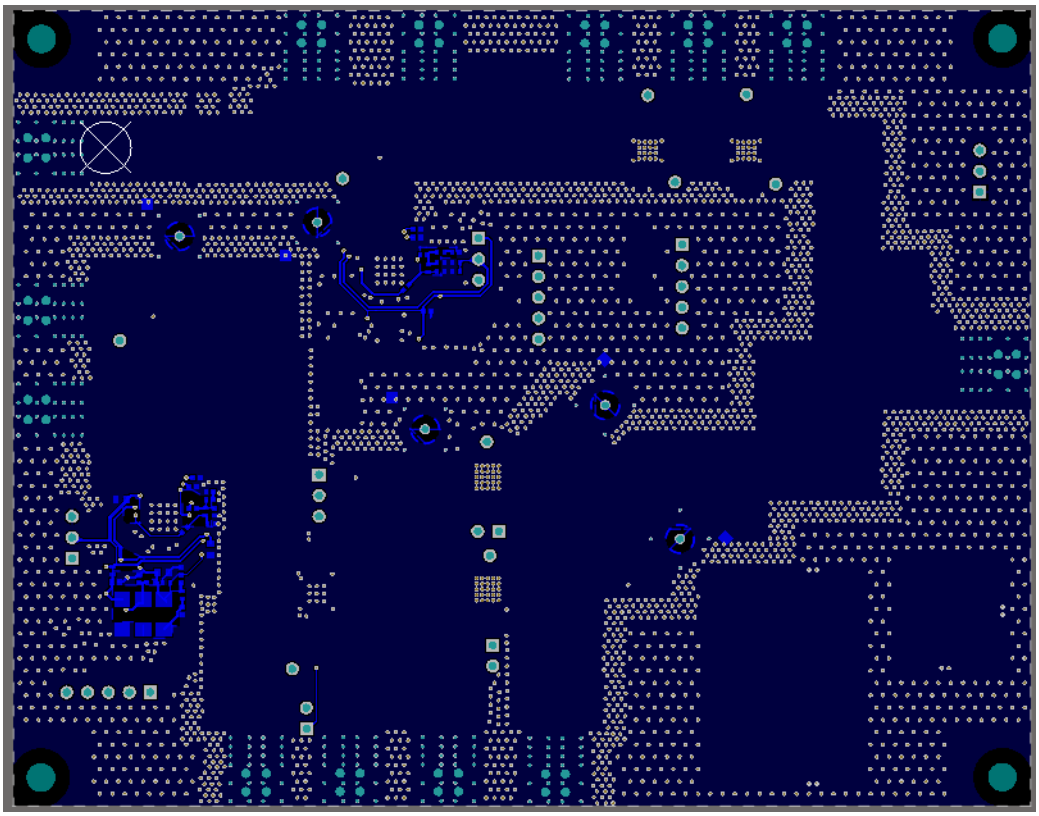

Figure 3.4 – RFFE transceiver Bottom Layer. Source: Own elaboration.

3.5 RF SYNTHESIZER

The RF synthesizer objective is to output the local oscillator frequency of 8.95 GHz into the mixer LO input for downconversion.

The chosen synthesizer was the ADF5355 from *Analog Devices* with the option of choosing a frequency from 6.8 GHz to 13.6 GHz controlled through a serial bus, is made using the SDP-S board from Analog Devices. In addition, the manufacturer provides the PLL software so the user can control the board and send the appropriate settings to the synthesizer.

3.6 RF MIXER

The RF mixer objective is to downconverter the Ku-Band signal (14-14.5 GHz) to intermediare frequency, in this project 3 GHz.

The mixer chosen was MACOM's MAMX-011021 because it is the most linear among those selected, as the mixer is the most critical element for the system's linearity in intermodulation products. This mixer has an 8 dB loss in Ku Band.

An alternative mixer was project to RFFE transceiver board lower the cost, spurious mixing products suppression, and better port-to-port isolation improvement using a 3 dB hibrid and a diode in balanced mixer topology.

Three commercial diodes were selected to test the mixer performance, MA4E2054D, BAT1504WK, and SMS7621. The Hybrid was designed and optimized using the ADS Method of Moments (MoM), and the substrate is the same one in the RFFE transceiver, AD250C from Rogers Corporation.

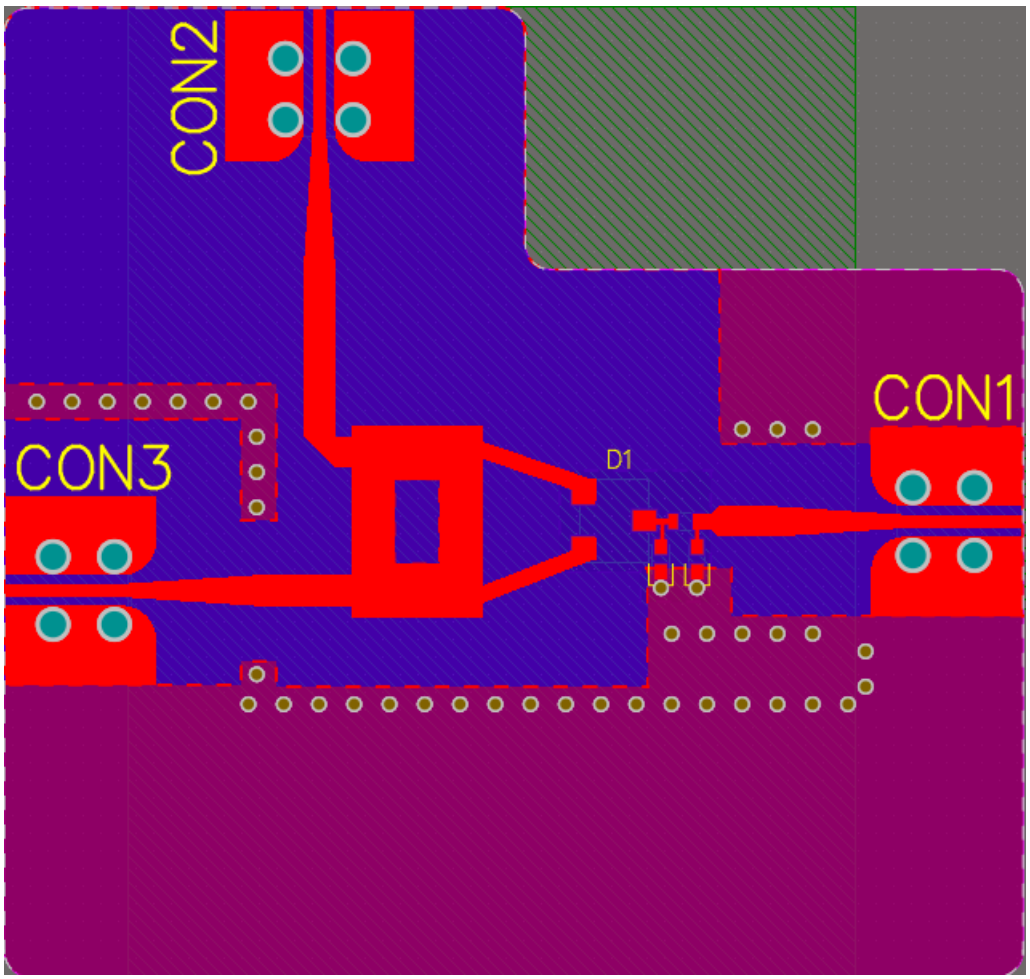

Figure 3.5 – Balanced mixer board layout. Source: Own elaboration.

3.7 LNA

A low noise amplifier is the receiver's most crucial component because it contributes most of the noise figure in the reception chain. LNA amplifies a very low-power signal without significantly degrading its signal-to-noise ratio.

LNA chosen was QORVO's QPA2609 for having the lowest noise figure, high gain, working in the specified frequency range, and having return loss below 12 dB among those

commercially researched.

An alternative LNA composed of GaAs FET transistors was designed to optimize and lower product costs. The transistor selected was CE3512K2 because the performance of up to 13.7 dB of gain and a minimum noise figure of 0.3 dB specified by its datasheet (ANDRADE; BARBOSA; RONDINEAU, 2020).

The first stage has been optimized to have a low noise figure using the noise figure circles and input matching, reaching 0.3 dB noise figure but decreasing the gain to 10 dB. In the second stage, the gain was improved with the matching between the stages and the output matching, reaching 14 dB.

The two stages were projected to respect the K-stability factor and μ-factor according to equations 2.20 and 2.21. A group of vias shielding was inserted in PCB inside the ground planes of the plate for the connection to GND with 1.5 mm spacing (spacing < $\frac{\lambda_g}{8}$ @ f = = 12 GHz),

The substrate chosen for the LNA project is the RO4350B from Rogers with a thickness of 0.508 mm (ϵ_r=3.48, $\tan\delta$= 0.0037 @ 10 GHz), due to higher availability and price in the market compared to RFFE transceiver substrate.

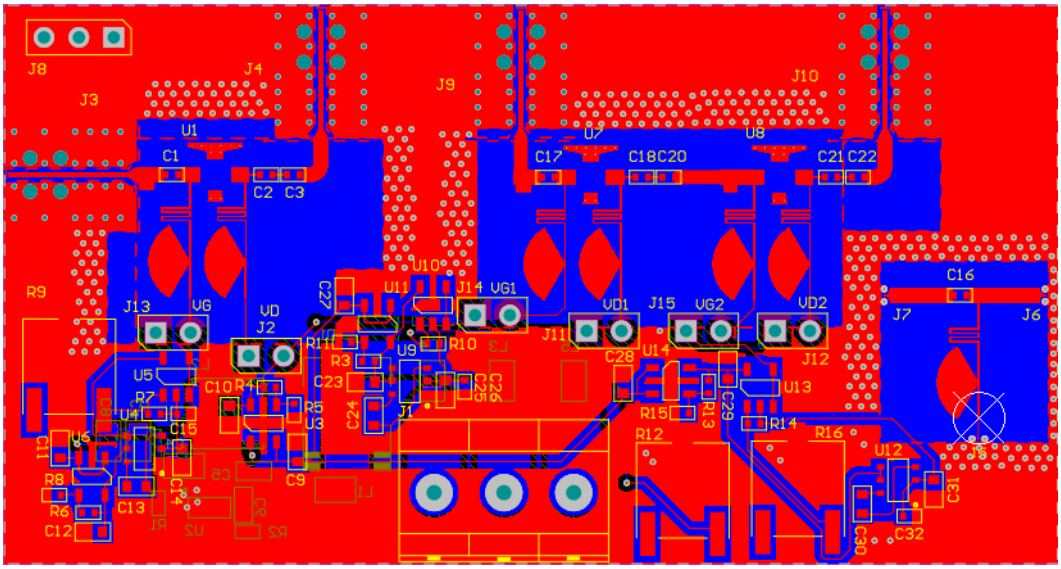

Figure 3.6 – LNA board layout. Source: Own elaboration.

3.8 PASSIVE COMPONENTS

A printed circuit board named PACBoard was manufactured to characterize the passive circuits designed and possible optimization in the RFFE transceiver. The substrate is AD250C from Rogers Corporation, having the dielectric constant (ϵ_r = 2.5) and ENIG finish.

The PACboard has the parallel coupled topology filter designed in this document. The Coupled Open-Loop Resonators Filter topology was designed by colleagues and characterized in this document with the TRL calibration method utilizing the probe station and vector network analyzer.

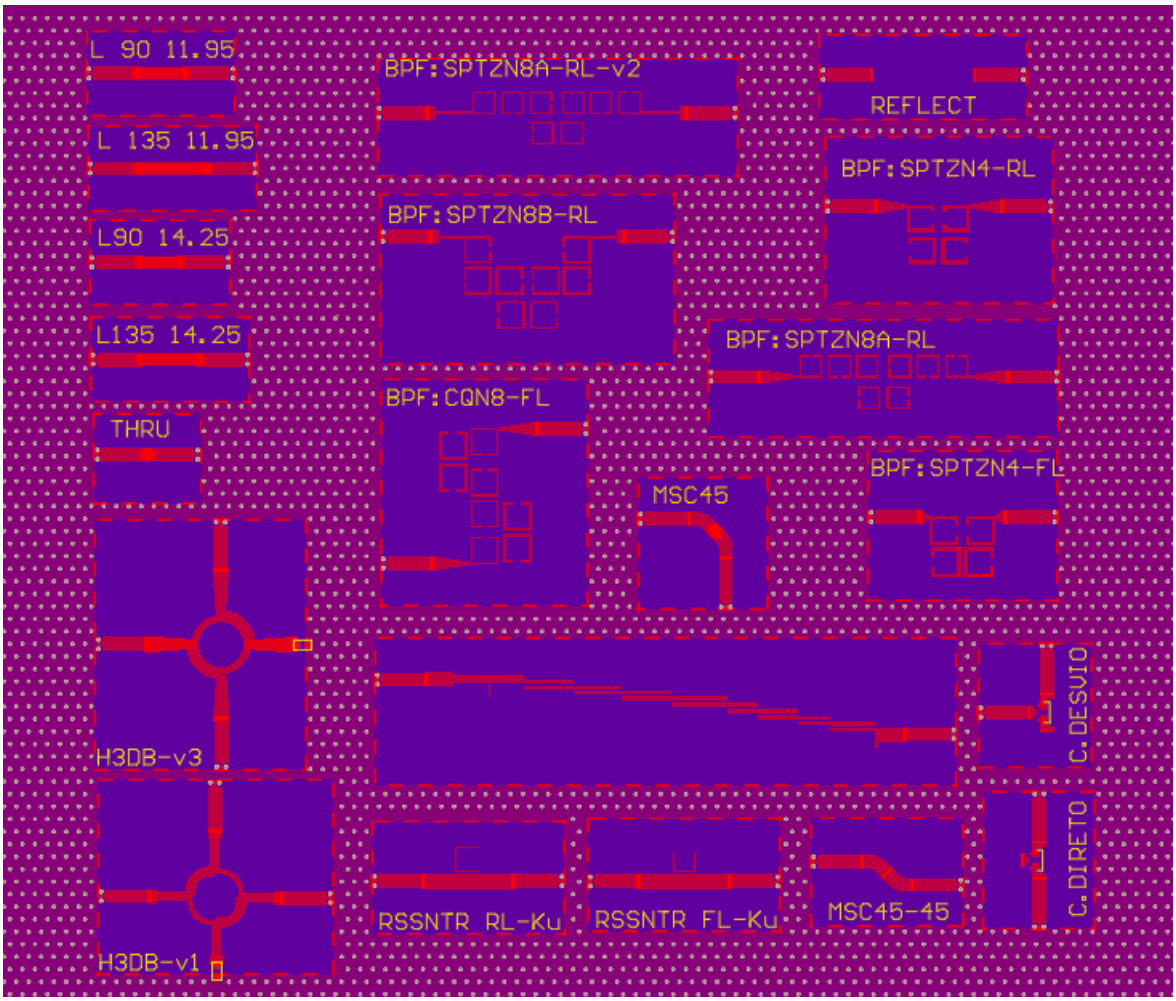

Figure 3.7 – PACBoard top layer layout. Source: Own elaboration.

The mixer generates copies of the input signal centered on f_1 + f_2 and f_1 - f_2, as shown in equation 2.29. Therefore, a bandpass filter is needed between the LNA and the mixer to attenuate the image frequency and not degrade the SNR.

This bandpass filter was designed with an 11.95 GHz center frequency, 500 MHz bandwidth, and a parallel coupling topology of order 8. Figure 3.8 shows the filter layout.

Figure 3.8 – Order 8 Parallel Couple filter with input and output stub for impedance matching. Source: Own elaboration.

The filter width is 48.37 mm and 7.27 mm in height. The filter's first and last transmission line has characteristic impedance lines access 50 Ohms for a center frequency of 11.95 GHz and two stubs for impedance matching. The parallel coupled filter sessions, according to figure 2.15 of subsection 2.12.1.2 shows their dimensions thicknesses (W), widths (L), and spacing (S) in table 3.3.

Table 3.3 – Order 8 Parallel Couple filter dimensions

Section	W [um]	L [um]	S [um]
1	328	4950	167
2	394	4900	111
3	400	4950	200
4	436	5600	103
5	496	3000	103
6	570	4000	104
7	340	3200	105
8	462	4530	103

3.9 POWER PRINTED CIRCUIT BOARD

It was necessary to design a new PCB to power the RF transceiver board with switched power supplies, containing the power supply for the low-noise amplifiers, power amplifiers, mixers, and synthesizers. The power PCB interconnection with the RF PCB will be done using flat cables.

The board has the layer configuration described in table 3.4. The FR-4 was chosen because it is a project with direct currents only and the substrate is cheaper and widely available on the market.

The initial design of the switching power supplies was modified to power the components using a 12 V battery source, requiring 3.5 V sources for the LNA's drain voltages, - 1.5 V for the LNA's V_g voltages, 0.5 V for the mixer V_g, and the synthesizer 3.3 V.

Table 3.4 – PCB Layers.

Layers	Name	Material	Thickness	Dielectric constant
1	*Top Overlay*	*Silk screen*		
2	*Top Solder*	*Solder Resist*	0,01 mm	
3	*Top Layer*	*Copper*	1 oz/ft^2	
4	*Dieletric 1*	FR-4	1,6 mm	4,4
5	*Bottom Layer*	*Cooper*	1 oz/ft^2	
6	*Bottom solder*	*Solder Resist*	0,01 mm	
7	*Bottom Overlay*	*Silk screen*		

For this objective, a load map was made where all the typical and maximum currents of the components are placed to know the total current for the switching power supply project, shown in figures A.1 and B.1.

The Step-Down Converters with part numbers TPS56120x, LM2841X, and TPS5450 generate voltages for four switched sources 7.5 V, 6 V, 5 V, and 3.3 V.

The LDO's LM2664M6/NOPB were used to achieve components and inverters voltages for the LNA gate, as they are negative. The project utilize LMV321 amplifiers to operate as buffers and divide the -3 V voltage at the input. 1 KΩ trimmer was used, which initially rotated to the maximum divides the output voltage to -1.5 V, making it possible to correctly adjust the voltage to carry out the polarization sequence of the low noise amplifiers, manually rotating them.

An adjustable 3.3 V to 2 V source output regulator AP2210K-ADJ was utilized for the mixer gate voltage. Then the op-amp LMV321 function is to buffer and voltage divider. Finally, the trimmer has a regulating mixer bias voltage function.

The linear regulator ADM7150ACPZ-3.3 was chosen to synthesizer power supplies with the 6 V Buck source to reach the required 5 and 3.3 voltages.

The board was manufactured in China with the capabilities described in the table 3.5.

Table 3.5 – Power printed circuit board fabrication capabilities.

Parameter	Value
Minimum space between tracks	6 mil (0.15 mm)
Minimum track width	6 mil (0.15 mm)
Diameter of holes	12 mil (0.3 mm)
Diameter of islands	24 mil (0.6 mm)
Maximum dimensions	100x100 mm

The tests were carried out with a 12 V voltage source, DC electronic load, multimeters, and digital oscilloscope. Appendices C and D show the test plans and their results, containing output voltage measurements, ripple, spike, and harmonic analysis.

3.10 LORA PROJECT

The Lora project implements the reading and treatment of four analog inputs for reading surge voltage, temperature, leakage current, and surge current and permanent regime over 50/60 Hz, 127/220 V electrical power networks in surge protection devices (DPS).

The choice of STM32WL55 is due to the microcontroller being an open platform supporting LoRa and specified considering the reliability, acquisition availability, and product life cycle.

The STM32WL55 microcontroller is a sub-GHz transceiver designed for high-efficiency long-range wireless applications, including the LoRa, so it is possible to transmit and receiver signal in 915 MHz.

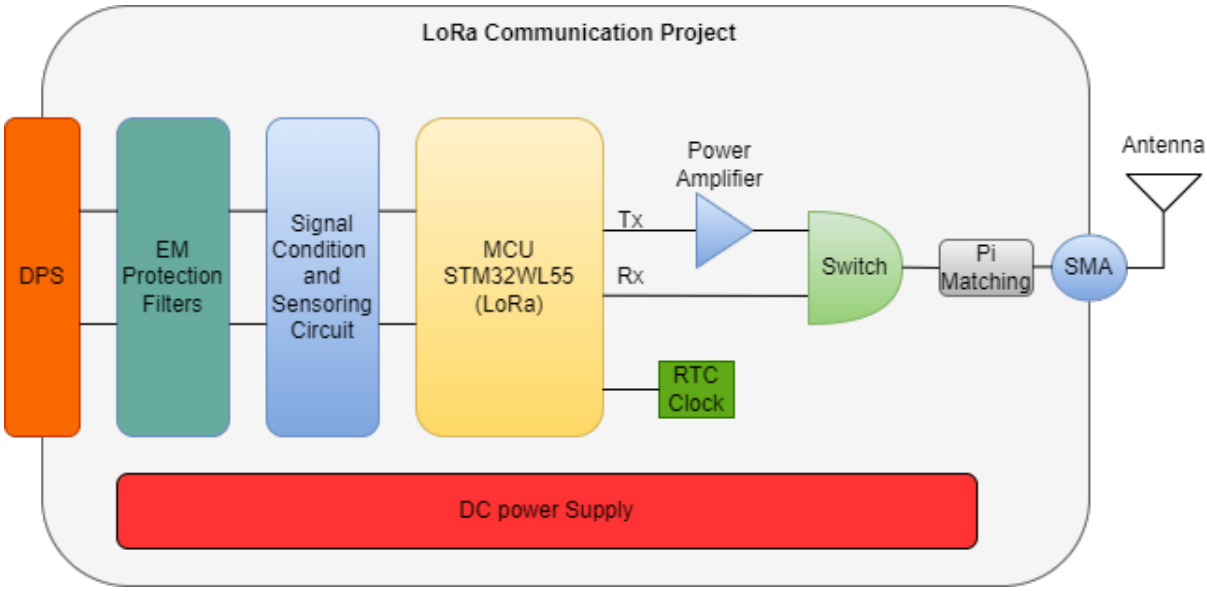

Figure 3.9 – LoRa communication project diagram. Source: Own elaboration.

3.10.1 Receiver

The LNA differential in single-ended needs a circuit with Balun for input transformation and the connection with the antenna. The impedance matching of the LNA with 50 Ohms is Zopt = 60 + j100 Ω for the package UFQFPN48 @915 MHz.

It is possible to have a more stable phase difference of 180 ° when utilizing the balun circuit compared to the circuit shown in the STM document (STMICROELECTRONICS, 2020). In contrast, according to the selected Balun datasheet, there is an additional 1.2 dB of loss.

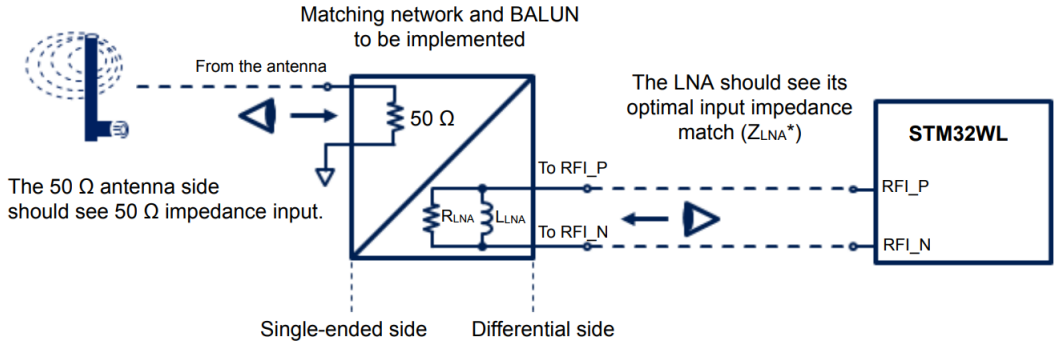

Figure 3.10 – Matching network and BALUN characteristics to be implemented with lumped components on PCB. Source: Reproduced from (STMICROELECTRONICS, 2020).

3.10.2 Transmitter

For a transmitter it is necessary to filter the signal due to the harmonics generated by it and project the impedance matching. Figure 3.11 shows the circuit according to the application note.

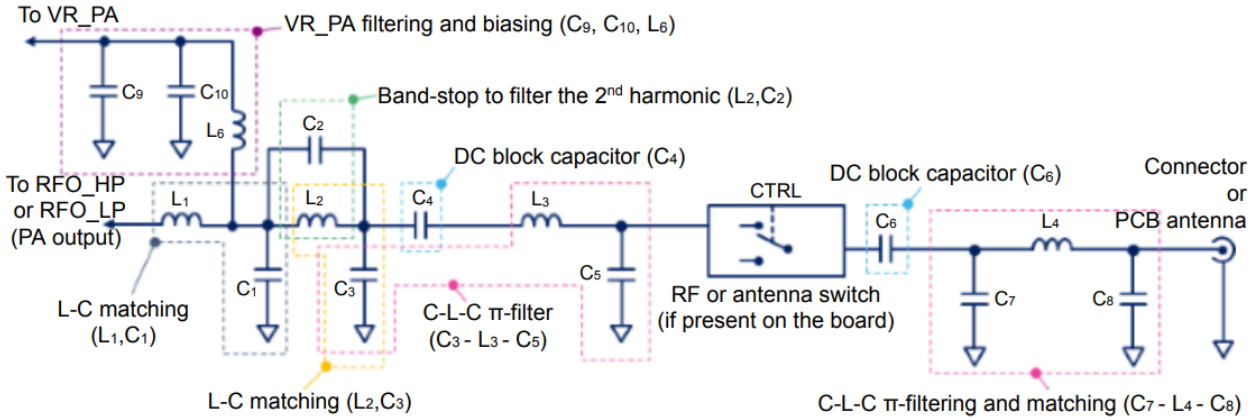

Figure 3.11 – Description of each part of the typical Tx application network. Source: Reproduced from (STMICROELECTRONICS, 2020).

Impedance Matching was designed for the package UFQFPN48, 22 dBm @915 MHz, VDDMCU = 3.3 V. Zopt= 10.71 + j1.85, 113.86 mA 21.5 dBm. Filter Band stop designed for 915 MHz and low pass filter for 1.2 GHz, all selected components are SMD 0603 available on the market.

3.11 HOMOLOGATION

In order to obtain approval and be certified, the transceiver product is designed to meet pre-established standards. Therefore, this product is part of the Category II telecommunica-

tion products classification (ANATEL, 2000). This classification fits the standards from the International Electrotechnical Commission to be followed listed below (ANATEL, 2018b).

- IEC 61000-4-2 (*Testing and measurement techniques – Electrostatic discharge immunity test*);
- IEC 61000-4-3 (*Radiated, radio-frequency, electromagnetic field immunity test*);
- IEC 61000-4-4 (*Electrical fast transient/burst immunity test)*;
- IEC 61000-4-6 (*Immunity to conducted disturbances, induced by radio-frequency fields*).

4 RESULTS AND DISCUSSION

The RF front-end receiver presentation includes LNA, mixer, filters, and RF LoRa measurement results.

4.1 RF FRONT END RECEIVER

The transceiver was designed so that it was possible to test each block individually with SMA connectors. As it is a project with more people involved, the printed circuit board contains the RFFE receiver and transmitter.

The complete Rx path was measured to evaluate the behavior of the RF system up to the IF filter output. The test simulates receiving a signal at the 11.95 GHz center frequency of Ku-band reception and converts it to an intermediate system frequency (3 GHz), filtering and amplifying the signal.

Agilent E8251A signal generator was configured in continuous wave (CW) operation mode, frequency 11.95 GHz, -111 dBm output power and connected at diplexer, the synthesizer generated frequency 8.95 GHz, 0 dBm output power. The spectrum analyzer was configured central frequency to 3 GHz, 10 MHz span, 1 MHz bandwidth and measured at IF filter output, according to table 5.1.

Table 4.1 – Power Measurement in Spectrum Analyser in the receiver system varying the input power.

Pin [dBm]	Pout [dBm]	Gain [dB]
-41.0	-13.9	27.1
-51.0	-22.2	28.8
-61.0	-31.7	29.3
-81.0	-41.7	39.3
-91.0	-51.5	39.5
-111.1	-71.0	40.1

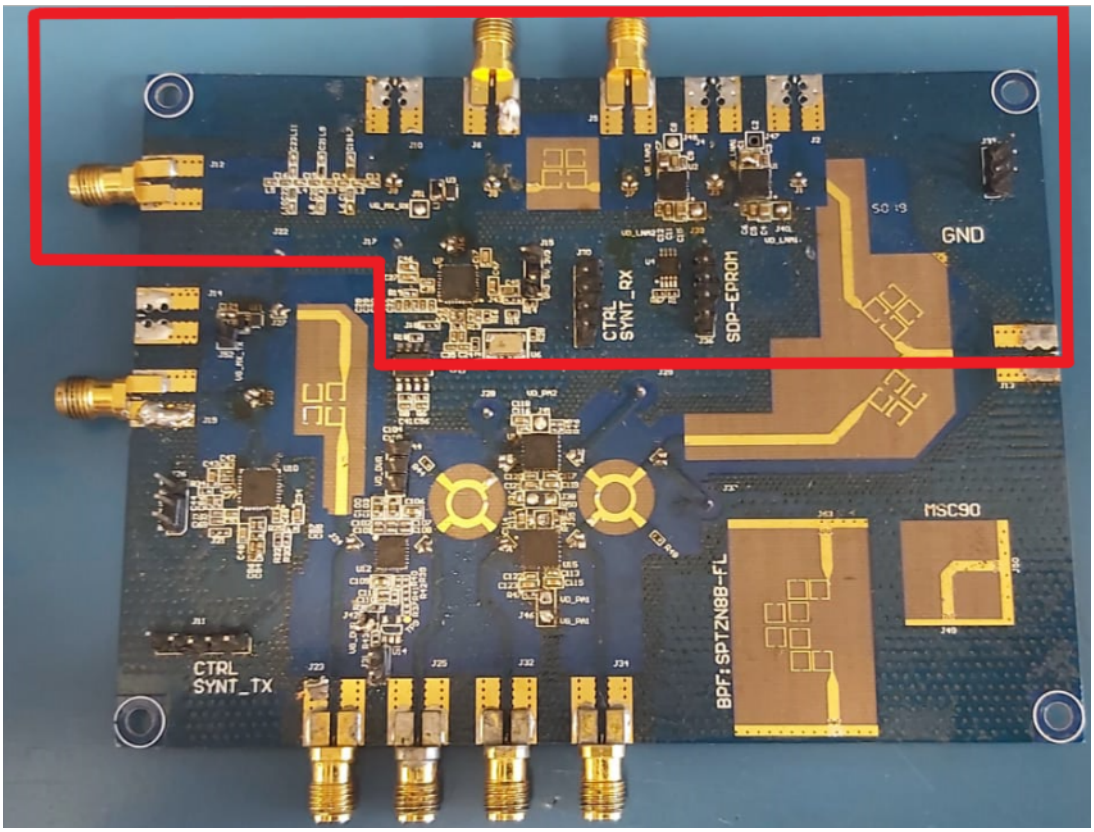

Figure 4.1 – RFFE transceiver PCB manufacturer by Lauquen, the red marking shows the receiver circuit design in this project. Source: Own elaboration.

4.2 SYNTHESIZER

The ADF5355 synthesizer component is controlled via a serial bus by an auxiliary board (SDP-S). The spectrum analyzer configures 8.95 GHz center frequency, 5 MHz span, 100 KHz bandwidth, and reference level at 0 dBm. In addition, the ADI software configures to disable the RFoutA output and enable the RFoutB output, 50 MHz in reference frequency and the VCO out 4475 MHz, this being half of the operating frequency to avoid spurious.

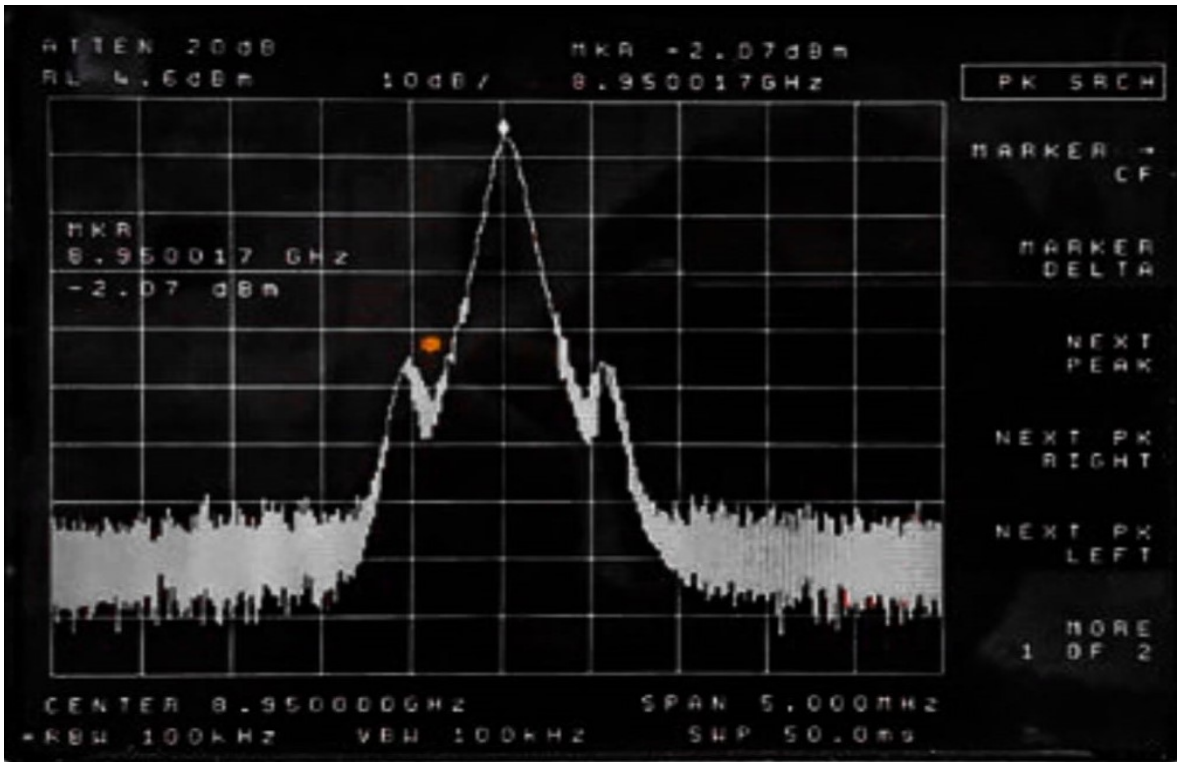

Figure 4.2 – Synthesizer measurement from the spectrum analyzer. Center frequency 8.95 GHz and power -2 dBm. Source: Reproduced from (ANDRADE; BARBOSA; RONDINEAU, 2020).

4.3 LNA

In the prototype, it was chosen the commercial component QPA2609 to transceiver integration. LNA composed of GaAs FET transistors was designed to optimize and lower product costs.

EM simulation was done in the Keysight Advanced Design System (ADS) with Momentum simulation tools. First, a DC analysis was done and the optimum NF and gain performance were achieved with Vd =2 V, and the drain current 10 mA (ANDRADE; BARBOSA; RONDINEAU, 2020).

The stability analyses simulated in ADS show that transistors are stable over the frequency bandwidth 11.7-12.2 GHz as seen in the figure 4.3. K-stability factor and μ-factor are respected according to the equations 2.20 and 2.21 (ANDRADE; BARBOSA; RONDINEAU, 2020).

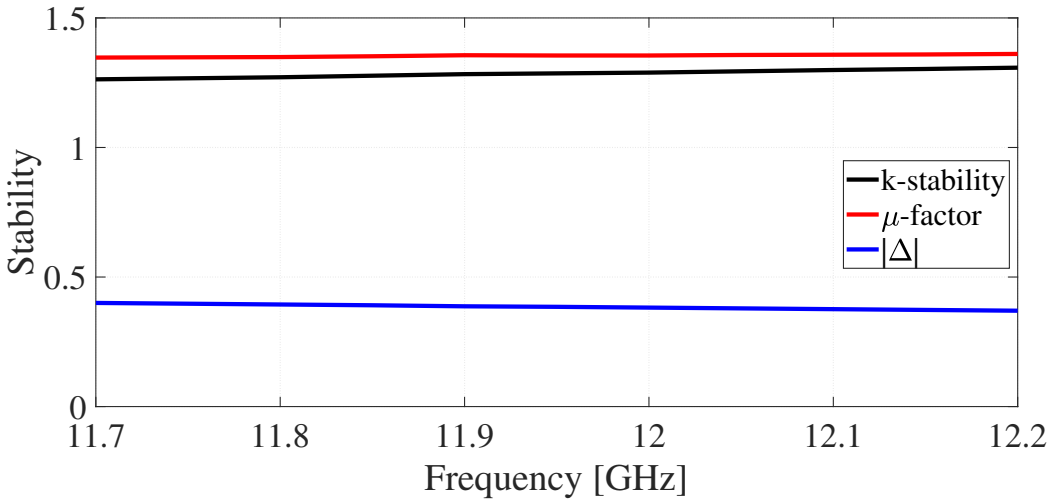

Figure 4.3 – LNA stability simulation in ADS. The simulation results show that LNA is stable in all bandwidth. Source: Reproduced from (ANDRADE; BARBOSA; RONDINEAU, 2020).

Only in the first version with a single stage amplifier was it possible to test and obtain results because, in the version with two stages, the current of the transistors rose too much due to the LNA oscillation. However, a metallic cover was added around the LNA to add a resonant cavity effect, unsuccessfully

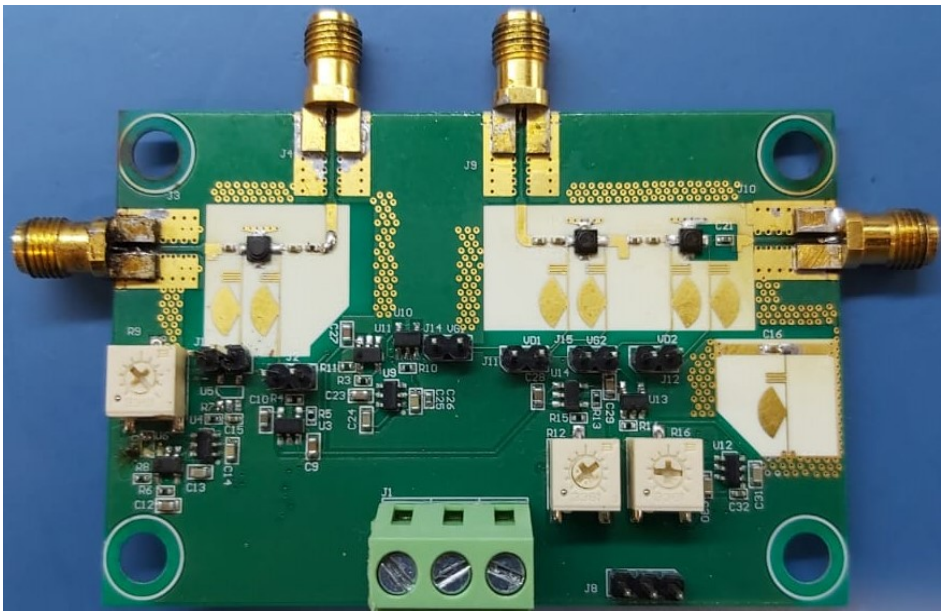

Figure 4.4 – LNA printed circuit board. Source: Reproduced from (ANDRADE; BARBOSA; RONDINEAU, 2020).

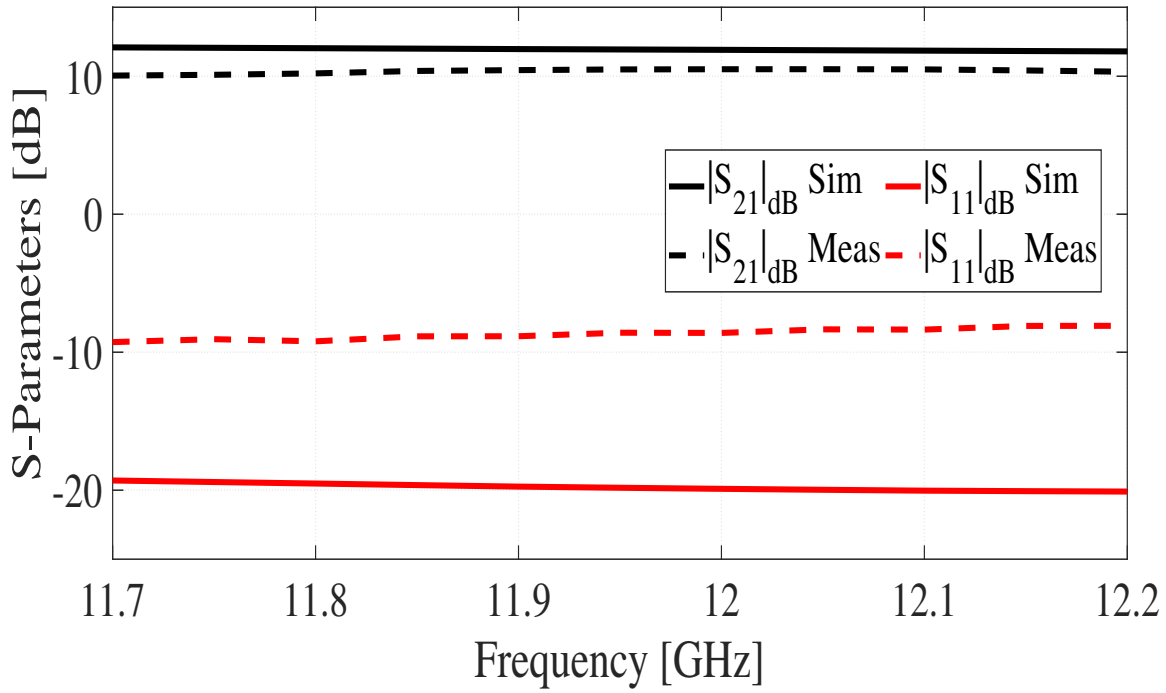

Figure 4.5 – LNA prototype scattering parameters simulated and measured results. Source: Reproduced from (ANDRADE; BARBOSA; RONDINEAU, 2020).

4.4 MIXER

The measurement was made with a spectrum analyzer, and two signal generators applied the LO and RF input signals. At the LO input, 2 dBm was already applied considering the cable loss, and at the RF input -15 dBm. Therefore, all losses due to the cables used were considered in measuring the gain conversion.

The three measured diodes presented the following conversion gain results:

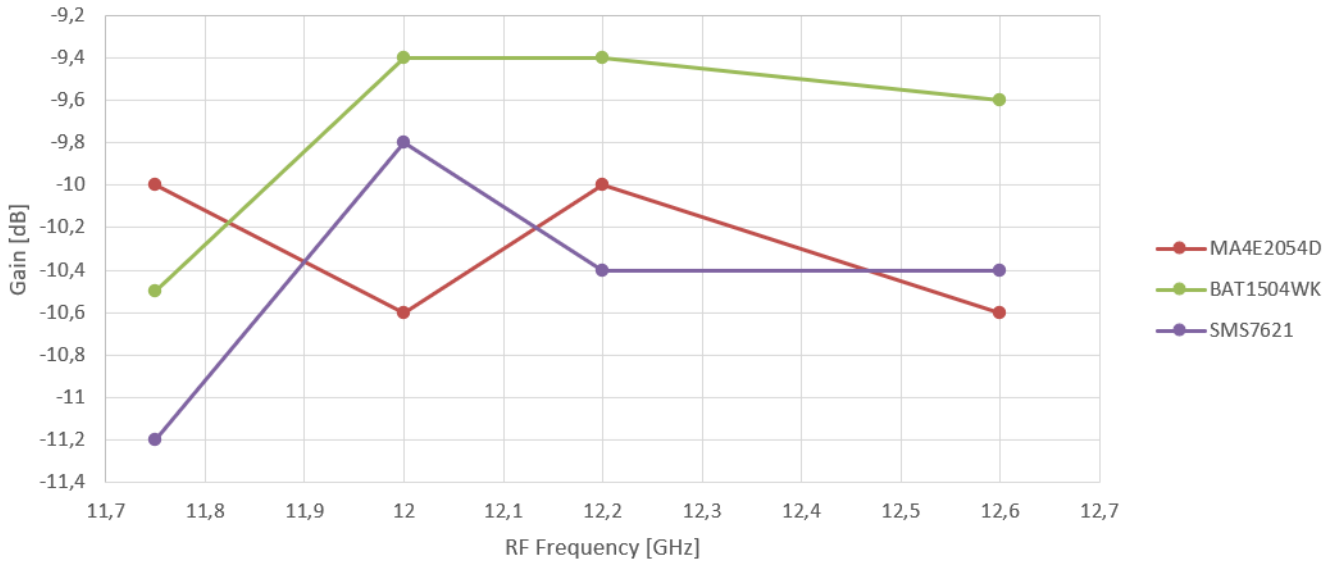

Figure 4.6 – Conversion gain mixer measurement along the frequency. Source: Own elaboration.

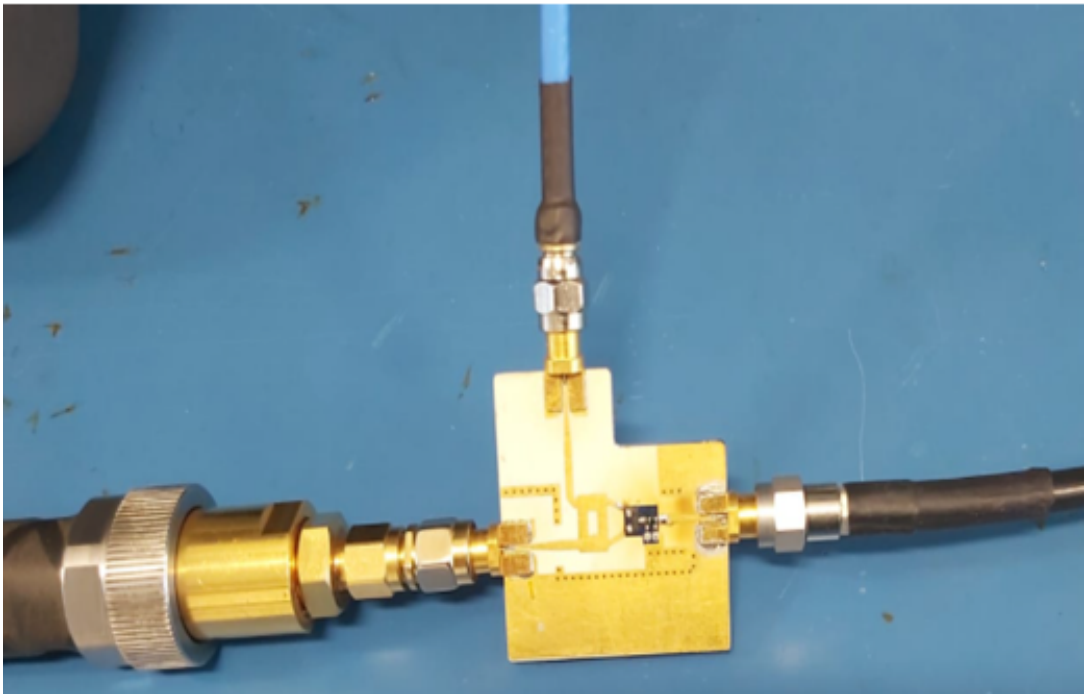

Figure 4.7 – Mixer measurement. Source: Own elaboration.

4.5 POWER PRINTED CIRCUIT BOARD

The manufactured power board has 94.72 mm X 96.85 mm dimensions. Figures 4.8 and 4.9 show the top and bottom views. Table 4.2 shows their results, and the test plans are in appendices C and D.

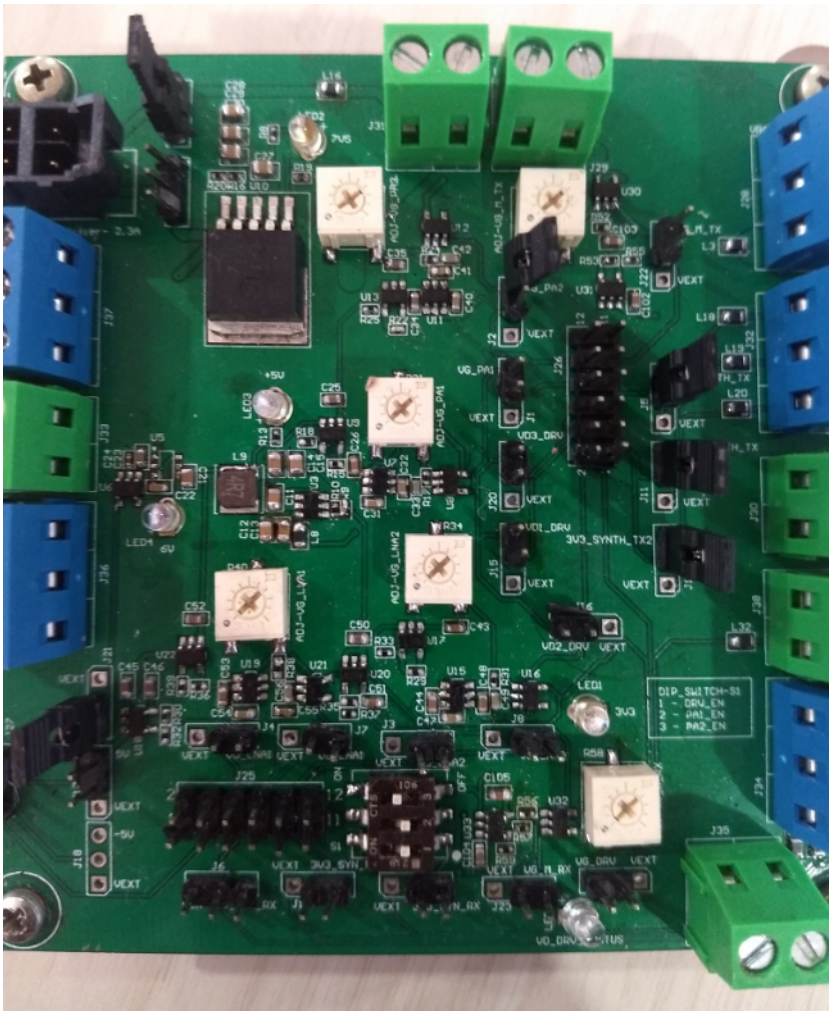

Figure 4.8 – Power printed circuit board top layer view. Source: Own elaboration.

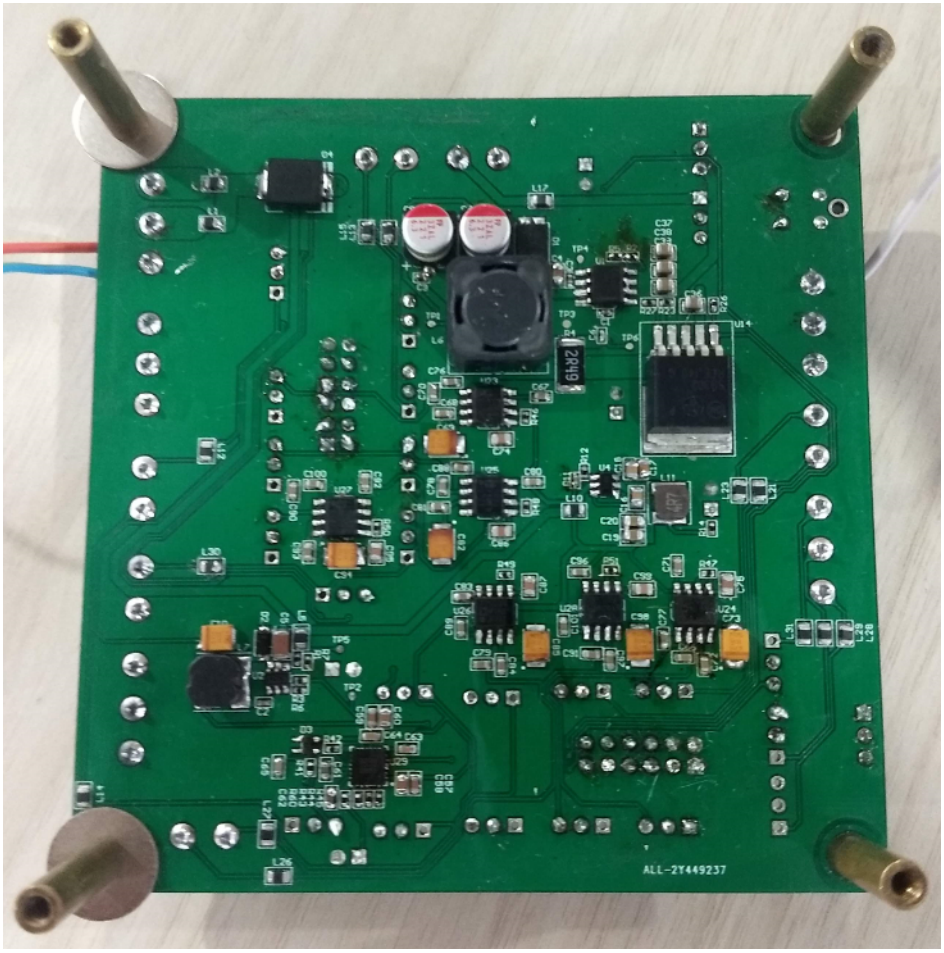

Figure 4.9 – Power printed circuit board bottom layer view. Source: Own elaboration.

Table 4.2 – Power printed circuit board results.

Parameter	Expected Voltage (V)	Measured Voltage (V)	Test current (mA)	Ripple (mV)	Spike (mV)
LNA (Vd)	3.5	3.48	120	75.1	109.1
LNA (Vg)	-1.5	-1.51	120	67.7	148.0
Sint 5V	5.0	4.98	195.6	46.0	195.6
Sint 3.3V	3.3	3.29	170	51.1	140.3
Mixer (Vg)	0.5	0.5	N/A	186.8	162.7

4.6 PASSIVE ELEMENTS

The printed circuit board contains the following passive elements, filter, diplexer, 50 Ω line, TRL lines, and 3 dB hybrid coupler, where the probe station measures all elements. However, only the elements influencing the reception chain will be presented.

A Vector network analyzer (VNA) does the measurement with TRL calibration inserted.

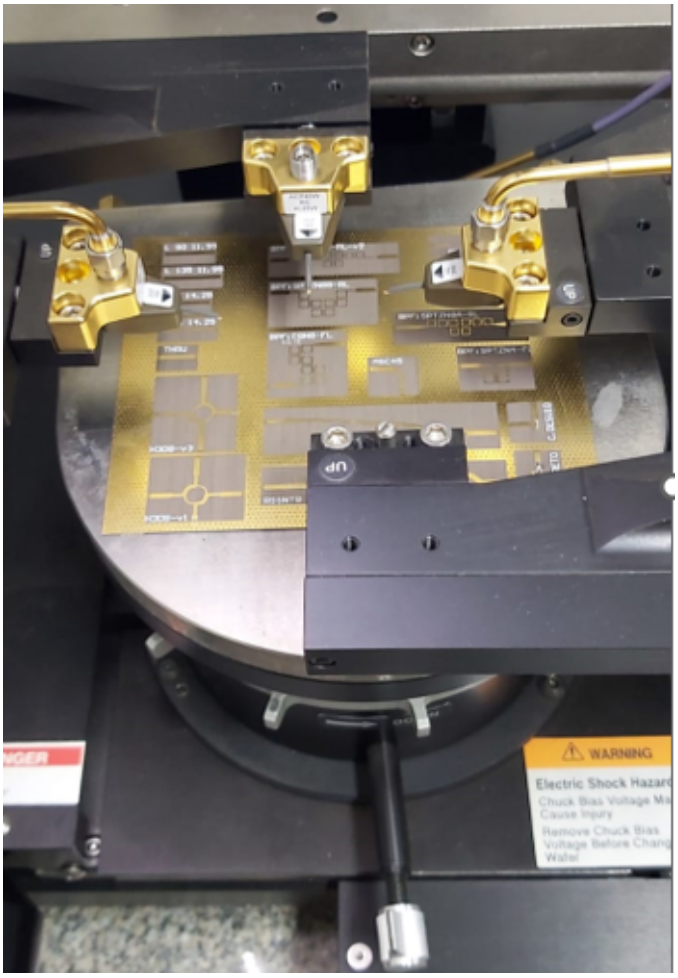

Figure 4.10 – Cascade microwave probe station measurements in passive components present in printed circuit board. Source: Own elaboration.

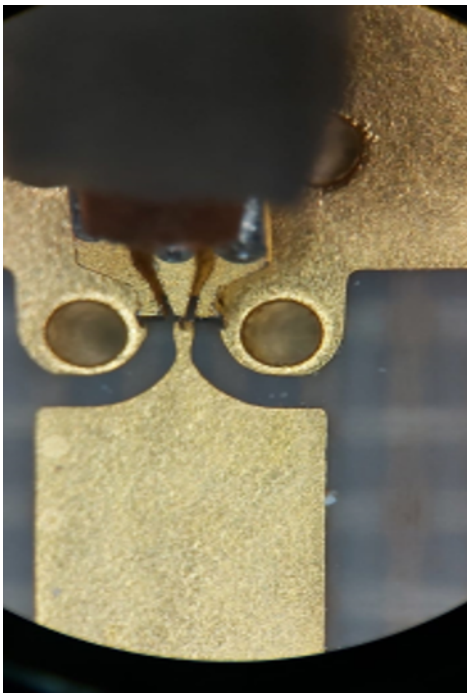

Figure 4.11 – ACP-GCG-200 connection in PACBoard. Source: Own elaboration.

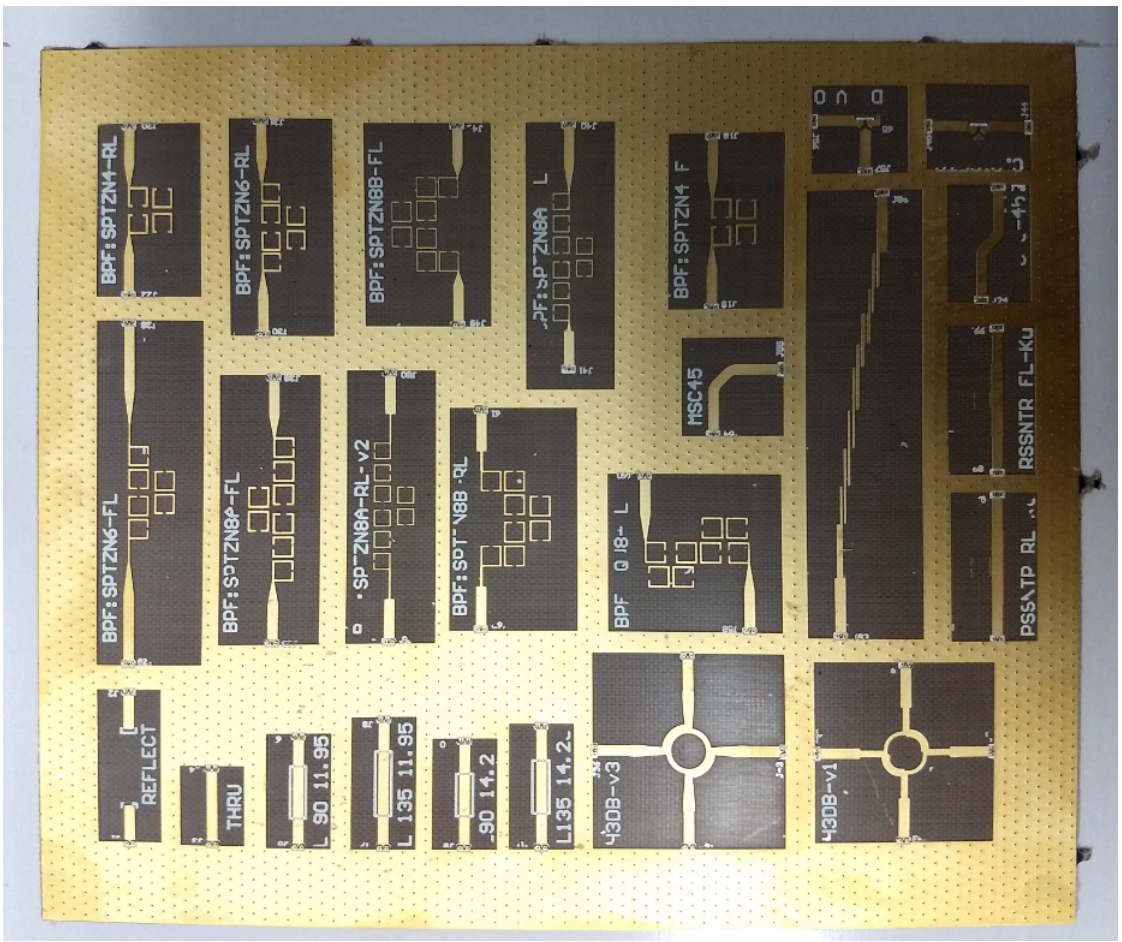

Figure 4.12 – Passive elements in PCB upper view. Source: Own elaboration.

Figure 4.13 – Order 8 Parallel Couple filter with input and output stub for impedance matching. Source: Own elaboration.

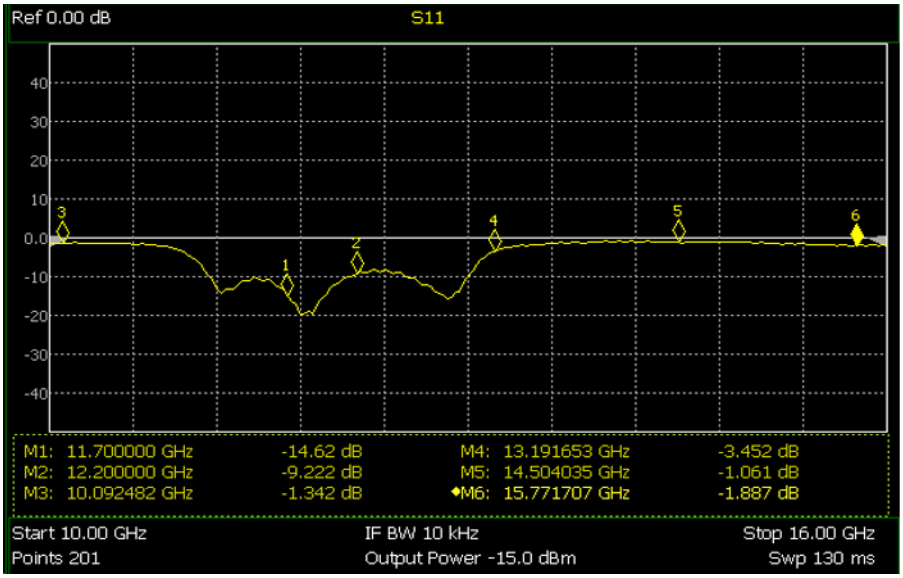

Figure 4.14 – Order 8 Parallel Couple filter S_{11}. Source: Own elaboration.

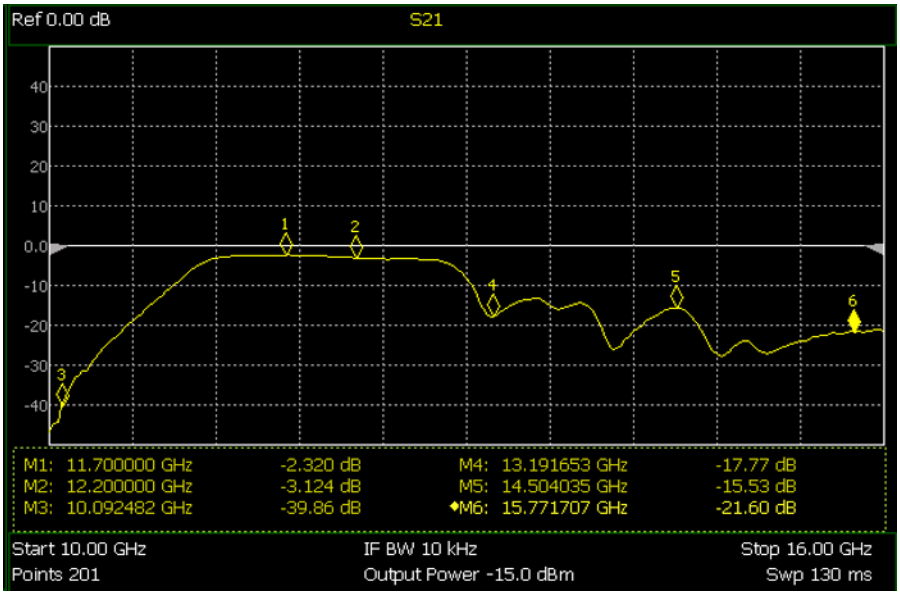

Figure 4.15 – Order 8 Parallel Couple filter S_{21}. Source: Own elaboration.

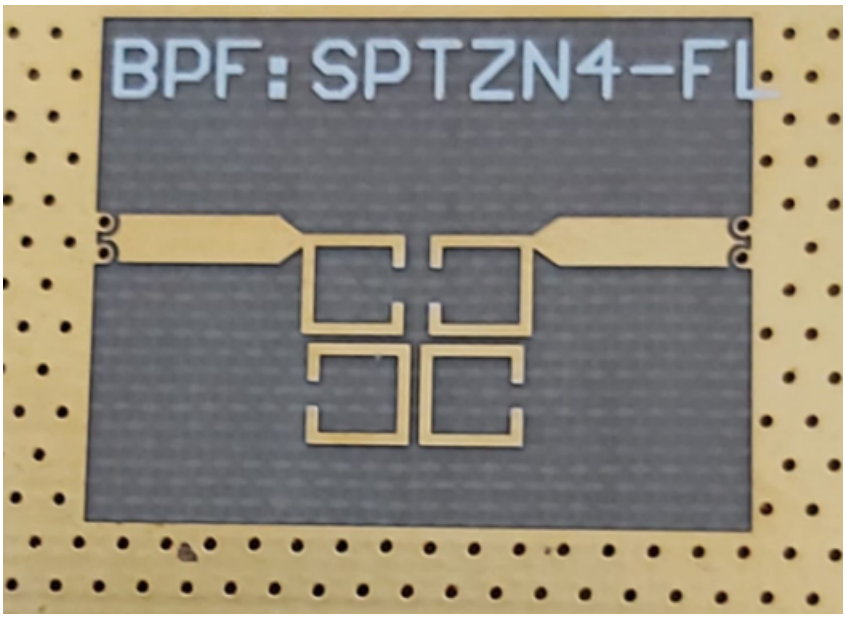

Figure 4.16 – Order 4 Coupled Open-Loop Resonator filter. Source: (SANTANA; BARBOSA; RONDINEAU, 2020)

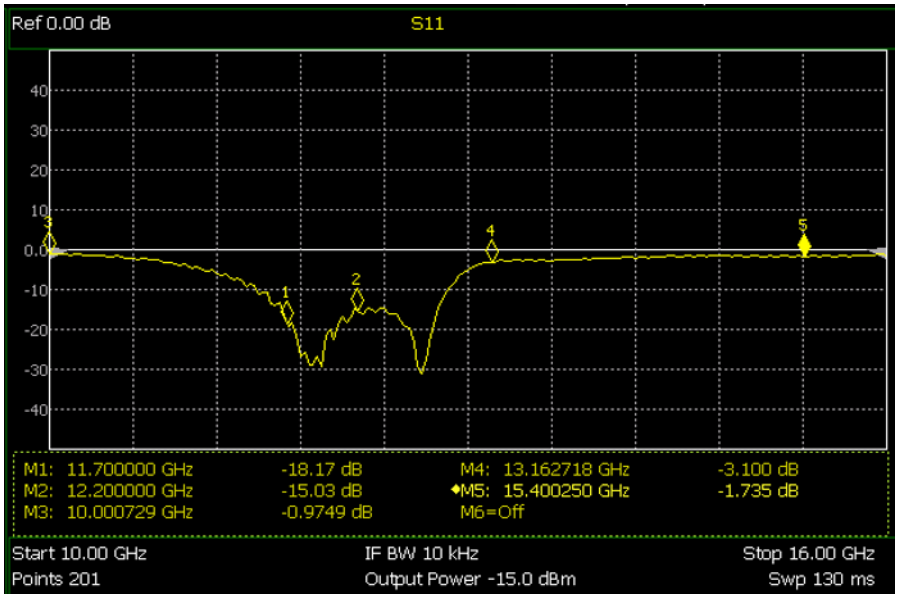

Figure 4.17 – Order 4 Coupled Open-Loop Resonator filter S_{11}. Source: Own elaboration.

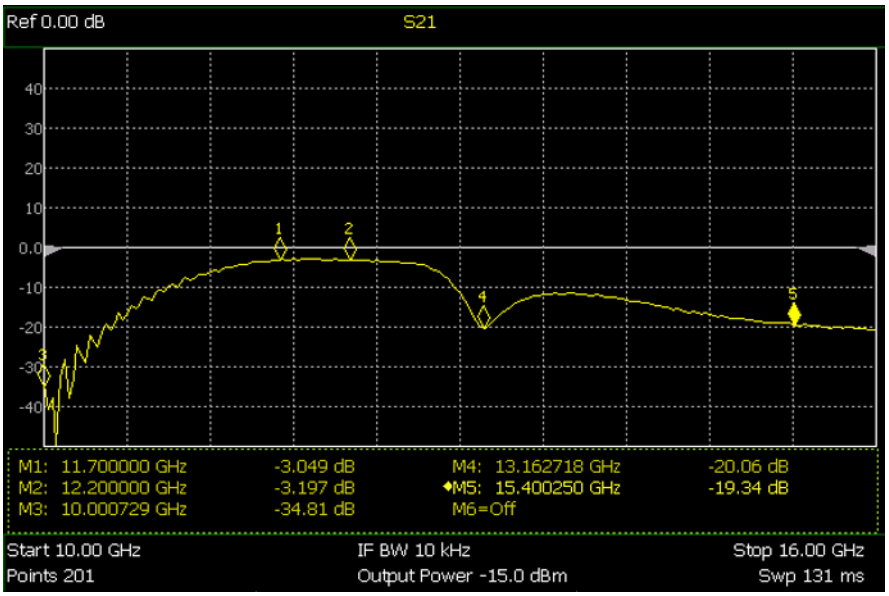

Figure 4.18 – Order 4 Coupled Open-Loop Resonator filter S_{21}. Source: Own elaboration.

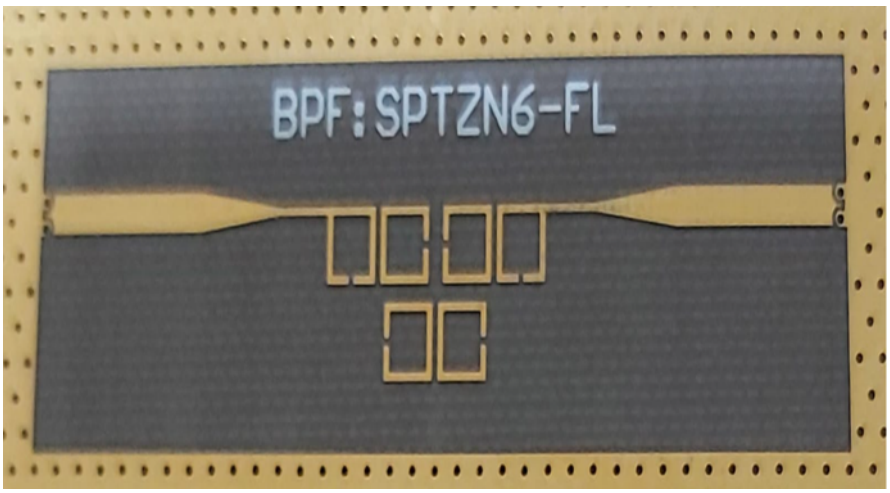

Figure 4.19 – Order 6 Coupled Open-Loop Resonator filter. Source: Own elaboration.

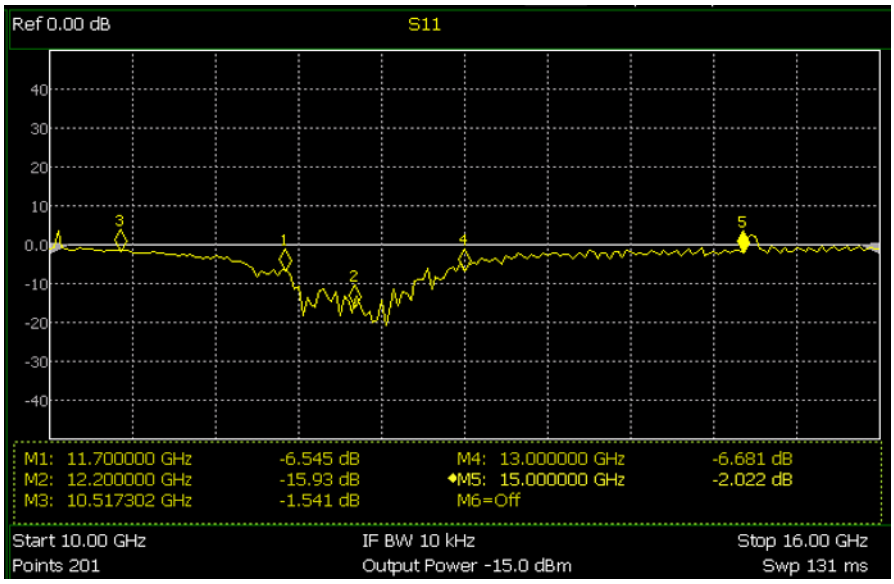

Figure 4.20 – Order 6 Coupled Open-Loop Resonator filter S_{11}. Source: Own elaboration.

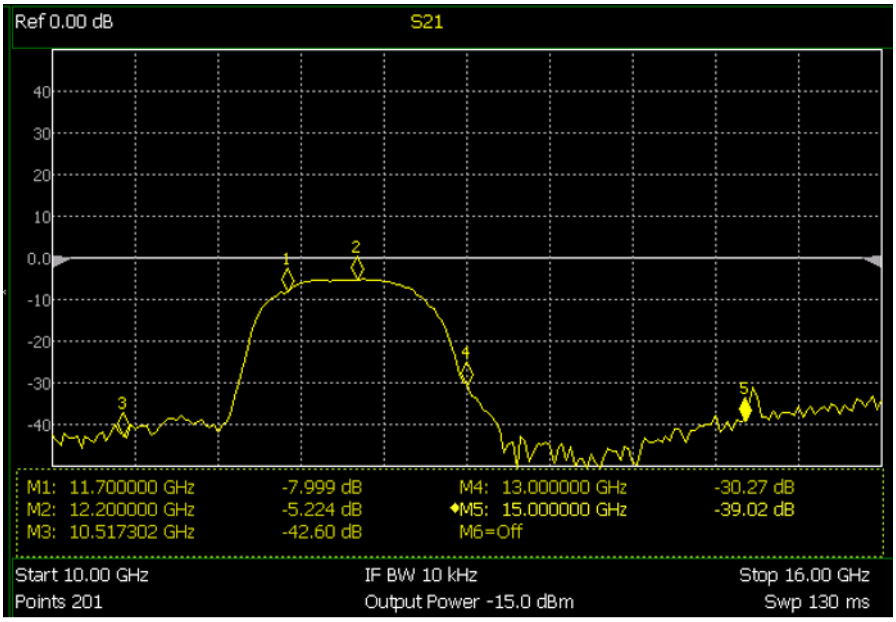

Figure 4.21 – Order 6 Coupled Open-Loop Resonator filter S_{21}. Source: Own elaboration.

Notably, increasing the filter order in coupled open-loop topology increases losses and rejection at other frequencies. Is it possible to reduce the losses in OSP finish.

4.7 LORA PROJECT

4.7.1 Receiver

Impedance matching was done in the software ADS, with the following electromagnetic simulation results for the layout already included in the PCB, according to figure 3.10, using the snp file Balun, capacitor and inductor components SMD 0603, provided by the manufacturers.

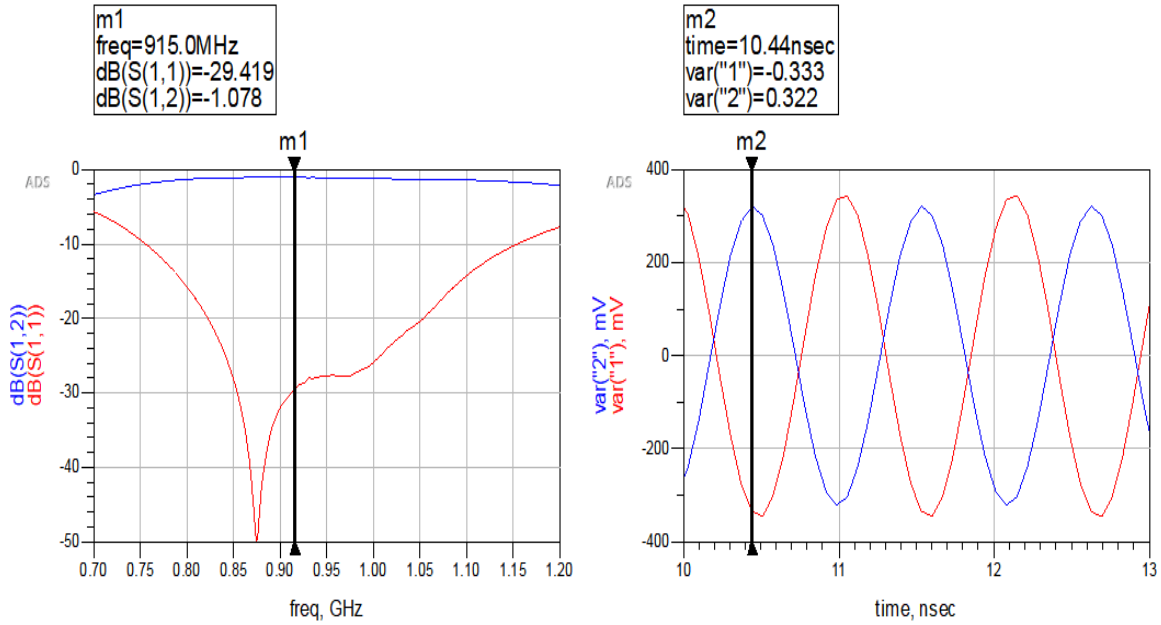

Figure 4.22 – Reflection coefficient, insertion loss and transient analysis of the LNA differential output. Source: Own elaboration.

4.7.2 Transmitter

In figure 4.23, it is possible to observe that in the second harmonic at 1.83 GHz there is an attenuation of 30 dB and at the frequency of interest, the circuit is matched to the PA to 50 Ohms to be possible for the connection with the antenna with maximum transmitted power.

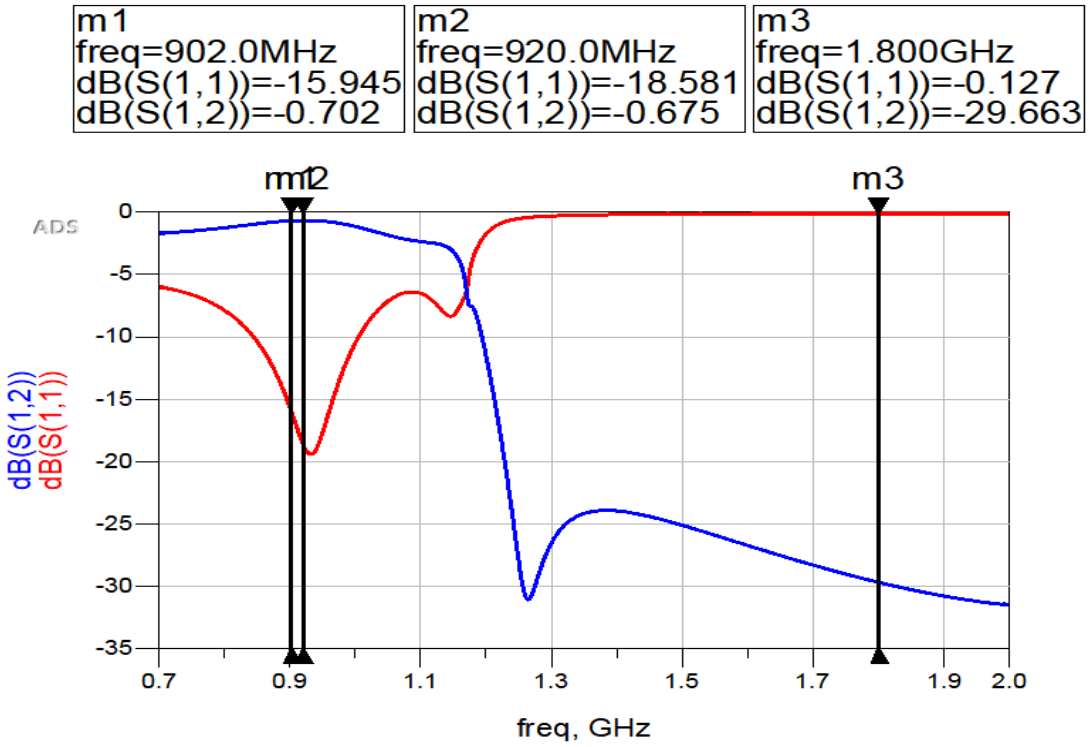

Figure 4.23 – Reflection coefficient (S_{11}) and insertion loss (S_{21}). Source: Own elaboration.

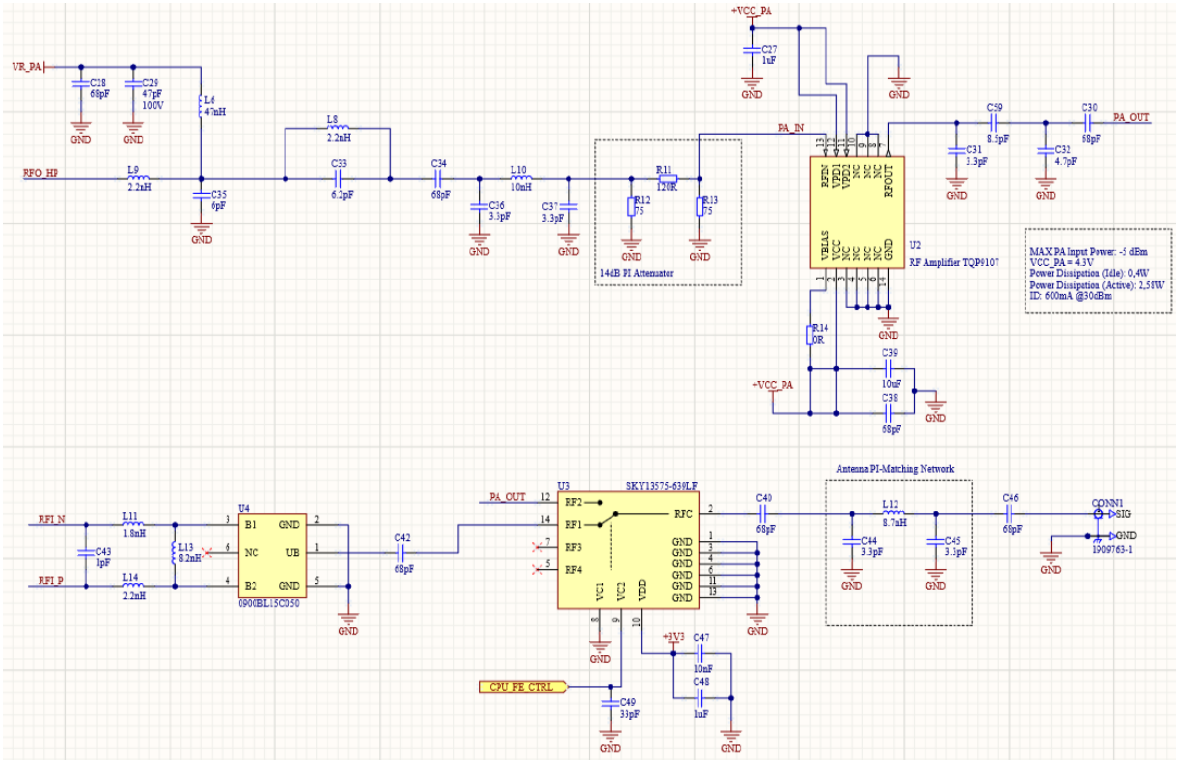

Figure 4.24 – LoRa schematic receiver and transmitter with power amplifier. Source: Own elaboration.

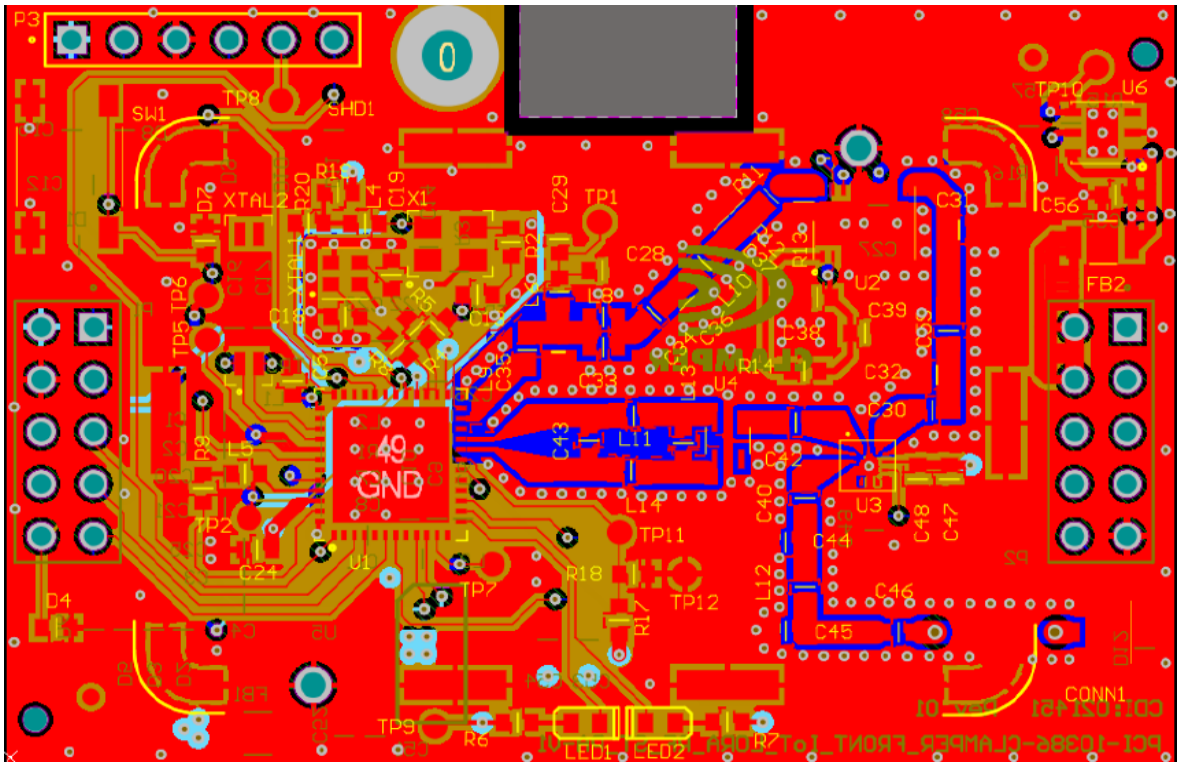

Figure 4.25 – Layout RF transmitter and receiver. Source: Own elaboration.

The first measurements were not giving the expected result, so it was decided to connect an RF probe and measure the signal at the input of the power amplifier, as shown in figure 4.26.

After discovering problems in the board assembly and carrying out the correction, it was possible to obtain 5.7 dBm according to the figure 4.27, adding the loss of the pi-attenuator of 14 dBm with the cable loss of 1.2 dB, reaching the STM32 projected 22 dBm.

The spectrum analyzer in figure 4.27 had problems and shifted the frequency by 1 MHz. The indication is that this equipment was not calibrated. When changing the equipment and measuring the power amplifier's output, the correct frequency is at 915 MHz.

In figure 4.28, we have the LoRa PCB output power measurement with 30.3 dBm

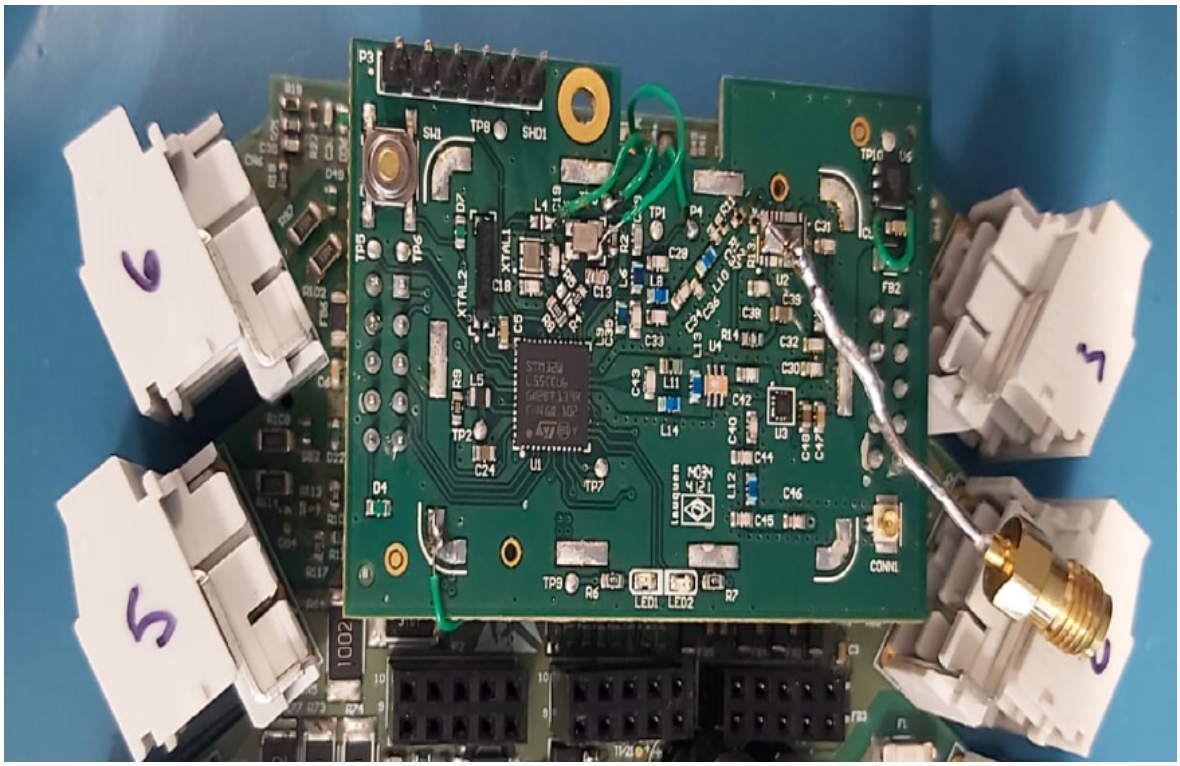

Figure 4.26 – Fabricated LoRa PCB. Source: Own elaboration.

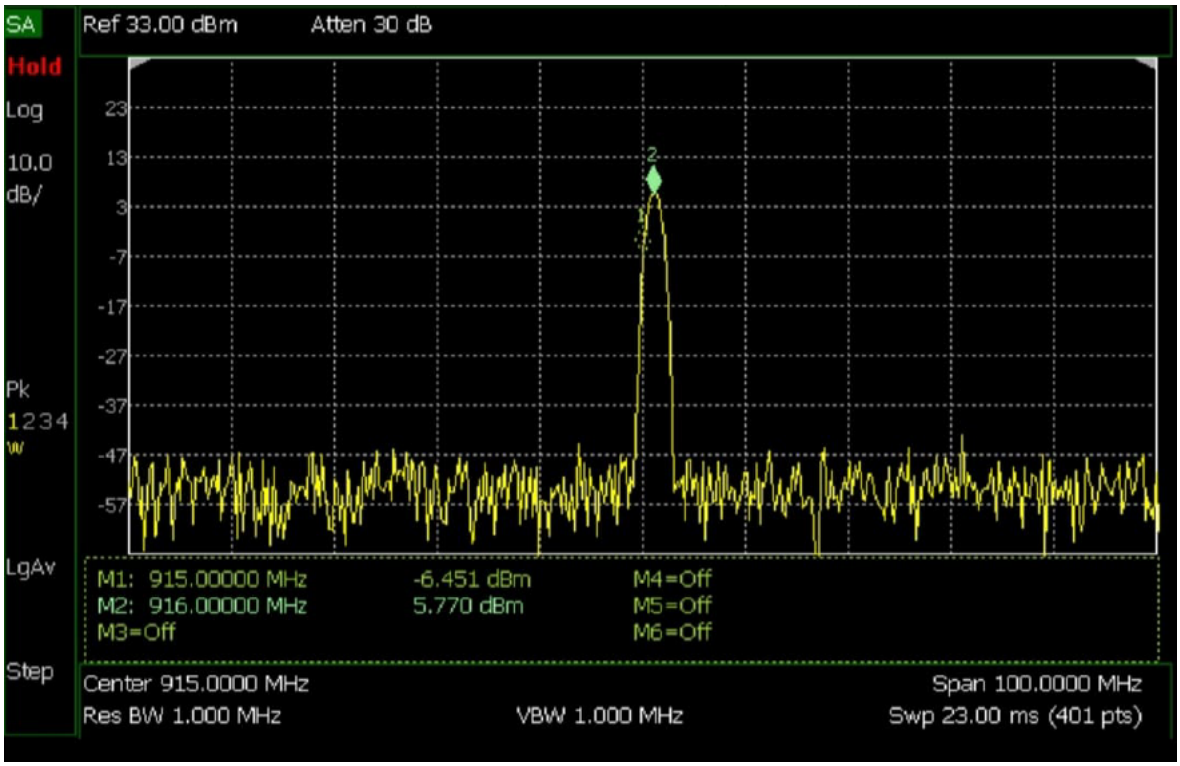

Figure 4.27 – Power measurement at the power amplifier input. Source: Own elaboration.

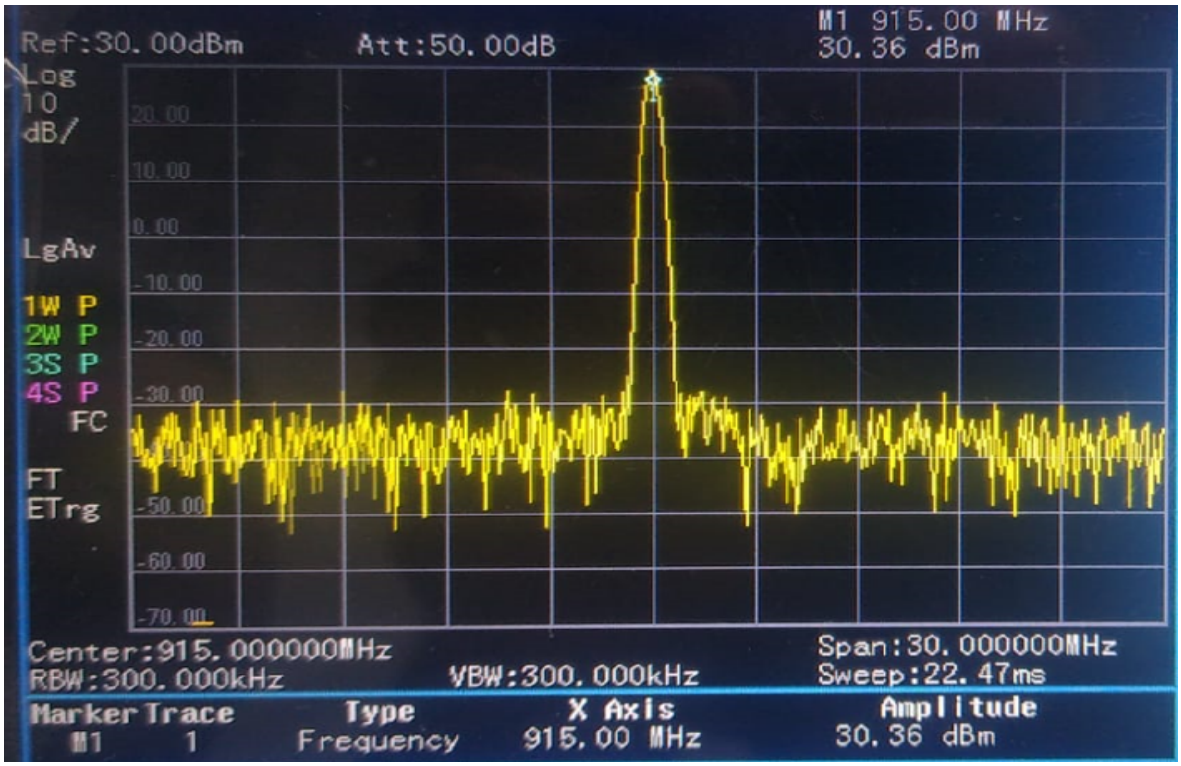

Figure 4.28 – Power measurement at the power amplifier output. Source: Own elaboration.

5 CONCLUSIONS AND FUTURE WORKS

Description of the conclusion of the work, presenting the final considerations, limitations of the work and some topics that can be addressed in future works.

This work was due to projects funded by companies, going beyond a research project, and emphasizing a product cycle methodology in applied engineering. The project's main focus was measurement results obtained to gather the maximum information and develop an optimized entire solution.

5.1 RFFE RECEIVER

In theory, adding the losses associated with the diplexer 3 dB, an LNA's cascade gain of 52 dB, filter loss of 3 dB, mixer loss of 8 dB, and filter loss in IF 0.5 dB, the reception gain must be at 37.5 dB. However, reaching up to 40.1 dB with an input power of -111.1 dBm was possible. The synthesizer worked as expected, generating a frequency of 8.95 GHz with a power of -2 dBm.

Table 5.1 – Comparison of expected and measured receiver output power.

Pin [dBm]	Pout expected [dBm]	Pout measured [dBm]
-61.0	-23.5	-31.7
-81.0	-43.5	-41.7
-91.0	-53.5	-51.5
-111.1	-73.5	-71.0

5.2 LNA

Only in the first version with a single stage was it possible to test and obtain results because the current of the transistors rose too much due to the LNA oscillation in the version with two stages.

The main aim of the LNA was that the two stages project in the version with transistors obtained a gain close to the commercial component QPA2609 of 26 dB. Being the first stage prioritized the noise figure reaching a gain of 11 dB, and the second stage prioritized the maximum gain of the transistor in 14 dB, matching the LNA integrated circuit present in the transceiver.

5.3 MIXER

The balanced mixer was designed to achieve a similar performance to the commercial mixer chosen to the transceiver with a conversion loss of 8 dB. After testing three different diodes, the better diode was the BAT1504WK, reaching a conversion loss of 9.6 dB.

5.4 POWER PRINTED CIRCUIT BOARD

The power supply board presented relevant results for its functioning, as they were within the power specifications of the respective elements of the RF board, and all switched power supplies worked correctly.

5.5 PASSIVE ELEMENTS

The passive elements have been tested and optimized for the Ku band reception from 11.7 GHz to 12.2 GHz. It was observed that increasing the filter order in coupled open-loop topology increases losses and rejection at other frequencies.

5.6 LORA PROJECT

It was possible to obtain the expected result in transmission of 30 dBm output power to the antenna. However, at the receiver, it was only possible to test the data reception from the software using another LoRa device at a distance of 1 Km.

5.7 FUTURE WORKS

A future work suggested is to design the IF chain for the connection with the RFFE transceiver, the modification of the commercial components LNA and mixer by the designed components, and the communication with the microcontroller.

In the LNA, work is still necessary to stabilize the project with the two-stage cascade to reach the requirements. The possible increase of a resistor in the second stage and some optimizations will make the LNA not oscillate.

BIBLIOGRAPHY

ABIDI, A. A. Direct conversion radio transceiver for digital communications. *IEEE*, v. 30, 1995.

ADAM, S. F. *Microwave Theory and Application*. 2. ed. [S.l.]: Prentice Hall, 1969.

ANATEL. *Regulamento para certificação e homologação de produtos para telecomunicações*. [S.l.], 2000. Disponível em: <http://pesquisa.in.gov.br/imprensa/jsp/visualiza/index.jsp?jornal=1&pagina=50&data=05/12/2000>.

ANATEL. *Plano de atribuição, destinação e distribuição de frequências no Brasil*. [S.l.], 2018. Disponível em: <http://www.anatel.gov.br/Portal/verificaDocumentos/documento.asp?numeroPublicacao=347196>.

ANATEL. *Requisitos técnicos e procedimentos de ensaios aplicáveis à certificação de produtos para telecomunicação de categoria II*. [S.l.], 2018. Disponível em: <https://sei.anatel.gov.br/sei/modulos/pesquisa/md_pesq_documento_consulta_externa.php?eEP-wqk1skrd8hSlk5Z3rN4EVg9uLJqrLYJw_9INcO40DYaeeyem-NQDAV_pnveKWqAHtqWyxyxOnFlatofywemJyllZ-keItLxCmEZNkXTSV4X4UrVT9YReFc9A9reH>.

ANDRADE, G. F. D.; BARBOSA, E. V. S.; RONDINEAU, S. R. Rf front-end receiver for vehicular satellite communications and lna gaas fet design in ku-band. In: *2020 Workshop on Communication Networks and Power Systems (WCNPS)*. [S.l.: s.n.], 2020. p. 1–6.

CHIANG, Y.-C.; HSIEH, W.-L.; CHUNG, M.-A. A method of synthesizing microwave bandpass filters constructed with symmetrical or asymmetrical compact microstrip resonators. *IEEE Transactions on Microwave Theory and Techniques*, v. 54, n. 11, p. 3947–3953, 2006.

Edwards, M. L.; Sinsky, J. H. A new criterion for linear 2-port stability using a single geometrically derived parameter. *IEEE Transactions on Microwave Theory and Techniques*, v. 40, n. 12, p. 2303–2311, 1992.

ELBERT, B. R. *Introduction to Satellite Communication*. 2. ed. [S.l.]: Artech House, 2008.

EMBRATEL. *Características do satélite Star One C1 para projeto técnico de redes de comunicações digitais em banda Ku*. [S.l.], 2017. Disponível em: <http://www.starone.com.br/internas/biblioteca/CTS/CTS-ENGSIS-17003-00(C1_Banda_Ku).pdf>.

FERKO, N. et al. Balloon based low altitude communication relay utilizing lora. In: *2022 International Symposium ELMAR*. [S.l.: s.n.], 2022. p. 97–100.

FREEMAN, R. L. *Radio System Design for Telecommunication*. [S.l.]: John Wiley & Sons, Inc, 2007.

GOLDBERG, B.-G. Rf synthesizers: Pll switching speed and speed-up techniques, a short review. In: *2001 IEEE MTT-S International Microwave Sympsoium Digest (Cat. No.01CH37157)*. [S.l.: s.n.], 2001. v. 2, p. 693–696 vol.2.

GUTTA, V.; FATTORINI, T.; PARKER, A. Intermodulation nulling in anti-parallel diode pair mixers. In: *2006 Asia-Pacific Microwave Conference*. [S.l.: s.n.], 2006. p. 461–464.

HERNANDEZ, L. M. M. *Body Area Networks using IEEE 802.15.6 : Implementing the ultra wide band physical layer*. [S.l.]: Academic Press, Elsevier Ltd, 2014.

HONG, J. Couplings of asynchronously tuned coupled microwave resonators. *IEE Proceedings - Microwaves, Antennas and Propagation*, Institute of Electrical Engineers, v. 147, n. 5, p. 354–358, out. 2000. ISSN 1350-2417.

HONG, J.-S. G.; LANCASTER, M. J. *Microstrip filters for RF/microwave applications*. [S.l.]: John Wiley & Sons, 2004. v. 167.

IPPOLITO, L. J. *Radiowave propagation in satellite communications*. [S.l.]: Springer Science & Business Media, 2012.

IPPOLITO, L. J.; JR, L. J. I. *Satellite communications systems engineering: atmospheric effects, satellite link design and system performance*. [S.l.]: John Wiley & Sons, 2017.

ITU-R. *Characteristics of precipitation for propagation modelling*. [S.l.], 2017. Disponível em: <https://www.itu.int/dms_pubrec/itu-r/rec/p/R-REC-P.837-7-201706-I!!PDF-E.pdf>.

JHA, C. K.; GUPTA, N. Design of a front end low noise amplifier for wireless devices. In: *2012 Students Conference on Engineering and Systems*. [S.l.: s.n.], 2012. p. 1–4.

KARUNAMURTHY, J. V. et al. Adaptive technique for lora communication with leo nanosatellite. In: *2021 IEEE Microwave Theory and Techniques in Wireless Communications (MTTW)*. [S.l.: s.n.], 2021. p. 182–187.

KHAN, Z. B. et al. Design and measurement of cavity enclosed microstrip edge-coupled bandpass filter at ku band. In: *2015 IEEE International Conference on Signal Processing, Communications and Computing (ICSPCC)*. [S.l.: s.n.], 2015. p. 1–4.

KRAUS, J. D. *Antennas*. 2. ed. [S.l.]: McGraw-Hill, 1988.

LATHI, B.; DING, Z. Sistemas de comunicações analógicos e digitais modernos. *LTC, Rio de Janeiro*, 2012.

LEE, T. H. *The Design of CMOS Radio-Frequency Integrated Circuits*. [S.l.]: Cambridge University Press, 2004.

LEENAERTS D.; TANG, J. v. d. *Circuit design for RF transceivers*. 1. ed. [S.l.]: ISBN 9781441949202,1441949208, 2001.

LEUNG, B. *VSLI for Wireless Communication*. 2. ed. [S.l.]: Springer Verlag NY, 2011.

LIU, Y. et al. Research on electromagnetic susceptibility of superheterodyne receiver rf front-end. In: *2013 5th IEEE International Symposium on Microwave, Antenna, Propagation and EMC Technologies for Wireless Communications*. [S.l.: s.n.], 2013. p. 576–581.

MINOLI, D. *Innovations in satellite communications and satellite technology*. [S.l.]: John Wiley & Sons, Inc., Hoboken, New Jersey., 2015.

POZAR, D. M. *Microwave engineering*. 4. ed. [S.l.]: John Wiley & Sons, 2012.

RAZAVI, B. *RF Microelectronics, 2nd Edition (Prentice Hall Communications Engineering and Emerging Technologies Series)*. 2. ed. [S.l.]: Prentice Hall, 2011.

RODDY, D. *Satellite Communications*. [S.l.]: CMcGraw-Hill, 2006.

ROGERS, C. P. J. *Radio Frequency Integrated Circuit Design*. [S.l.]: Artech House, INC., 2003.

SANTANA, M. P.; BARBOSA, E. V.; RONDINEAU, S. R. Design of ku-band filters and diplexer for a heterodyne transceiver using coupled open-loop resonator cells. In: *2020 Workshop on Communication Networks and Power Systems (WCNPS)*. [S.l.: s.n.], 2020. p. 1–6.

STEER, M. *Microwave and RF Design: A System Approach*. [S.l.]: SciTech Publishing, Inc., 2010.

STMICROELECTRONICS. *AN5457 Application note. RF matching network design guide for STM32WL Series.* [S.l.], 2020. Rev. 2.

SULAEMAN, Y. et al. S-band two stage low-noise-amplifier using single stub matching network. In: *2016 International Conference on Radar, Antenna, Microwave, Electronics, and Telecommunications (ICRAMET)*. [S.l.: s.n.], 2016. p. 63–66.

TERROVITIS, M.; MEYER, R. Intermodulation distortion in current-commutating cmos mixers. *IEEE Journal of Solid-State Circuits*, v. 35, n. 10, p. 1461–1473, 2000.

VASILESCU, G. *Electronic Noise and Interfering Signals Principles and Applications*. [S.l.]: Springer Berlin Heidelberg, 1999.

WANG, K.-A. et al. 0.35-m sige bicmos weaver image rejection receiver with 60-ghz double-quadrature sub-harmonic schottky diode mixer and 10-ghz double quadrature gilbert mixer. In: *2017 IEEE Asia Pacific Microwave Conference (APMC)*. [S.l.: s.n.], 2017. p. 899–902.

XU, S.; RAHMAT-SAMII, Y. Numerical evaluation of antenna noise temperature for optimal reflector antenna designs. In: *2011 IEEE International Symposium on Antennas and Propagation (APSURSI)*. [S.l.: s.n.], 2011. p. 3330–3332.

ZHANG, C. et al. A novel orthogonal lora multiple access algorithm for satellite internet of things. *China Communications*, v. 19, n. 3, p. 279–289, 2022.

ZHANG, L. et al. A ka-band monolithic doubly balanced up- and down-conversion mixer. In: *2018 Asia-Pacific Microwave Conference (APMC)*. [S.l.: s.n.], 2018. p. 258–260.

ZHAO, W.; ZHANG, Y.; ZHAN, M. Design and performance of a w-band microstrip rat-race balanced mixer. In: *2010 International Conference on Microwave and Millimeter Wave Technology*. [S.l.: s.n.], 2010. p. 713–716.

APPENDIX

A CURRENT ANALYSIS

Figure A.1 – Total current analysis. Source: Own elaboration.

B LOAD MAP

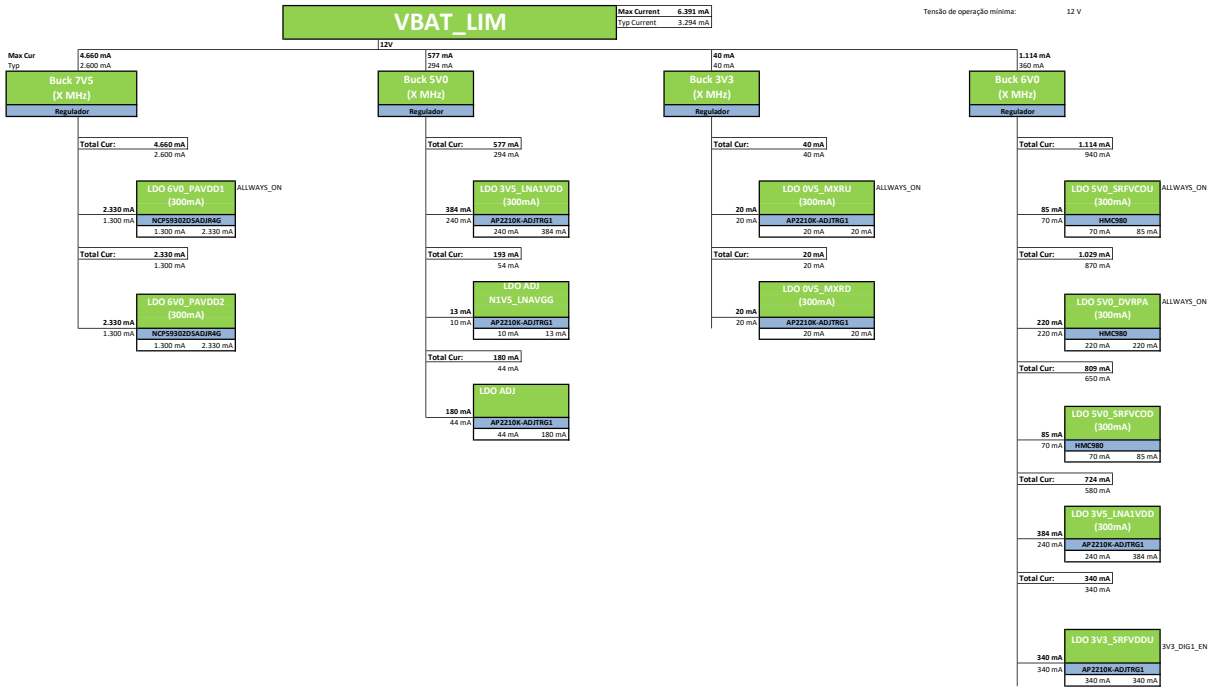

Figure B.1 – Power printed circuit board load map. Source: Own elaboration.

C LNA POWER SUPPLIER TEST PLANS

PSUBoard - LNA - Teste de alimentação

Última Modificação	Tensões de saída
Responsável:	Guilherme
Revisor:	Rev2
Data:	18/07/2019

STATUS GERAL DO TESTE	OK
Não Avaliado	0
OK	4
Warning	0
Fail	0

Índice

Home

CASO DE TESTE	VERSÃO	STATUS	DATA	RESPONSÁVEL	REVISOR
Tensões de saída	1	OK	18/07/2019	Guilherme	Rev2
Teste com carga resistiva	1	OK	18/07/2019	Guilherme	Rev2
Harmônicos espúrios	1	OK	18/07/2019	Guilheme	Rev2
Medida de spike e ripple	1	OK	18/07/2019	Guilherme	Rev2

Materiais e Ferramentas

Índice

LNA- QPA2609

Observações:

R5 deve ser substituído por um resistor de 2.32 kOhm

Componentes extras à BOM:

Periféricos:

Não constam.

Dispositivos auxiliares:

Fonte de bancada DC

Instrumentos de medição:

Osciloscópio
Carga eletrônica
Múltimetro

Softwares:

Não constam

Tensões de saída

Índice

OK **Versão:** 1

Objetivo

Avaliar a integridade dos sinais de alimentação do LNA do receptor.

Procedimentos

Introdução teórica :

As fontes servem para a alimentação do LNA, onde Vg é a tensão de gate e Vd é a tensão de Dreno. O sinal de alimentação vai para o conector J25, no qual os pinos 6 e 10 são para Vd e os pinos 8 e 12 para Vg do LNA 1 e 2 respectivamente.
O datasheet recomenda que faça o procedimento de Bias para alimentar o LNA, primeiramente aplica-se Vg=-1.5V, em seguida Vd=3.5V e aumenta-se a tensão Vg até atingir uma corrente de dreno Id = 120mA, onde Vg deve ser próximo a -0.46V

Procedimento 1 :

Rotacionar todos os Trimmers até o fim do curso no sentido anti-horário.
Conectar os Jumpers de controle J3, J4, J7 e J8 na posição de fonte interna (Pino 2 ligado ao Pino 3), retirar os demais Jumpers.
Conectar o pino +12V da fonte externa na entrada VBAT do conector borne J28 e o GND ao GND indicado no mesmo conector.
Conectar o cabo de referência do multímetro a uma das portas GND disponíveis (J37).
Ajustar o multímetro para medição de tensão, na escala de 20V.
Realizar as medições no pino 6, 8, 10 e 12 do conector J25-
Rotacionar os Trimmers R34 e R40, no sentido horário, até atingir a tensão de -1.3V nos pinos J25-12 e J25-8 respectivamente.
Rotacionar os Trimmers R34 e R40, no sentido horário, até atingir a tensão de -0.46V nos pinos J25-12 e J25-8 respectivamente.

Critérios

Pino (J25)	Tensão Mínima (V)	Tensão Esperada (V)	Tensão Máxima (V)
6	3.4	3.5	3.6
10	3.4	3.5	3.6
8	-1.6	-1.5	-1.4
12	-1.6	-1.5	-1.4

Após rotacionar os Trimmers, devem ser observadas as tensões indicada no procedimento

Dados Obtidos

Dados do procedimento 1:

Pino (J25)	Tensão Esperada (V)	Tensão Medida (V)
6	3.5	3,483
10	3.5	3,484
8	-1.5	-1,51
12	-1.5	-1,47

Tensões do procedimento atingidas (•) Sim ( ) Não

Análise dos Testes **Data** **18/07/2019**
STATUS: OK Responsável: Guilherme
Revisor: Rev2

Teste com carga resistiva

Índice

OK **Versão:** 1

Objetivo

Avaliar a capacidade da fonte em manter a corrente e tensão projetadas

Procedimentos

Introdução teórica :

Procedimento 1 :

Com a fonte extena desligada, conectar a carga eletrônica, também desligada, ao pino 6 do conector J25 (ponteira positiva).
Conectar a ponteira negativa da carga eletrônica ao GND
Colocar a carga em modo corrente constante (CC) e ajustar a corrente para 120 mA.
Ligar a fonte externa regulada para +12V e a carga eletrônica. Verificar a tensão medida pelo equipamento.
Desligar a carga e a fonte.
Repetir o procedimento para o pino 10 do conector J25
Repetir o procedimento para os pins 8 e 12 do conector J25, com o ajuste de corrente para 5mA

Critérios de Avaliação

Condições em que a solução de engenharia será aprovada ou reprovada.

Pino (J25)	Tensão Mínima (V)	Tensão Esperada (V)	Tensão Máxima (V)
6	3.4	3.5	3.6
10	3.4	3.5	3.6
8	-1.6	-1.5	-1.4
12	-1.6	-1.5	-1.4

Dados Obtidos

Dados do procedimento 1:

Pino (25)	Medida 1	Medida 2	Medida 3	Tensão Média	Desvio Padrão
6	3,46	3,46		3,46	0,00
10	3,42	3,42		3,42	0,00
8	-1,47	-1,46		-1,465	0,01
12	-1,46	-1,47		-1,465	0,01

Análise dos Testes **Data** **18/07/2019**
STATUS: OK Responsável: Guilherme
Revisor: Rev2

Harmônicos espúrios

Índice

OK **Versão:** 1

Objetivo

Observar a presença de ruído na alimentação do LNA em decorrência da fonte chaveada.

Procedimentos

Introdução teórica :

Procedimento 1 :

Utilizar a mesma configuração de jumpers do caso anterior.

Com o osciloscópio na função FFT, realizar medições nos pinos 6, 8, 10 e 12 do conector J25
Observar as componentes de frequência até 1 MHz.

Dados Obtidos

Dados do procedimento 1:

Na figura 1 e 2 utilizou-se a função de FFT do osciloscópio e observou-se picos nas frequências mostrada na tabela a seguir.

Frequência (KHz)	Magnitude (dBm)
138	-26,32
171	-45,83
42.9	-40,39
14.3	-41,48
286	-47,57

Procedimento associado

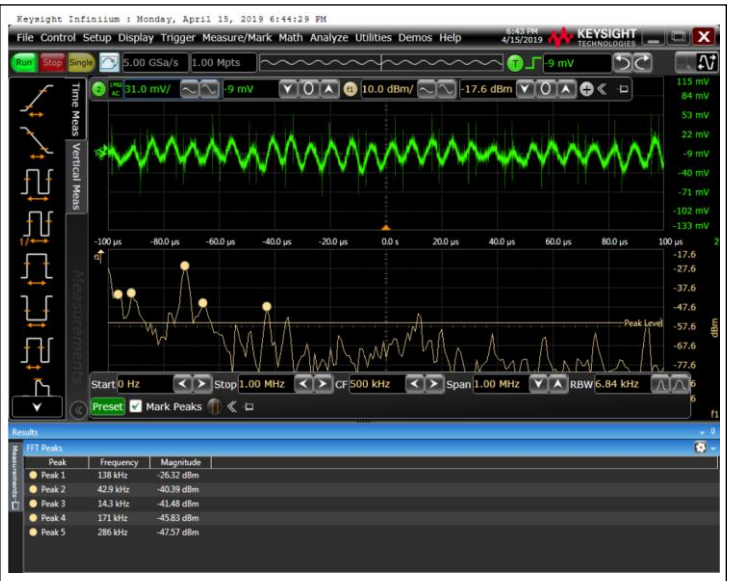

Figura 1 - Harmônicos de 0-100MHz

Procedimento associado

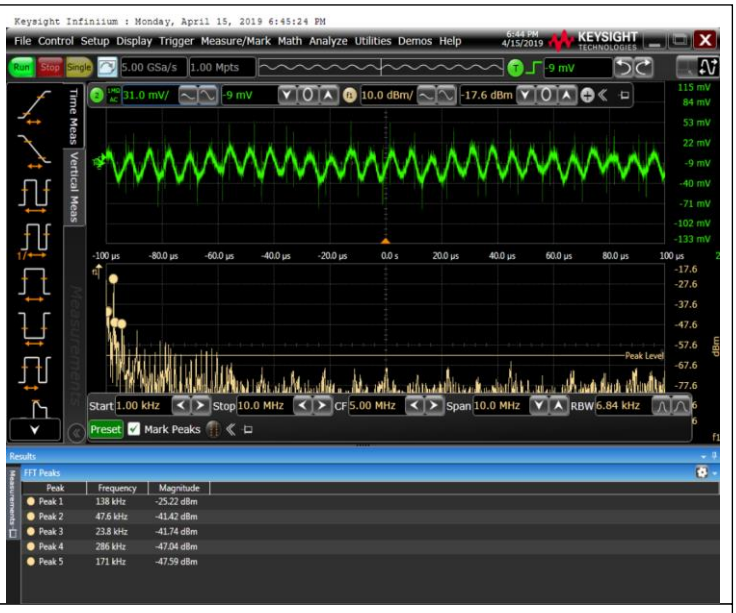

Figura 2 - Harmônicos

Análise dos Testes

STATUS: OK

Data **18/07/2019**

Responsável: Guilheme

Revisor: Rev2

Medida de spike e ripple

Índice

OK **Versão:** 1

Objetivo

Medir nível de skipe de tensão pico-a-pico e nível de ripple.

Procedimentos

Introdução teórica :

A caracterização de nível de spike e ripple e de importância para garantir que sejam preservados os estágios seguintes. Os Spikes, ou picos de tensão possuem um menor nível de energia se comparado ao ripple e ocorrem em transições de nível por chaveamento ou ativação do sistema. O pico causado pelo spike de tensão pode danificar o estágio seguinte, caso não esteja em um nível aceitável. O ripple é uma flutuação AC somada ao nível DC de interesse que não foi removido pelos filtros passa baixas. O nível de ripple, caso não controdado pode extrapolar os níveis de máximo e mínimo do estágio seguinte, fazendo com que o mesmo sai de operação, aqueça ou até mesmo se danifique.

Procedimento 1 :

Adicionar procedimentos para ligar o circuito de interesse e desligar os demais;
Conecte a carga eletrônica entre os pinos de Vdd (J25-6) e o GND (J25-4)

Conecte o osciloscópio digital entre os pinos deVdd (J25-6) e o GND (J25-4). A conexão deve ser feita entre o pino de GND mais próximo possível do Vdd com um cabo com pequeno caminho de GND para evitar a adição de componentes indutivas, o que pode afetar a medida;
Configure o osciloscópio para ter acoplamento AC, habilite a opção de persistência infinita e set o trigger para rising edge;
Ajuste a escala para 0.5V/div, 10ns/div (ou mais conviente);
Configure a carga eletrônica para o modo de CC, pressionando I-SET, configurando para 192 mA, depois apertar ON, para ativar a carga;
Conectar o pino +12V da fonte externa na entrada VBAT do conector borne J28 e o GND ao GND indicado no mesmo conector;
Ligue a fonte de tensão externa;
Ajuste a escala se necessário, ajuste os marcadores para a medida pico-a-pico e registre a medida do spike;
Desligue a fonte externa e repita o procedimento de medida para o outro spike.

Procedimento 2 :

Adicionar procedimentos para ligar o circuito de interesse e desligar os demais;
Conecte a carga eletrônica entre os pinos de Vdd (J25-6) e o GND (J25-4)
Conecte o osciloscópio digital entre os pinos de Vdd (J25-6) e o GND (J25-4). A conexão deve ser feita entre o pino de GND mais próximo possível do Vdd com um cabo com pequeno caminho de GND para evitar a adição de componentes indutivas, o que pode afetar a medida;
Configure o osciloscópio para ter acoplamento AC;
Ajuste a escala para 0.5V/div, 10ns/div (ou mais conviente);
Configure a carga eletrônica para o modo de CC, pressionando I-SET, configurando para 192 mA, depois apertar ON, para ativar a carga;
Conectar o pino +12V da fonte externa na entrada VBAT do conector borne J28 e o GND ao GND indicado no mesmo conector;
Ligue a fonte de tensão externa e espere o sinal entrar em regime estacionário;
Ajuste a escala se necessário, ajuste os marcadores para a medida pico-a-pico e registre a medida do ripple;

Repetir os procefimentos para os pinos 8, 10 e 12 do conector J25 Nos pinos 8 e 12 ajustar a corrente da carga eletrônica para 5 mA

Dados Obtidos

Dados do procedimento 1:

Medidas de tensão do procedimento 1.

Pino (J25)	Spike (mV)	Ripple (mV)
6	109,10	75,1
8	148,00	67,70
10	117,40	50,20
12	147,80	59,60

Figuras do procedimento 1.

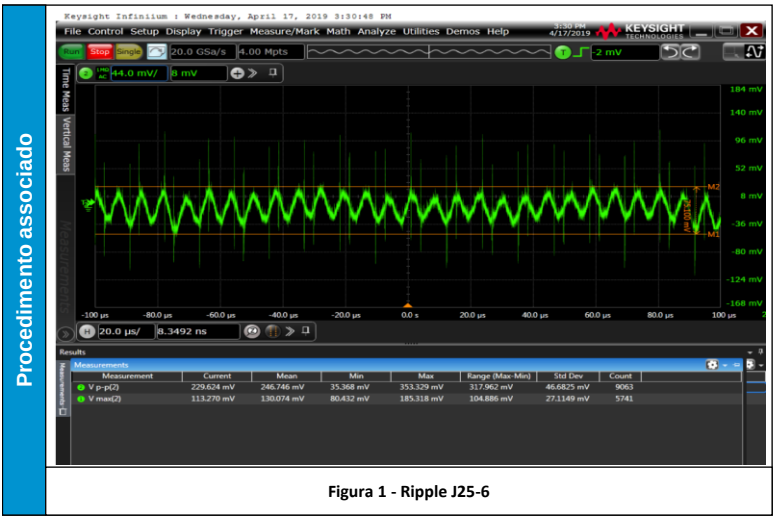

Figura 1 - Ripple J25-6

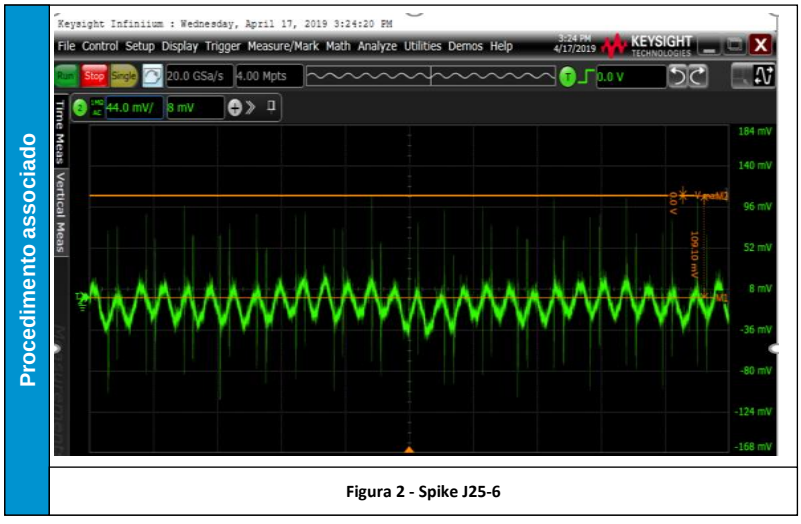

Figura 2 - Spike J25-6

Procedimento associado

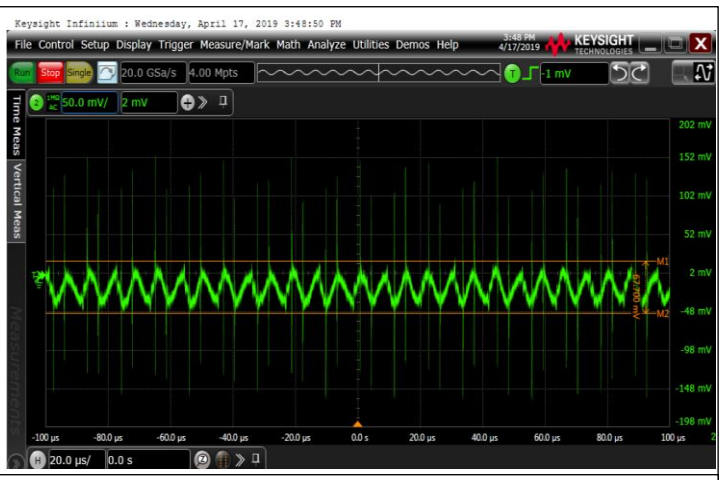

Figura 3 - Ripple J25-8

Procedimento associado

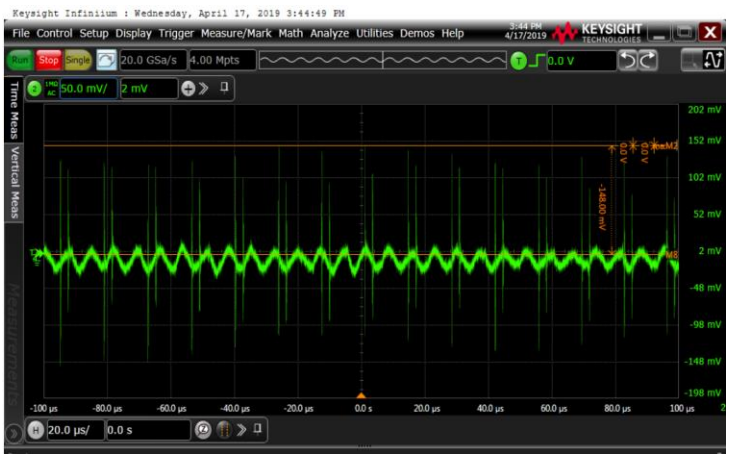

Figura 4 - Spike J25-8

Procedimento associado

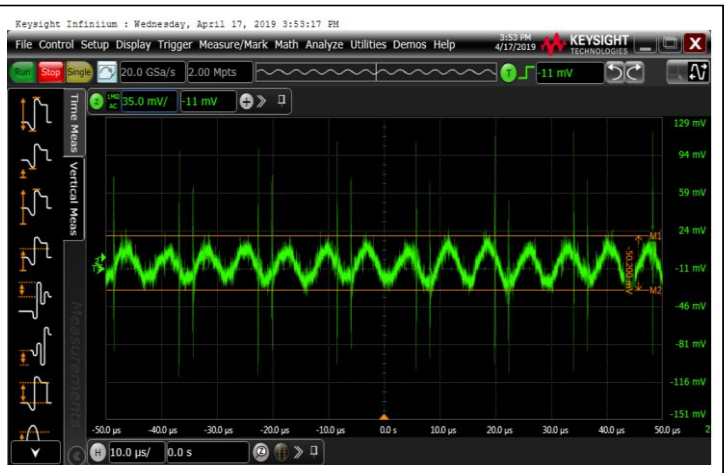

Figura 5 - Ripple J25-10

Procedimento associado

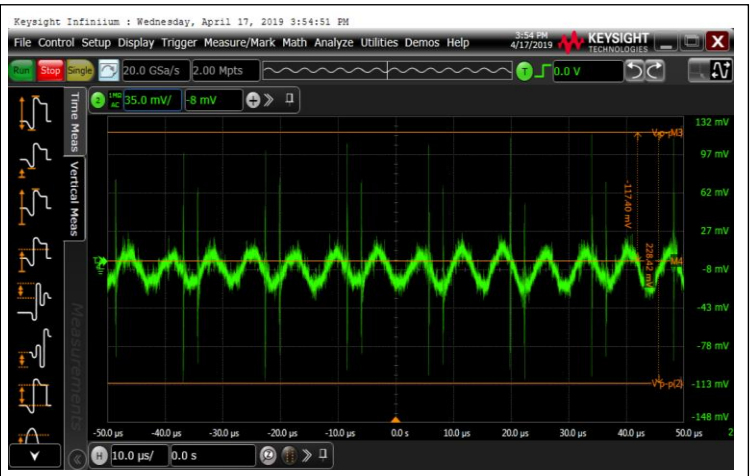

Figura 6 - Spike J25-10

Procedimento associado

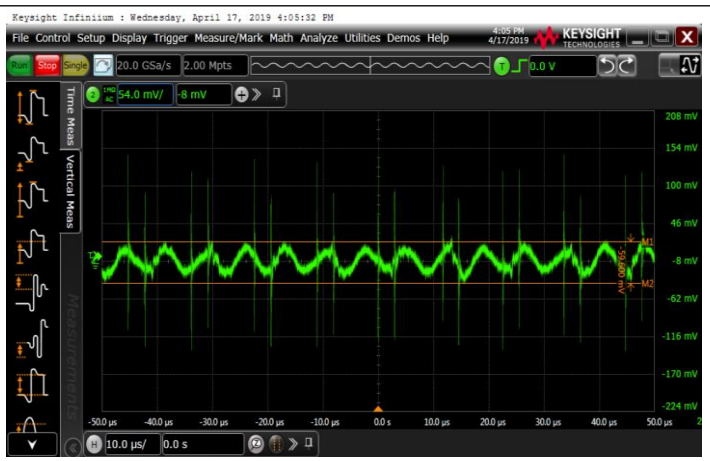

Figura 7 - Ripple J25-12

Procedimento associado

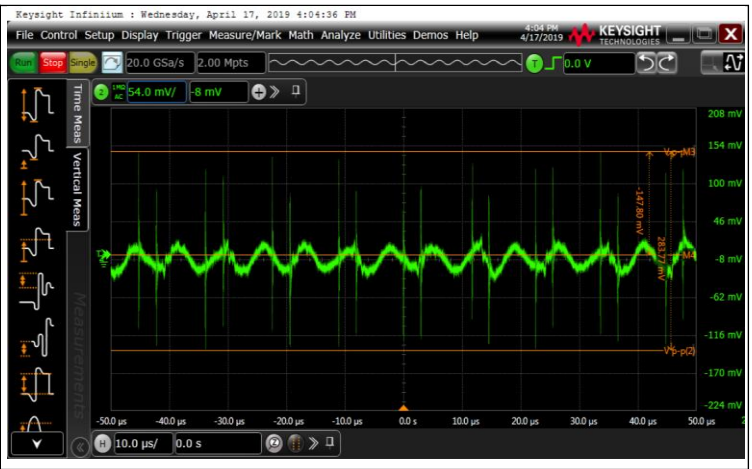

Figura 8 - Spike J25-12

Análise dos Testes

STATUS: OK

Data **18/07/2019**

Responsável: Guilherme

Revisor: Rev2

D SYNTHESIZER POWER SUPPLIER TEST PLANS

Última Modificação	Tensões de saída
Responsável:	Guilherme
Revisor:	Rev2
Data:	08/08/2019

STATUS GERAL DO TESTE	OK
Não Avaliado	0
OK	4
Warning	0
Fail	0

Índice

Home

Materiais e Ferramentas

Índice

Sintetizador -ADF5356

Observações:
R5 deve ser substituído por um resistor de 2.32 kOhm

Componentes extras à BOM:
Não constam

Periféricos:
Não constam.

Dispositivos auxiliares:
Fonte de bancada DC

Instrumentos de medição:
Múltimetro
Carga eletrônica

Softwares:
Não constam

Tensões de saída

Índice

OK **Versão:** 1

Objetivo

Avaliar o nivel de tensão de alimentação do sintetizador do receptor

Procedimentos

Introdução teórica :

Os pinos de saída alimentarão o sintetizador do receptor. Os sinais vem do LDO ADM7150 (U24, U26 e U28). Este dispositivo tem sua tensão de saída pré determinada de acordo com o Part Number.

Procedimento 1 :

Colocar todas as portas do DIP Switch S1 na posição OFF.
Rotacionar todos os Trimmers até o fim do curso no sentido anti-horário.
Conectar os Jumpers de controle J6, J12 e J14 na posição de fonte interna (Pino 2 ligado ao Pino 3), retirar os demais Jumpers.
Conectar o pino +12V da fonte externa na entrada VBAT do conector borne J28 e o GND ao GND indicado no mesmo conector.
Conectar o cabo de referência do multímetro a uma das portas GND disponíveis (J37).
Ajustar o multímetro para medição de tensão, na escala de 20V. Realizar as medições no pinos 5, 7 e 9 do conector J25.

Critérios de Avaliação

As tensões observadas devem estar dentro dos seguintes limites (definidos de acordo com o datasheet do sintetizador)

Pino (J25)	Tensão Mínima (V)	Tensão Esperada (V)	Tensão Máxima (V)
5	4,75	5,0	5,25
7	3,15	3,3	3,45
9	3,15	3,3	3,45

Dados Obtidos

Dados do procedimento 1:

Pino (J25)	Medida 1	Medida 2	Medida 3	Tensão Média	Desvio Padrão
5	4,98	4,98		4,98	0,00
7	3,29	3,29		3,29	0,00
9	3,27	3,29		3,28	0,01

Análise dos Testes **Data** **08/08/2019**

STATUS: OK Responsável: Guilherme

Revisor: Rev2

Teste com carga resistiva

Índice

OK **Versão:** 1

Objetivo

Avaliar o provisionamento de corrente para a alimentação do sintetizador do receptor

Procedimentos

Introdução teórica :

Procedimento 1 :

Seguir a mesma configuração de jumpers do Caso anterior
Com a fonte extena desligada, conectar a carga eletrônica, também desligada, ao pino 5 do conector J25 (ponteira positiva)
Colocar a carga em modo corrente constante (CC) e ajustar a corrente para 85 mA.
Ligar a fonte externa regulada para +12V e a carga eletrônica. Verificar a tensão medida pelo equipamento.
Desligar a carga e a fonte.

Repetir os procedimentos para os pinos J25-7 e J25-9, ajustando a s correntes para 170 mA em ambos.

Critérios de Avaliação

Após aplicada a carga, a tensão nos terminais deve se manter nos seguintes níveis (definidos de acordo com o datasheet do

Pino (J25)	Tensão Mínima (V)	Tensão Esperada (V)	Tensão Máxima (V)
5	4,75	5,0	5,25
7	3,15	3,3	3,45
9	3,15	3,3	3,45

Dados Obtidos

Dados do procedimento 1:

Pino (25)	Medida 1	Medida 2	Medida 3	Tensão Média	Desvio Padrão
5	4,95	4,95		4,95	0,00
7	3,26	3,26		3,26	0,00
9	3,24	3,24		3,24	0,00

Análise dos Testes **Data** **08/08/2019**

STATUS: OK Responsável: Guilherme

Revisor: Rev2

Harmônicos espúrios

Índice

OK **Versão:** 1

Objetivo

Observar a presença de ruído na alimentação do sintetizador RX em decorrência da fonte chaveada.

Procedimentos

Introdução teórica :

Procedimento 1 :

Utilizar a mesma configuração de jumpers do caso anterior.
Ligar a fonte de alimentação
Com o osciloscópio na função FFT, realizar medições nos pinos 5, 7 e 9 do conector J25
Observar as componentes de frequência até 1 MHz.
Salvar arquivo pino 9 com nome - Harmonico-1M-SRx
Salvar arquivo pino 5 com nome - Harmonico-1M-SRx_V1

Procedimento 2 :

Repetir procedimento 1 com frequencia até 10MHz
Salvar arquivo pino 9 com nome - Harmonico-10M-SRx
Salvar arquivo pino 5 com nome - Harmonico-10M-SRx_V1

Dados Obtidos

Dados do procedimento 1:

Na figura 1 e 2 utilizou-se a função de FFT do osciloscópio e observou-se picos nas frequências mostrada na tabela a seguir.
Na figura 1 utilizou-se frequência de 0-1MHz e na figura 2 0-10MHz
A medição foi no conector J25-9

Frequência (KHz)	Magnitude (dBm)
138	-27,22
45,9	-44,74
559	-48,52
1,78	-49,64
230	-50,67

Procedimento associado

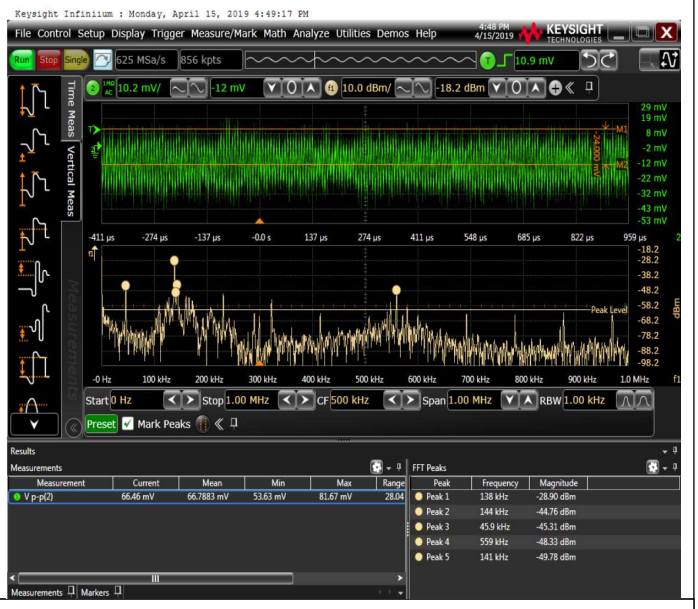

Figura 1 - Conector J25-9 1MHz

Procedimento associado

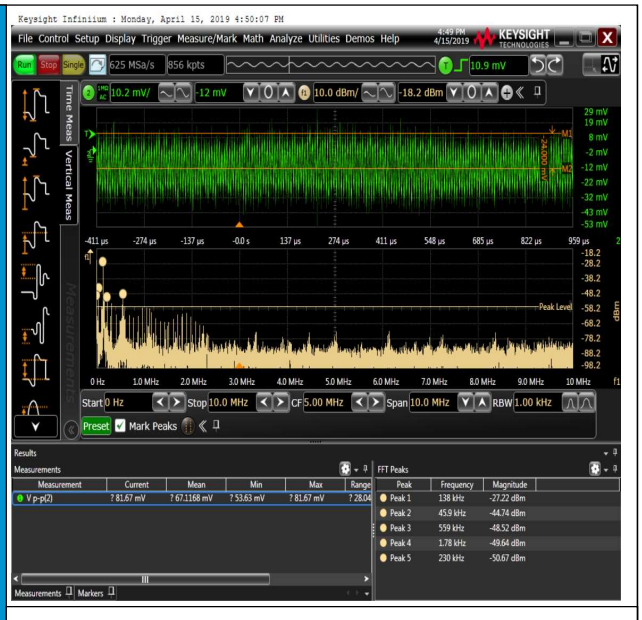

Figura 2 - Conector J25-9 10MHz

Na figura 1 e 2 utilizou-se a função de FFT do osciloscópio e observou-se picos nas frequências mostrada na tabela a seguir.
Na figura 1 utilizou-se frequência de 0-1MHz e na figura 2 0-10MHz
A medição foi no conector J25-5

Frequência (KHz)	Magnitude (dBm)
138	-26,24
141	-44,11
45,9	-45,82
559	-47,47
230	-47,82

Procedimento associado

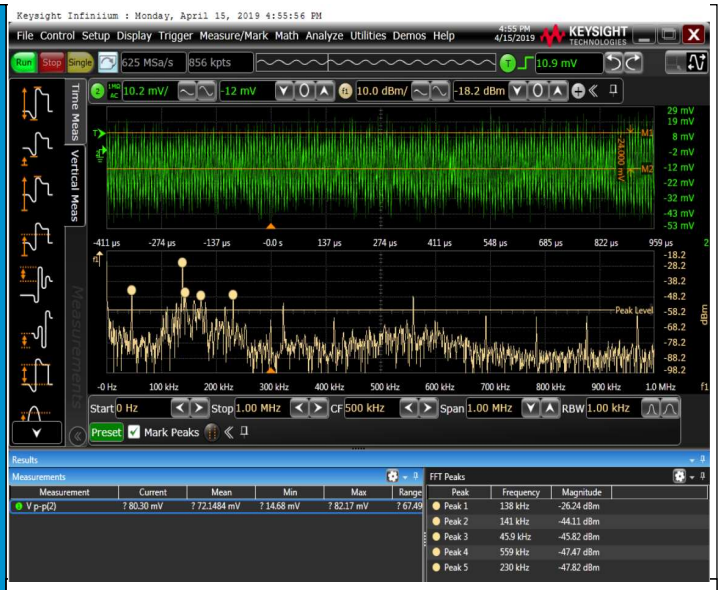

Figura 1 - Conector J25-5 1MHz

Procedimento associado

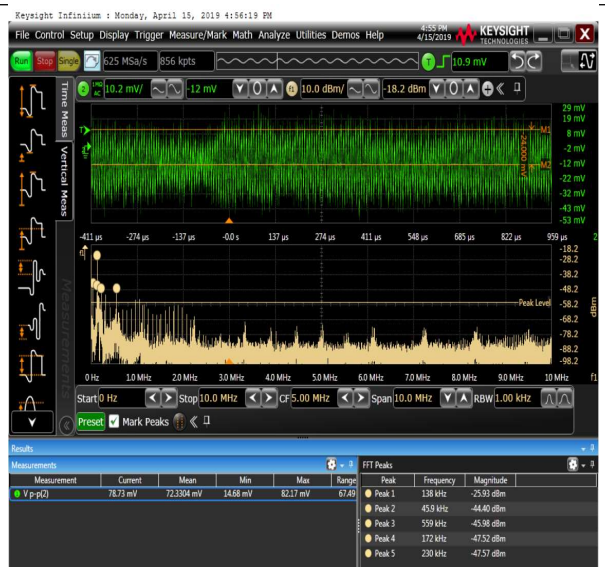

Figura 2 - Conector J25-5 10MHz

Análise dos Testes **Data** **08/08/2019**

STATUS: OK Responsável: Guilherme

Revisor: Rev2

Medida de spike e ripple

Índice

OK **Versão:** 1

Objetivo

Medir nível de skipe de tensão pico-a-pico e nível de ripple.

Procedimentos

Introdução teórica :

A caracterização de nível de spike e ripple é de importância para garantir que sejam preservados os estagios seguintes. Os Spikes, ou picos de tensão possuem um menor nível de energia se comparado ao ripple e ocorrem em transições de nível por chaveamento ou ativação do sistema. O pico causado pelo spike de tensão pode danificar o estágio seguinte, caso não esteja em um nível aceitável. O ripple é uma flutuação AC somada ao nível DC de interesse que não foi removido pelos filtros passa baixas. O nível de ripple, caso não controdado pode extrapolar os níveis de máximo e mínimo do estágio seguinte, fazendo com que o mesmo sai de operação, aqueça ou até mesmo se danifique.

Procedimento 1 :

Adicionar procedimentos para ligar o circuito de interesse e desligar os demais;
Conecte a carga eletrônica entre os pinos de Vdd (J25-5) e o GND (J25-1)
Conecte o osciloscópio digital entre os pinos de Vdd (J25-5) e o GND (J25-1). A conexão deve ser feita entre o pino de GND mais próximo possível do Vdd com um cabo com pequeno caminho de GND para evitar a adição de componentes indutivas, o que pode afetar a medida;
Configure o osciloscópio para ter acoplamento AC, habilite a opção de persistência infinita e set o trigger para rising edge;
Ajuste a escala para 0.5V/div, 10ns/div (ou mais conviente);
Configure a carga eletrônica para o modo de CC, pressionando I-SET, configurando para 85 mA, depois apertar ON, para ativar a carga;
Conectar o pino +12V da fonte externa na entrada VBAT do conector borne J28 e o GND ao GND indicado no mesmo conector;
Ligue a fonte de tensão externa;
Ajuste a escala se necessário, ajuste os marcadores para a medida pico-a-pico e registre a medida do spike;
Desligue a fonte externa e repita o procedimento de medida para o outro spike.

Procedimento 2 :

Adicionar procedimentos para ligar o circuito de interesse e desligar os demais;
Conecte a carga eletrônica entre os pinos de Vdd (J25-5) e o GND (J25-1)
Conecte o osciloscópio digital entre os pinos de Vdd (J25-5) e o GND (J25-1). A conexão deve ser feita entre o pino de GND mais próximo possível do Vdd com um cabo com pequeno caminho de GND para evitar a adição de componentes indutivas, o que pode afetar a medida;
Configure o osciloscópio para ter acoplamento AC;
Ajuste a escala para 0.5V/div, 10ns/div (ou mais conviente);
Configure a carga eletrônica para o modo de CC, pressionando I-SET, configurando para 85 mA, depois apertar ON, para ativar a carga;
Conectar o pino +12V da fonte externa na entrada VBAT do conector borne J28 e o GND ao GND indicado no mesmo conector;
Ligue a fonte de tensão externa e espere o sinal entrar em regime estacionário;
Ajuste a escala se necessário, ajuste os marcadores para a medida pico-a-pico e registre a medida do ripple;

Repetir os procefimentos para os pinos 7 e 9 do conector J25, alterando a corrente da carga eletrônica para 170 mA

Dados Obtidos

Pino (J25)	Spike (mV)	Ripple (mV)
5	195,6	46
7	140,30	51,10
9	124,6	43

Figuras do procedimento 1.

Procedimento associado

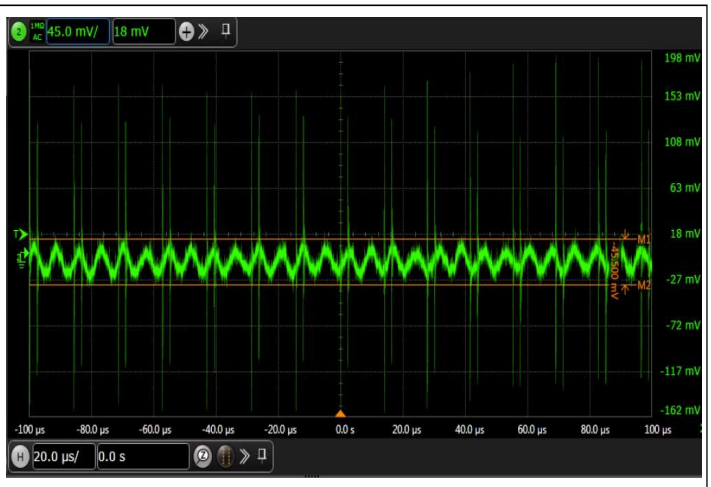

Figura 1 - Ripple J25-5

Procedimento associado

Figura 2 - Spike J25-5

Procedimento associado

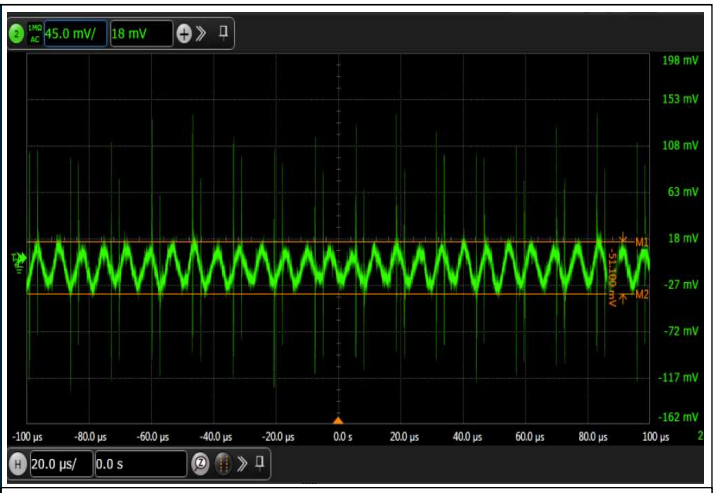

Figura 3 - Ripple J25-7

Procedimento associado

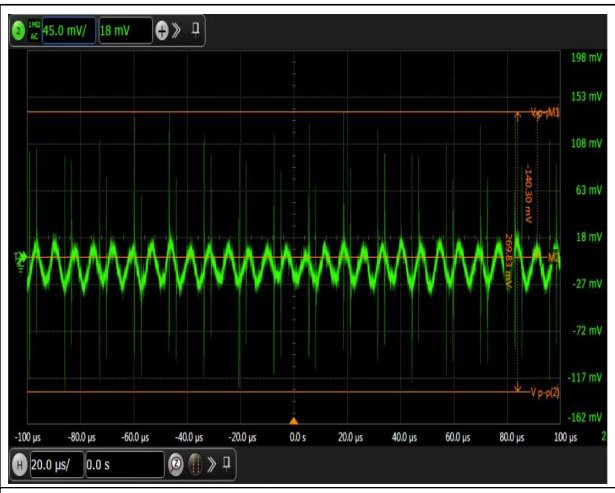

Figura 4 - Spike J25-7

Procedimento associado

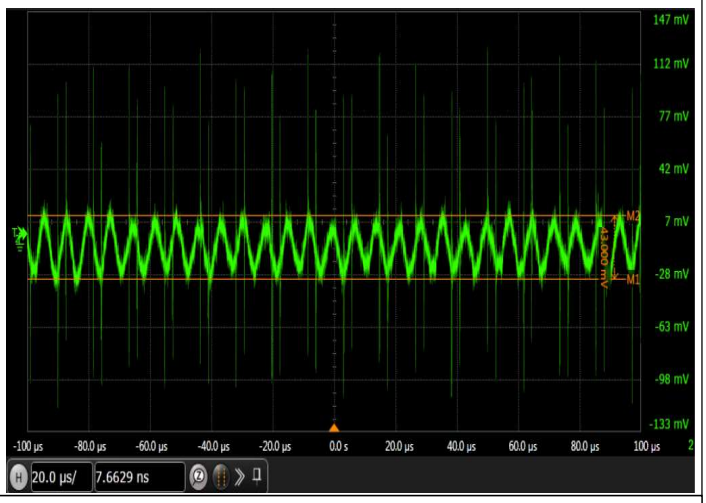

Figura 5 - Ripple J25-9

Procedimento associado

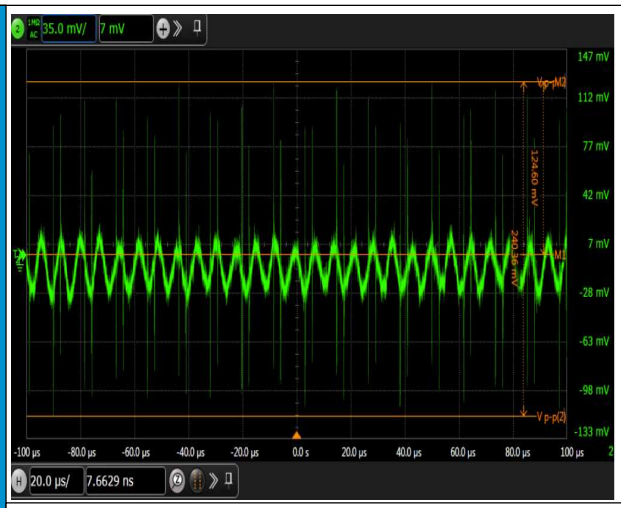

Figura 6 - Spike J25-9

Análise dos Testes

STATUS: OK

Data **08/08/2019**

Responsável: Guilherme

Revisor: Rev2